

Conceptual Design of a Blended Wing Body Airliner

a project presented to
The Faculty of the Department of
Aerospace Engineering San José State
University

in partial fulfillment of the requirements for the degree
Master of Science in Aerospace Engineering

by

Jeffrey Trac-Pho

December 2022

approved by

Sean Montgomery
Faculty Advisor



San José State
UNIVERSITY

© 2022
Jeffrey Trac-Pho
ALL RIGHTS RESERVED
ABSTRACT

Conceptual Design of a Blended Wing Body Airliner

Jeffrey Trac-Pho

Currently the aviation industry makes up 2% of all CO₂ emissions around the world. With current aviation technology plateauing, the need for an innovative aircraft design that can drastically reduce fuel emissions is imperative. It is also no surprise that airliners make up most of the CO₂ emissions in the aviation industry due to their prevalence in business and trade across the world. The blended wing body is an aircraft that consists of using multiple airfoils for its fuselage instead of the typical tube for improved aerodynamic efficiency. Improving the aerodynamic efficiency will reduce gas emissions and improve the global environment. This paper will present a feasible blended wing body aircraft design capable of carrying 500 passengers across 6,000 nmi at a cruise speed of 0.80 Mach number while still being FAR part 25 certifiable.

ACKNOWLEDGEMENTS

I would like to thank my family and my advisor for their continuous support throughout my master's project. My advisor, Sean Montgomery, has done a wonderful job guiding me throughout my project with his expertise in aircraft design. In addition, I will be forever grateful for my family's encouragement to do my master's and help me pursue my passion in aerospace engineering.

TABLE OF CONTENTS

ABSTRACT	iii
ACKNOWLEDGEMENTS	iv
LIST OF TABLES.....	ix
LIST OF FIGURES.....	xi
NOMENCLATURE	xiv
1. Mission Specifications & Comparative Study.....	1
1.1 Introduction	1
1.1.1 Motivation	1
1.1.2 Literature Review	1
1.1.3 Project Proposal.....	7
1.1.3.1 Mission Requirements	7
1.1.3.2 Critical Mission Requirements	7
1.1.3.3 Mission Profile	8
1.1.4 Mission Methodology.....	8
1.2 Comparative Study of Similar Aircraft	9
1.2.1 Mission Capabilities and Configuration Selection	9
1.2.2 Comparison of Important Design Parameters	11
1.2.3 Discussion.....	14
1.3 Conclusion	14
2. Weight Sizing & Weight Sensitivities	15
2.1 Introduction	15
2.2 Mission Weight Estimates.....	15
2.2.1 Database for Takeoff Weights and Empty Weights of Similar Airplanes	15
2.2.2 Determination of Regression Coefficients A and B	16
2.2.3 Determination of Mission Weights.....	16
2.2.3.1 Manual Calculation of Mission Weights	16
2.2.3.2 Calculation of Mission Weights using RDS Program	19
2.3 Takeoff Weight Sensitivities.....	20
2.3.1 Manual Calculation of Takeoff Weight Sensitivities	20
2.3.2 Trade Studies	21
2.4 Discussion	22
2.5 Conclusion.....	23
3. Performance Constraint Analysis	24
3.1 Introduction	24
3.2 Manual Calculation of Performance Constraints	24
3.2.1 Stall Speed	24
3.2.2 Takeoff Distance.....	25
3.2.3 Landing Distance	26
3.2.4 Drag Polar Estimation	27
3.2.5 Climb Sizing Estimation for FAR 25 Regulations	30
3.3 Calculation of Performance Constraints with RDS Software	34

3.4 Discussion	39
3.5 Conclusion.....	40
4. Configuration Selection.....	41
4.1 Introduction	41
4.2 Discussion of Items which have Major Impact on Design.....	41
4.2.1 List of Items with Major Impact on the Design.....	41
4.2.2 Discussion.....	41
4.3 Comparative Study of Airplanes with Similar Mission Performance.....	42
4.3.1 Recap of Similar Aircraft Studies.....	42
4.3.2 Configuration Selection of Similar Airplanes	45
4.3.3 Discussion.....	47
4.4 Selection of Propulsion System.....	47
4.4.1 Selection of the Propulsion System Type.....	47
4.4.2 Number of Engines.....	47
4.5 Configuration Selection.....	48
4.5.1 Overall Configuration.....	48
4.5.2 Wing Configuration.....	48
4.5.3 Empennage Configuration.....	48
4.5.4 Integration of Propulsion System	48
4.5.5 Landing Gear Disposition.....	49
4.5.6 Configuration Proposal.....	49
5. Fuselage Design.....	51
5.1 Introduction	51
5.2 Layout Design of the Cockpit	52
5.3 Layout Design of the Fuselage.....	53
5.4 Discussion	54
6. Wing, High-Lift System & Lateral Control Design	56
6.1 Introduction	56
6.2 Wing Planform Design.....	57
6.3 Airfoil Selection	62
6.4 Wing Design Evaluation	64
6.5 Design of the High-Lift Devices	64
6.6 Design of the Lateral Control Surfaces	68
6.7 Wing Drawings	69
6.8 Discussion	70
7. Design of the Empennage & Control Surfaces	71
7.1 Introduction	71
7.2 Overall Empennage Design.....	71
7.3 Design of the Vertical Stabilizer	73
7.4 Empennage Design Evaluation	74
7.5 Design of the Longitudinal and Directional Controls	74
7.6 CAD Drawings	75
7.7 Discussion	76
8. Landing Gear Design.....	77

8.1	Introduction	77
8.2	Estimation of the Center of Gravity Location	77
8.3	Landing Gear Design	78
8.3.1	Tire Design Choices	78
8.3.2	Strut Design Choices	79
8.3.3	Preliminary Arrangement	80
8.3.4	Retraction Feasibility	83
8.4	Discussion	84
9.	Weight & Balance Analysis	85
9.1	Introduction	85
9.2	Component Weight Breakdown	85
9.3	Center of Gravity Location for Various Loading Scenarios	89
9.4	Discussion	90
10.	Stability Analysis	91
10.1	Introduction	91
10.2	Static Margin	91
10.3	Discussion	91
11.	Drag Polar Estimation.....	92
11.1	Introduction	92
11.2	Drag Polars	92
11.3	XFLR 5 Calculations.....	95
11.4	Discussion	95
12.	Drawings, Environmental and Safety Considerations	96
12.1	Drawings	96
12.2	Environmental Considerations	98
12.3	Safety Consideration	98
13.	Drag Polar Estimation – Class II	99
13.1	Introduction	99
13.2	Wing Drag Estimation.....	99
13.3	Empennage Drag Estimation.....	103
13.4	Nacelle Drag Estimation	105
13.5	Flap Drag Estimation	108
13.6	Landing Gear Drag Estimation	111
13.7	Raymer’s Calculations	112
13.8	Discussion	114
14.	Weight and Balance Analysis – Class II.....	115
14.1	Introduction	115
14.2	Component Weight Breakdown	115
14.3	Discussion	119
15.	V-N Diagram	120
15.1	Introduction	120
15.2	V-N Diagram.....	120
16.	Installed Thrust and Power Characteristics	123
16.1	Introduction	123

16.2 Installed Thrust Calculations.....	123
17. Critical Performance Requirements.....	125
17.1 Introduction	125
17.2 Critical Performance Calculations	125
17.3 Discussion	128
18. Initial Structure Arrangement	129
18.1 Introduction	129
18.2 Discussion	129
19. Airplane Subsystem Arrangement.....	131
19.1 Introduction	131
19.2 Flight Control Systems Layout Design	131
19.3 Propulsion System Design	132
19.4 Fuel System Layout Design	132
19.5 Hydraulic System Layout Design	133
19.6 Electrical System Layout Design	133
19.7 Environmental Control System Layout Design	133
19.8 Cockpit Instrumentation, Flight Management and Avionics System Layout Design.....	134
19.9 De-Icing, Anti-Icing, Rain Removal, and Defog Systems Layout Design	134
19.10 Escape System Layout Design	135
19.11 Water and Waste Systems Layout Design	135
19.12 Safety and Survivability Considerations	135
20. Stability and Control Analysis – Class II	136
20.1 Introduction	136
20.2 Discussion	136
21. Cost Analysis.....	137
21.1 Design and Development Cost	137
21.2 Manufacturing Cost.....	137
21.3 Operating Cost.....	138
22. Conclusion	139
22.1 Conclusion	139
References.....	140
Appendix.....	143
A. Raymer’s Weight Calculations.....	143
B. Roskam’s Weight Calculations.....	145
C. Matlab Code.....	146
C.1. Breguet’s Range Equation	146
C.2. Sweep Angle Equation	147
C.3. CG Excursion Equation	148
C.4. Drag Polar Graph Equation	149
C.5. Drag Polar Graph Equation of Raymer’s and Roskam’s Methods.....	150
C.6. V-N Diagram	151
C.7. DAPCA IV Cost Model.....	153

LIST OF TABLES

Table 1.1 – X-48 advantages and challenges report of the blended wing-body concept [2].....	4
Table 1.2 – Similar conventional aircraft study [12].....	11
Table 1.3 – Similar winged body aircraft study [2][12].....	13
Table 2.1 – Similar airplane weight database [12][13][14][15].....	15
Table 2.2 – Roskam’s fuel fraction table [14].....	18
Table 2.3 – Fuel ratios of the 500 - BWB airliner.....	18
Table 2.4 – RDS screenshot of weight distributions.....	20
Table 3.1 – Roskam’s estimate for C_D increments [14].....	29
Table 3.2 – Drag polar data for various configurations.....	30
Table 3.3 – RDS inputs of performance module.....	34
Table 3.4 – Performance analysis summary.....	35
Table 3.5 –Wing and propulsion sizing comparison analysis with RDS.....	39
Table 4.1 – Similar conventional aircraft study [12].....	42
Table 4.2 – Similar winged body aircraft study [2][12].....	44
Table 4.3 – Engine specifications [17].....	47
Table 6.1 – Wing planform design.....	60
Table 6.2 – NASA SC (2) 0412 airfoil profile parameters.....	63
Table 6.3 – NACA 25118 airfoil profile parameters.....	63
Table 6.4 – Approximated change in local section lift coefficient with arbitrary Swf/S values.....	66
Table 7.1 – Vertical stabilizer parameters.....	73
Table 7.2 – Roskam’s table for vertical tail design parameters [19].....	73
Table 7.3 – XFLR5 empennage inputs.....	74
Table 7.4 – XFLR5 empennage outputs.....	74
Table 8.1 – CG location at critical loading scenarios.....	77
Table 8.2 – Roskam’s tire size reference table [19].....	78
Table 8.3 – Main landing gear tires.....	78
Table 8.4 – Nose landing gear tires.....	78
Table 8.5 – Main landing gear struts.....	79
Table 8.6 – Nose landing gear struts.....	79
Table 9.1 – CG inputs in Excel for the X-location.....	86
Table 9.2 – CG outputs in Excel for the X-location.....	87
Table 9.3 – CG inputs in Excel for the Z-location.....	88
Table 9.4 – CG outputs in Excel for the Z-location.....	89
Table 11.1 – Roskam’s estimates for C_D increments [14].....	93
Table 11.2 – Drag polar data for various configurations.....	94
Table 12.1 – Blended wing body aircraft parameters.....	98
Table 13.1 – Landing gear component drags [22].....	113
Table 13.2 – Drag coefficients summary.....	114
Table 14.1 – CG inputs in Excel for the X-location using Roskam’s method.....	116
Table 14.2 – CG outputs in Excel for the X-location using Roskam’s method.....	117

Table 14.3 – CG inputs in Excel for the Z-location using Roskam’s method.....	118
Table 14.4 – CG outputs in Excel for the Z-location using Roskam’s method.....	119
Table 14.5 – Component weight comparison with various methods	119
Table 16.1 – Summary of power extraction requirements [23].....	124
Table 17.1 – Parameter values for equation 17.4 [25].....	126

LIST OF FIGURES

Figure 1.1 – Dr. Robert H. Liebeck’s initial design of a blended wing body [2].....	2
Figure 1.2 – BWB-450 in NASA Langley Research Center’s wind tunnel [3].....	3
Figure 1.3 – X-48B [5]	3
Figure 1.4 – Multi-bubble shell cabin concept [7].....	5
Figure 1.5 – Airbus MAVERIC [6]	6
Figure 1.6 – Mission profile for blended wing body airliner	8
Figure 1.7 – Boeing 747-400 [8].....	9
Figure 1.8 – Airbus 340-600 [9]	9
Figure 1.9 – Boeing 777-300 [10].....	9
Figure 1.10 – Northrop Grumman B-2 Spirit [1].....	10
Figure 2.1 – Trend line for determining regression coefficients A and B.....	16
Figure 2.2 – Range and payload trade study	22
Figure 3.1 – FAR 25 take-off distances [14]	25
Figure 3.2 – FAR 25 landing distances [14].....	26
Figure 3.3 – Equivalent parasitic area and wetted area in Roskam’s textbook [14]	28
Figure 3.4 – Estimated drag polar	29
Figure 3.5 – RDS takeoff analysis part 1.....	36
Figure 3.6 – RDS takeoff analysis part 2.....	37
Figure 3.7 – RDS landing analysis	38
Figure 4.1 – Boeing 747-400 [8]	45
Figure 4.2 – Airbus 340-600 [9].....	45
Figure 4.3 – Boeing 777-300 [10]	46
Figure 4.4 – X-48B [5]	46
Figure 4.5 – Airbus MAVERIC [6].....	46
Figure 4.6 – Northrop Grumman B-2 Spirit [11]	46
Figure 4.7 – Proposed configuration front view.....	49
Figure 4.8 – Proposed configuration side view	49
Figure 4.9 – Proposed configuration top view	50
Figure 4.10 – Proposed configuration isometric view.....	50
Figure 5.1 – Side cockpit view for the blended wing body design	52
Figure 5.2 – Top cockpit view for the blended wing body design	52
Figure 5.3 – Side fuselage view for the blended wing body design.....	53
Figure 5.4 – Top fuselage view for the emergency exits.....	53
Figure 5.5 – Top fuselage view for the blended wing body design.....	54
Figure 5.6 – Top fuselage dimensions for the blended wing body design	55
Figure 6.1 – Top view of wing planform from XFLR5.....	57
Figure 6.2 – Mean aerodynamic center and location.....	58
Figure 6.3 – Trapezoidal area of wing planform [20]	59
Figure 6.4 – The sweep angle combinations curve from 0° to 90° for current aircraft parameter...	62
Figure 6.5 – NASA SC (2) 0412 airfoil profile	62

Figure 6.6 – NACA 25118 airfoil profile	63
Figure 6.7 – Local lift coefficient across mean aerodynamic chord with XFLR5	64
Figure 6.8 – Effect of airfoil thickness on CLMAX [19].....	65
Figure 6.9 – Flap length concerning chord length and its impact of flap deflection angle [19]	66
Figure 6.10 – Flap deflection angle and its impact on variable K' [19].....	67
Figure 6.11 – High-lift device placement.....	69
Figure 6.12 – Side view of aircraft wing.....	69
Figure 7.1 – Location estimates of empennage parts [14].....	72
Figure 7.2 – XFLR5 CAD of the vertical tail.....	75
Figure 7.3 – XFLR5 ruddervators placement of the vertical tail.....	75
Figure 7.4 – NACA 0012 rudder airfoil	75
Figure 8.1 – Geometric definition for static load on landing gear	79
Figure 8.2 – Longitudinal and lateral ground clearance criteria [19].....	80
Figure 8.3 – Lateral tip-over criteria [19].....	80
Figure 8.4 – Longitudinal tip-over criteria [19]	81
Figure 8.5 – Longitudinal ground clearance criterion for the blended wing body aircraft	81
Figure 8.6 – Lateral ground clearance criterion for the blended wing body aircraft.....	81
Figure 8.7 – Longitudinal tip-over criterion at the most forward C.G.	82
Figure 8.8 – Longitudinal tip-over criterion at the most aft C.G.....	82
Figure 8.9 – Lateral tip-over criterion at the most forward C.G.	83
Figure 8.10 – Retraction feasibility of landing gears	83
Figure 9.1 – CG excursion diagram.....	89
Figure 11.1 – Typical compressibility drag behavior.....	93
Figure 11.2 – Manually calculated drag polar estimation for various configuration	94
Figure 11.3 – XFLR5 calculations for cruise clean (white) and takeoff (green) configurations	95
Figure 12.1 – Front view of modeled blended wing body aircraft.....	96
Figure 12.2 – Side view of modeled blended wing body aircraft.....	96
Figure 12.3 – Top view of modeled blended wing body aircraft	96
Figure 12.4 – Iso view of modeled blended wing body aircraft.....	96
Figure 13.1 – Lifting surface correction factor [23].....	100
Figure 13.2 – Turbulent mean skin-friction coefficient [23].....	101
Figure 13.3 – Zero-lift wave drag coefficient [23].....	102
Figure 13.4 – Transonic drag due to lift from the wing [23].....	103
Figure 13.5 – Transonic drag due to lift from the empennage [23].....	105
Figure 13.6 – Transonic fairing for fuselage base drag coefficient [23]	107
Figure 13.7 – Wave drag coefficient for parabolic fuselages [23]	107
Figure 13.8 – Profile drag increment: plain flaps [23]	109
Figure 13.9 – Induced drag factor for uninterrupted flaps [23].....	110
Figure 13.10 – Equivalent parasitic drag increment for gears with multiple wheel bogies [23].....	111
Figure 13.11 – Drag polar comparison with other methods	114
Figure 15.1 – V-N gust diagram.....	121
Figure 15.2 – V-N maneuver diagram.....	122
Figure 16.1 – Effect of Mach number on K_t [23].....	123
Figure 18.1 – Internal wing structure arrangement iso view	129

Figure 18.2 – Internal wing structure arrangement front view130
Figure 18.3 – Internal wing structure arrangement top view130
Figure 19.1 – Boeing 767 flight control features [26].....131
Figure 19.2 – Boeing 767 fuel system layout [26]132
Figure 19.3 – Boeing 767 pressurization system layout [26]134
Figure 19.4 – Boeing 767 water system system layout [26]135

NOMENCLATURE

Symbol	Definitions	Units (SI)
AR	Wing Aspect Ratio	N/A
AoA (α)	Angle of Attack	degrees ($^{\circ}$) / radians
b	Wingspan	ft (m)
c	Wing Chord	ft (m)
\bar{c}	MAC	ft (m)
C_D	Coefficient of Drag	N/A
CG	Center of Gravity	ft (m)
C_L	Coefficient of Lift	N/A
C_m	Coefficient of Moment	N/A
e	Oswald Efficiency Factor	N/A
L	Length of Fuselage	ft (m)
L/D	Lift-to-drag ratio	N/A
i_w	Incidence Angle of Wing	degrees ($^{\circ}$) / radians
NP	Neutral Point	ft (m)
S	Wing area	ft ² (m ²)

SM	Static Margin	N/A
S_{TO} / S_L	Takeoff / Landing Distance	ft (m)
TSFC	Thrust Fuel Consumption	lb/lbf/hr (g/kN/s)
T/W	Thrust-to-Weight Ratio	lbf/lbf (N/N)
$V_{(H,V)}$	Horizontal/ Vertical Stabilizer Tail Volume Coefficient	N/A
$W_{(CREW,E,F,P,0)}$	Weight (Crew weight, Empty, Fuel, Payload, Gross takeoff)	lbs (N)
W/S	Wing Loading	lb/ft ² (N/m ²)
\bar{y}	Aerodynamic Center Lateral Location	ft (m)
λ	Taper Ratio	N/A
ρ	Atmospheric Density at altitude	lb/ft ³ (kg/m ³)
σ	Atmospheric Density Ratio	N/A
μ	Dynamic Viscosity	lb-s/ft ² (kg/m ³)
Λ_{LE}	Sweep Angle at Leading Edge	degrees (°) / radians
$\Lambda_{C/4}$	Sweep Angle (Quarter-Chord)	degrees (°) / radians
Λ_{TE}	Sweep Angle at Trailing Edge	degrees (°) / radians
Γ	Dihedral Angle	degrees (°) / radians

1. Mission Specification & Comparative Study

1.1 Introduction

1.1.1 Motivation

Air transportation has become more prevalent within the past few decades as more and more people have begun using it to travel for work conferences, vacations, and visiting their friends and families. Airliners were designed to meet the high demand of people who wanted to travel to popular locations around the world. Conventional airliners use a tube-and-wing (TAW) configuration which consists of a cylindrical fuselage and wings attached to either side of the fuselage. The fuselage carries the payload and passengers whereas the wings produce the lift necessary for flight. The tube-and-wing configuration is well proven over the years and has been continually improved upon by various aircraft manufacturers, such as Boeing and Airbus to improve its efficiency; however, the technical optimization of airliners has slowly begun to plateau and a change in airliner configuration is necessary to meet the growing prices of airline fuel as well as the concerning environmental pollution that conventional airliners create.

Many environmentally friendly transportation methods have been proposed with electric vehicles and aircraft being on the rise due to their zero-carbon emission. Although electric vehicles and aircraft are a hot topic of research, the technology needed to design an electrical airliner still needs more research. One alternative for eco-friendlier long-range transportation is a blended wing body (BWB) airliner. BWB configuration consists of a fuselage and the wing being combined into one homogenous lifting surface. The single surface airframe increases the aerodynamic efficiency because of the shape of the body thereby increasing the fuel efficiency of the aircraft as well. Research has discovered that the energy to revenue work ratios of the BWB was 31.5% to 40% higher than the TAW counterparts [1]. Research needs to be done to help develop high-performing aircraft with minimal negative consequences on the environment.

This report will discuss a conceptual design of a large BWB airliner capable of holding up to 500 passengers.

1.1.2 Literature Review

The blended wing body is significantly different than the conventional tube and wing configuration, having no fuselage or horizontal stabilizer. Instead, the airfoil cross-section runs along the entire surface of the aircraft, creating one single aerodynamic surface. In this sense, the entire aircraft can be modeled as a wing. It should be noted that the control surfaces are the main way to control the aircraft's pitch due to the absence of the horizontal stabilizer. A vertical stabilizer can be implemented to help control the yaw of the aircraft. Many engineers in the early to mid-1900s conceptualized the blended wing body design but were quickly regarded as a novel idea due to stability and control issues. However, due to the technological advances, control algorithms have improved

making this configuration feasible.

The development of a blended wing body configuration airliner started in the late 20th century with Dennis Bushnell from NASA Langley Research Center challenging the conventional concept of the tube and wing configuration for an airliner. By the late 20th century, many novel aircraft design concepts were already designed and built, such as the flying wing, and tailless aircraft. Both of which would heavily become the inspiration for the BWB [2].

McDonnell Douglas, an American aerospace manufacturing company, accepted the challenge and began funding research for more unconventional aircraft designs. Dr. Robert H. Liebeck and other engineers from McDonnell Douglas designed the first blended wing body transport aircraft with theoretical L/D ratios up to 28.

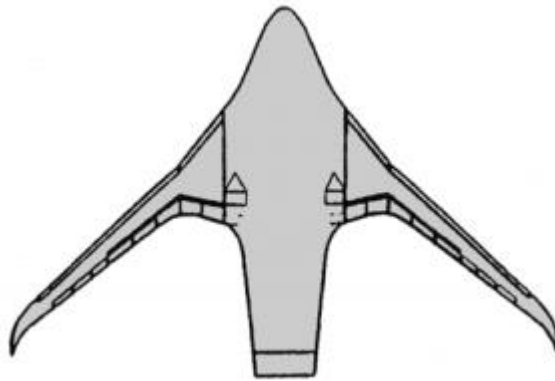


Figure 1.1. Dr. Robert H. Liebeck’s initial design of a blended wing body [2]

This initial concept would eventually lead to the experimental design of the X-48, an experimental aircraft design by Boeing. A lot of engineers were in strong agreement that more research should be put into the BWB configuration because of its major aerodynamic advantage; however, many passengers did not feel comfortable in the BWB configuration due to its safety concerns, which stemmed from the placements of exits due to its unconventional configuration. Unlike the conventional tube and wing configuration, the blended winged body had a “theater-like” seating arrangement for its passengers. This meant that there were fewer safety exits, making it difficult for people in the middle of the aircraft to evacuate to safety. The lack of windows also did not make passengers in blended wing bodies feel safe. Although the blended wing body configuration was not commercialized in the airline industry, it was widely accepted into the military.

The BWB’s efficient configuration allows the aircraft to consume 20% less fuel on average over a 7,000 nmi flight. The design of this aircraft can greatly cut fuel emissions, saving both the environment and money for aircraft manufacturers. In addition, the wingspan is only slightly greater than the Boeing 747, allowing these unconventional aircraft to operate in conventional airport terminals [3]. In addition, the BWB configuration was not only more aerodynamic and fuel efficient, but also lighter. The researchers at McDonnell Douglas discovered that the BWB had 15% lower takeoff weight, and 12% lower empty operating weight [4].

Although McDonnell Douglas designed the blended wing concept, Boeing pushed for the further

development and research of the BWB configuration. This sparked the development of the X-48 which went through many iterations to determine the feasibility of the aircraft. Before the production of the X-48 experimental aircraft, the BWB-450, a 3% BWB scaled model, was simulated under Langley's wind tunnel to obtain empirical data. Testing under the wind tunnel for the BWB-450 model included low-speed simulations and forced oscillations.

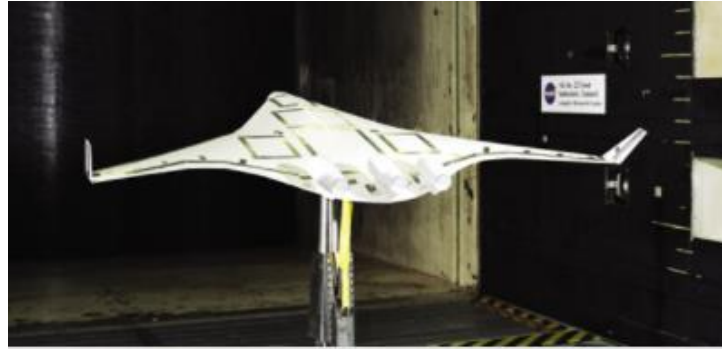


Figure 1.2. BWB-450 in NASA Langley Research Center's wind tunnel [3]

The X-48A was the initial proposed concept which was about 35 ft wide but was eventually canceled before production. The X-48B was a scaled version used for flight testing. It was scaled at 8.5% and had a wingspan of 20.4 feet and could reach up to 118 knots. The X-48C iteration was generally used to test low-speed stability as well as determine noise pollution caused by the plane. This version kept the dimensions of its predecessor but had a wider wingspan and a more developed flight control system [5].



Figure 1.3. X-48B [5]

All iterations of the X-48 were unmanned aerial vehicles (UAV) because it was an experimental research project. Ground control stations were implemented during flight testing. In application, many more monitors and sensors would need to be implemented to allow the pilot operating in the ground control station to be informed of external interferences [4].

In the X-48 study, John Fielding and Howard Smith discussed the possible advantages and challenges of the blended wing body concept.

Table 1.1. X-48 advantages and challenges report of the blended wing-body concept [2]

Factors	Advantages
Aerodynamics	Low wetted-area-to-volume ratio Form conducive to low interference drag
Structures	Efficient deep sections Favorable spanloading
Human Factors	High volumetric capacity Flexible cabin layout potential
Systems	Potential for highly integrated airframe/engine Ideal configuration for application of laminar flow technology Significant advantages from control configuring the vehicle
Economics	Particularly suitable for high-capacity applications Significant reduction in direct operating costs should be achievable
Factors	Challenges
Systems	Design of fully integrated and novel propulsion systems Design and integration of possible laminar-flow systems Control allocation
Operations	Span/wheel track limits Airport passenger handling
Manufacturing	Manufacture/assembly of very large components (probably composite)
Aerodynamics	Drag of thick airfoils and the achievement of laminar flow
Structures	Unconventional layout Noncircular cabin Aeroelasticity Major cutouts for exits
Human Factors	Embarkation time Passenger comfort and appeal No windows Emergency evacuation Pilot workload
Airworthiness Requirements	Safety Evacuation Stability augmentation
Conceptual Design	Tools Methods

Noise pollution comparison is another factor that has been investigated by many research papers. The BWB configuration has various noise reduction technologies to help reduce aircraft noise pollution. This includes the noise shielding shape, propulsion system, and landing gear technology that apply to the BWB configuration. It is projected that the noise reduction can be anywhere from 4 dB to 26.6 dB

when compared to modern large airliners such as the Boeing 787 or the Airbus A380 [6].

Structurally, the walls of the blended wing body's interior, specifically the cabin, are stouter than the usual tube and wing configuration. This is due to the geometry of the passenger cabin no longer being a cylinder. Conventional tube and wing airliners have a cylinder-shaped fuselage which means that the stress was distributed evenly. In contrast, the blended wing body has a non-circular, non-uniform fuselage creating several areas where stress is greater, specifically towards the edges of the aircraft. [2] To compensate for the edges that may increase the pressure within the cabin, a "multi-bubble shell" where multiple rounded cylinders would be used to reduce pressure at the edges. [7]

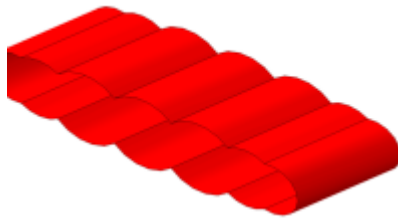


Figure 1.4. Multi-bubble shell cabin concept [7]

Engines in blended wing bodies are generally placed towards the aft of the fuselage to allow for boundary layer swallowing. This would in turn reduce drag and be beneficial for fuel consumption during flight. The placement of the engines also helped with the balance of the aircraft. Because a blended winged body has no large empennage, the engines were used to help balance the aircraft [2].

Yaw control in a blended wing body is a major concern due to the lack of horizontal stabilizers. Winglets were theorized to be the main form of yaw control in the past; however, studies have found that winglets alone are not enough to perform adequate yaw control. The inclined vertical stabilizer, as well as thrust vectoring from the engines, can help supplement the winglets for yaw control and compensate for the lack of a full empennage. [1]

Recently, more companies have decided to investigate BWB aircraft with Airbus designing the MAVERIC, a UAV demonstrator used to test the feasibility of BWB's unconventional configuration using the current state of the art technology. This aircraft is 2 meters long and 3.2 meters wide but is speculated to be able to reduce fuel consumption by up to 20%. Many people were initially skeptical about Airbus' statement about a BWB airliner; however, within 3 years of its announcement, Airbus managed to develop a scaled prototype to push the capabilities of future airliners.



Figure 1.5. Airbus MAVERIC [6]

Although the BWB configuration was first regarded as a novel concept, improvements in technology have reintroduced the concept as a feasible airliner design. With the growing prices of fuel and pollution, the need for more efficient aircraft, specifically large commercial airliners, is imperative.

1.1.3 Project Proposal

1.1.3.1 Mission Requirements

The mission for this aircraft is to carry up to 500 passengers on a transcontinental flight. Takeoff and landing will be done in a conventional airport while meeting FAR requirements. An approximated 6,000 nmi range is estimated for these intercontinental flights. The aircraft will climb and descend in flight and cruise at 35,000 feet before landing at their destination.

The aircraft will meet the following requirements:

- Must meet FAR 25 certification requirements
- Payload: 500 passengers, 125,000 lbs (55,699 kg) if each person weights approximately 200lbs and each passenger has 50 lbs of luggage
- 12 Crew Members and gear, 2,800 lbs (1,270 kg), assuming that each crew member weighs 200 lbs and there are 400 lbs of equipment
- Total payload weight: 127,800 lbs (56,969 kg)
- Range: 6,000+ nmi (11,112 km)
- Cruise velocity: 460+ kts or 0.80 Mach (852 km/h)
- Clean stall velocity/ land stall velocity: 143 kts (2 km/h)
- Cruise altitude: 35,000 ft (10,688 m)
- Takeoff field length: < 13,000 ft (3,962 m)
- Landing field length: < 8,500 ft (2,591 m)

1.1.3.2 Critical Mission Requirements

The passengers and their safety are the most critical mission requirements. The maximum load of the total amount of passengers and safety exits should all be accounted for in the BWB design. In addition, the cruise velocity and range are all key factors that determine the efficiency of the aircraft. Having a higher cruise velocity will allow the passengers to get to their destinations faster and a longer range will allow more options for flights. In addition, takeoff distance and rate of climb should also be accounted for because this unconventional configuration will need to be able to take off and depart in a conventional airport. To summarize, the following are key aspects to the success of the mission:

- Maximum Passenger Weight
- Passenger Safety
- Cruise Velocity
- Range
- Takeoff Distance
- Rate of Climb

1.1.3.3 Mission Profile

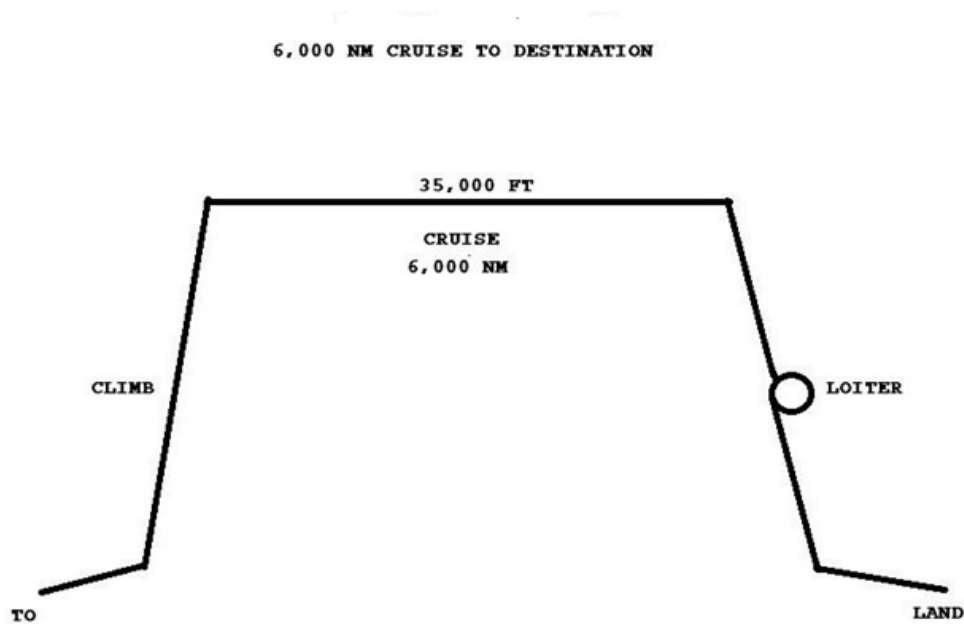


Figure 1.6. Mission profile for blended wing body airliner

1.1.4 Project Methodology

The preliminary sizing and design process are determined by researching previous aircraft designs that have similar mission objectives. In this case, research of large airliners carrying about 500 passengers will be first analyzed to determine a ballpark range for the preliminary design of the blended wing body aircraft. Using Roskam's Airplane Design textbook, equations to perform weight and performance sizing can be estimated early. Advanced equations and detailed graphs can be done using MATLAB. Configuration selection can be done using SolidWorks to determine a rough sketch of the preliminary design. In addition, RDS can also be used to model aircraft performance and provide rough weight estimates. XFLR5 will be used to analyze the aerodynamics, stability, and control of the aircraft. SolidWorks will also be used to perform weight and balance estimates. Roskam's class II methods will later be used when going into detail about certain aspects of the aircraft.

1.2 Comparative Study of Similar Aircraft

1.2.1 Mission Capabilities and Configuration Selection

Several similar aircraft will be studied to determine feasible dimensions for the BWB concept. The Boeing 747-400 is a 400-passenger airliner designed by Boeing. The 747-400 had a conventional tube and wing configuration with 4 turbofan jet engines. Similar aircraft that also held similar number of passengers were later produced to optimize efficiency or to compete with the standard Boeing 747-400 large airliner. The Airbus A340-600, a competing airliner that used the conventional tube and wing design with 4 turbofan jet engines, operated on newer engines as well as improved the cabin layout, making passengers feel more at ease. The Boeing 777-300 is another large airliner that used 2 turbofan jet engines because it is a relatively new aircraft when compared to the Boeing 747-400 and Airbus A340-600. More recent engines would be more efficient and powerful and as such, the Boeing 777-300 only relied on 2 turbofan jet engines.



Figure 1.7. Boeing 747-400 [8]



Figure 1.8. Airbus 340-600 [9]



Figure 1.9. Boeing 777-300 [10]

In addition to conventional tube-and-wing aircraft, several unconventional blended with body aircraft will also need to be compared for this design. The X-48B, the 8.5% scale of the blended wing body concept proposed by Boeing and NASA will be compared. This aircraft bears the most similarity to the conceptual design, having a similar mission profile as the 500-passenger blended wing body airliner. In addition, the B-2 Spirit designed by Northrop Grumman will also be analyzed due to the similarities of being a winged body. Despite being a strategic stealth bomber, the geometry and design of this winged body aircraft should have several similarities for a blended wing body airliner.



Figure 1.10. Northrop Grumman B-2 Spirit [1]

1.2.2. Comparison of Important Design Parameters

Table 1.2. Similar conventional aircraft study [12]

	Boeing 747-400	Airbus A340-600	Boeing 777-300
Configuration	Conventional TAW configuration with 4 turbofan jet engines	Conventional TAW configuration with 4 turbofan jet engines	Conventional TAW configuration with 2 turbofan jet engines
Payload Weight	Maximum Structural Payload: 165,082 lbs (74,880 kg) Max number of passengers: 416	Maximum payload weight: 148,150 lbs (67,200 kg) Max number of passengers: 380	Maximum payload weight: 157,145 lbs (71,280 kg) Max number of passengers: 398
Crew Member Weight	Crew Members: 12 Gear: 400 lbs Total Crew Weight: 2,800 lbs	Crew Members: 12 Gear: 400 lbs Total Crew Weight: 2,800 lbs	Crew Members: 12 Gear: 400 lbs Total Crew Weight: 2,800 lbs
Empty Weight	402,300 lbs (182,480 kg)	391,760 lbs (177,700 kg)	353,800 lbs (160,500 kg)
Gross Takeoff Weight	Maximum Take-off Weight: 800,000 lbs (362,870 kg)	Maximum Take-off Weight: 804,690 lbs (365,000 kg)	Maximum Take-off Weight: 666,000 lbs (299,370 kg)
Maximum Fuel Weight	203,520 Liters of Jet A-1 (360,742 lbs)	194,897 Liters of Jet A-1 (345,364 lbs)	171,176 Liters of Jet A-1 (303,411 lbs)
Wing Loading	137 lbf/ft ² (670 kg/m ²)	171 lbf/ft ² (835 kg/m ²)	143 lbf/ft ² (700 kg/m ²)
Thrust-to-Weight Ratio	0.270 (lbf/lbf) 4 GE CF6-80C2B5F Engines (Manufactured by General Electric)	0.298 (lbf/lbf) 4 Rolls-Royce Trent 500 (Manufactured by Rolls-Royce)	0.350 (lbf/lbf) 2 General Electric GE90 Engines (Manufactured by General Electric)
Engine Maximum Thrust	62,100 lbf (276.23 kN)	60,000 lbf (267 kN)	115,540 lbf (514 kN)

Thrust Specific Fuel Consumption	0.344 lbs/lbf/h (1.24 g/kN/s)	0.542 lbs/lbf/h (1.95 g/kN/s)	0.545 lbs/lbf/h (1.96 g/kN/s)
Engine Weight	9,854 lbs(4,470 kg)	11,000 lbs(4,990 kg)	19,316 lbs (8,762 kg)
Engine Length	168 in (4.27 m)	184.6 in (4.69 m)	286.67 in (7.281 m)
Engine Diameter	106 in (2.69 m)	97.4 in (2.47 m)	128 in (3.30 m)
Range	7,262 nmi (13,450) km at maximum take-off weight	7,500 nmi (13,890 km)	6,006 nmi (11,120 km)
Cruise Velocity	Mach 0.855 (495 kts) [917 km/h]	Mach 0.83 (475 kts) [880 km/h]	Mach 0.84 (488 kts) [904 km/h]
Cruise Altitude	35,000 ft (11,000 meters)	41,100 ft (12,525 m)	35,000 ft (11,000 m)
Maximum Velocity	Mach 0.92 (533 kts) [987 km/h]	Mach 0.86 (493 kts) [913 km/h]	Mach 0.89 (513 kts) [950 km/h]
Cruise Lift-to-drag Ratio	15.5	19.0	19.3
Landing Stall Velocity	160 kts (296 km/h)	156 kts (290 km/h)	149 kts (276 km/h)
Maximum Rate of Climb	3600 ft/min (1100 m/min)	2300 ft/min (700 m/min)	3,500 ft/min (1067 m/min)
Maximum Service Ceiling	45,069 ft (13,747 m)	41,000 ft (12,500 m)	43,100 ft (13,140 m)
Takeoff Distance	9,236 ft (2,815 m)	10,300 ft (3,140 m)	11,120 ft (3,380 m)
Landing Distance	6,250 ft (1,905 m)	6,200 ft (1,890 m)	6,050 ft (1844 m)
Wing Area	5,825 ft ² (541.2 m ²)	4,704.8 ft ² (437 m ²)	4,604.8 ft ² (427.80 m ²)
Wing Span	211.3 ft (64.4 m)	198 ft (60.40m)	200 ft (60.9 m)
Wing Chord	48 ft (14.63 m)	40 ft (12.20 m)	45.4 ft (13.85 m)
Wing Aspect Ratio	7.7	9.3	8.7
Fuselage Length	225.2 ft (68.63 m)	246 ft (74.96 m)	206 ft (62.74 m)
Fuselage Width	21.3 ft (6.50 m)	18.5 ft (5.64 m)	20 ft (6.20 m)

Table 1.3. Similar winged body aircraft study [2][12]

	Boeing X-48B	Northrop Grumman B-2 Spirit
Configuration	Blended Winged Body Design with 3 turbojet engines	Flying Wing Design with 4 turbofan jet engines
Payload Weight	N/A	Bomb weight capacity: 40,000 lbs (18,143 kg)
Crew Member Weight	N/A	Crew Members:12 Gear: 400 lbs Total Crew Weight: 2,800 lbs
Gross Takeoff Weight	523 lbs (227 kg)	335,600 lbs (152,633 kg)
Engine	3 JetCat USA P200 Gas Turbine Engine	4F118-GE-100 Engines
Engine Thrust	54 lbf (0.24 kN)	60,000 lbf (267 kN)
Engine Weight	5.53 lbs (2.51 kg)	19,000 lbs(1,500 kg)
Engine Diameter	5.12 in (0.130 m)	46.5 in (1.18 m)
Engine Length	N/A	101 in. (2.60 m)
Range	N/A (Endurance of 30 minutes)	6,000 nmi (11,100 km)
Cruise Velocity	118 kts [219 km/h]	486 kts 900 km/h
Cruise Altitude	9,843 ft (3,000 meters)	49,900 ft (15,200 m) (Service Ceiling)
Cruise Lift-to-drag Ratio	N/A	21.5 (at 35,000 ft)

Landing Distance	6,250 ft (1,905 m)	6,200 ft (1,890 m)
Wing Area	100.5 ft ²	4,704.8 ft ² (437 m ²)
Wing Span	20.4 ft	198 ft (60.40m)
Wing Chord	48 ft (14.63 m)	40 ft (12.20 m)
Wing Aspect Ratio	5.1	5.87

Although data from the B-2 bomber and the X-48B was retrieved, certain specific information like the wing loading cannot be found simply because of the confidentiality and the limited number of manufactured unconventional aircraft.

1.2.3. Discussion

The mission requirements are straightforward due to the aircraft being an airliner. The mission payload weight and range should be like those of the similar aircraft study. These requirements will most likely not change since they are a standard for airliners that fly transcontinental. The areas that would require the most research would be the performance and the wing design of this aircraft. A full-scale BWB aircraft has yet to be built and as such, these requirements are still tentative.

1.3. Conclusion

Studying both conventional and unconventional aircraft has helped outline basic mission requirements that a blended wing body should fulfill. In addition, the data from similar aircraft can be used to verify and validate calculations for weight sizing and performance estimates. The literature review provides the necessary background information to assist in the early development of the blended wing body design. All this information will be useful in beginning the preliminary design concept of the 500-passenger blended wing body concept.

2. Weight Sizing & Weight Sensitivities

2.1 Introduction

In this conceptual design for a blended wing body airliner, Roskam's textbook, *Airplane Design* [14], will be used as a reference to determine early estimates for weight sizing. This textbook has equations and tables to help determine fuel usage and a method for estimating empty weight. These manual calculations will be verified using the RDS software program to determine the validity of the results. RDS software program has a "quick initial sizing" tool that can help determine preliminary weight estimates.

2.2 Mission Weight Estimates

2.2.1 Database for Takeoff Weights and Empty Weights of Similar Airplanes

Table 2.1. Similar airplane weight database [12][13][14][15]

Aircraft	Takeoff Weight (lb)	Empty Weight (lb)	Airplane Type
Northrop B-2 Spirit	335,600	160,000	Stealth BWB Bomber
Northrop YB-49	194,000	88,400	Military BWB
Boeing 747-400	800,000	402,300	Conventional TAW
Boeing 747-400 ER	910,000	406,900	Conventional TAW
Boeing 777-300	666,000	353,800	Conventional TAW
Boeing 777-300 ER	775,000	366,940	Conventional TAW
Airbus A340-500	820,100	376,800	Conventional TAW
Airbus A340-600	804,690	319,760	Convectional TAW
Airbus A340-800	1,235,000	608,400	Conventional TAW

2.2.2 Determination of Regression Coefficients A and B

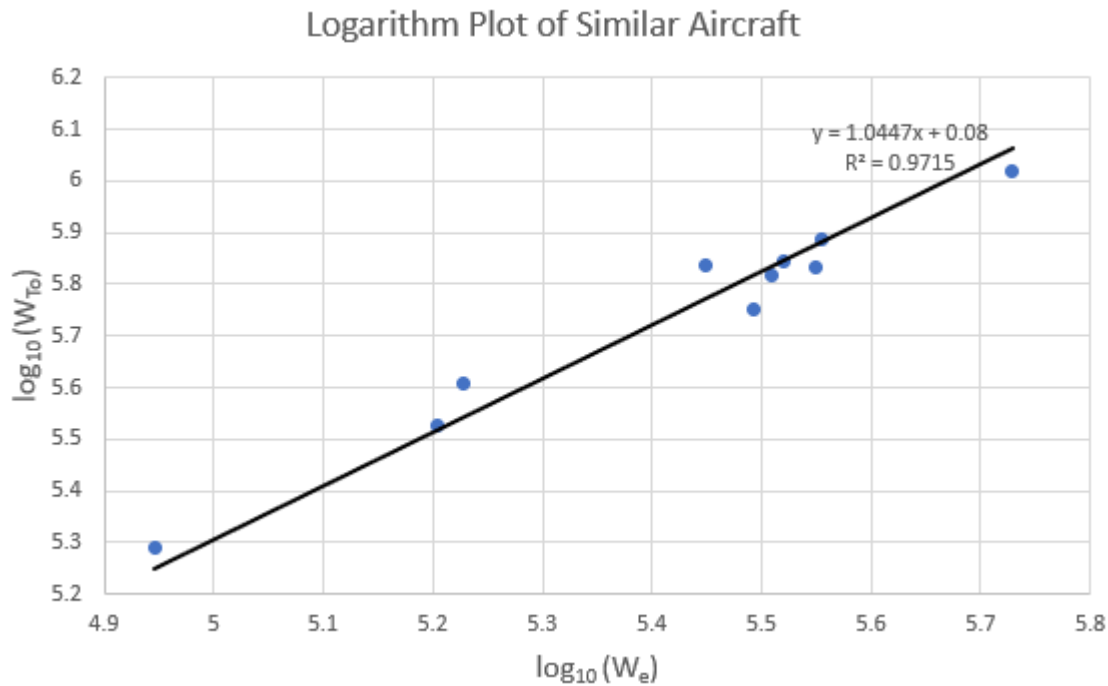


Figure 2.1. Trend line for determining regression coefficients A and B

From the regression plot, the constants of A and B can be assumed to be 0.080 and 0.1045 respectively. This was done using the similar aircraft data in Table 2.1 and plotting their log values onto a graph. A linear form trendline can be used to estimate regression coefficients. It should also be noted that when using similar aircraft data, all conventional tube and wing configured aircraft had their weights decreased to assume blended wing-body configuration. As stated before, “BWB had 15% lower takeoff weight, and 12% lower empty operating weight” [4].

2.2.3 Determination of Mission Weights

2.2.3.1 Manual Calculation of Mission Weights

The payload weight, empty weight, maximum takeoff weight, and fuel weight all play a significant portion in the performance of the aircraft. Assumptions will need to be made to obtain an initial weight estimate. These assumptions include the lift-to-drag ratio, Oswald efficiency, aspect ratio, and specific fuel consumption. The values listed below for the blended wing body aircraft were estimated from the literature review and Roskam’s textbook [14].

- $L/D = 22$
- $e = 0.85$
- $c = 0.65$
- $AR = 8.5$

The payload weight of this aircraft includes the 500 passengers that will be in the blended wing body aircraft. In addition, the aircraft must be able to hold 12 crew members as this is the minimum according to FAR 25 regulations. A good assumption for each passenger's weight is 250 lbs. Each passenger is assumed to weigh no more than 200 lbs on average and carry no more than 50 lb of luggage onto the aircraft. Airliner equipment and luggage such as food, beverages, and equipment will weigh in about 400 lbs.

Below is a total list of weights for the aircraft's payload.

- Passenger Capacity = 500
- Passenger Weight and luggage weight = $(500)(200) + (500)(50) = 125,000$ lbs
- Crew Capacity = 12
- Crew + Equipment = $(12+2)(200) = 2,800$ lbs
- Total Payload Weight: 127,800 lbs
- $W_p = 127,800$ lbs (58,000 kg)

The total payload weight of this airliner is approximated to be about 127,800 lbs.

The maximum takeoff weight used for this blended wing body is 950,000 lbs. A conventional tube and wing airliner that could carry 500 passengers would weigh in about 1,100,000 lbs. Using the literature review research, an expected 15% maximum takeoff weight reduction seems reasonable for this design.

From Figure 2.1, the regression coefficient A and B can be found as 0.080 and 1.045 respectively.

- $A = 0.080$
- $B = 1.045$
- $W_E = \text{invlog}_{10}\{(\log_{10}W_{TO} - A)/B\} = W_E = \text{invlog}_{10}(5.665)$
- $W_E = 440,306$ lbs (199,580 kg)
- Plugging in the guessed W_0 in this equation gives a W_E : $W_E = 462,457$ lbs (199,580 kg)

Table 2.2. Roskam's fuel fraction table [14]

Table 2.1 Suggested Fuel-Fractions For Several Mission Phases

Mission Phase No. (See Fig.2.1)	1	2	3	4	7	8
Airplane Type:	Engine Start, Warm-up	Taxi	Take-off	Climb	Descent	Landing Taxi, Shutdown
1. Homebuilt	0.998	0.998	0.998	0.995	0.995	0.995
2. Single Engine	0.995	0.997	0.998	0.992	0.993	0.993
3. Twin Engine	0.992	0.996	0.996	0.990	0.992	0.992
4. Agricultural	0.996	0.995	0.996	0.998	0.999	0.998
5. Business Jets	0.990	0.995	0.995	0.980	0.990	0.992
6. Regional TBP's	0.990	0.995	0.995	0.985	0.985	0.995
7. Transport Jets	0.990	0.990	0.995	0.980	0.990	0.992
8. Military Trainers	0.990	0.990	0.990	0.980	0.990	0.995
9. Fighters	0.990	0.990	0.990	0.96-0.90	0.990	0.995
10. Mil. Patrol, Bomb, Transport	0.990	0.990	0.995	0.980	0.990	0.992
11. Flying Boats, Amphibious, Float Airplanes	0.992	0.990	0.996	0.985	0.990	0.990
12. Supersonic Cruise	0.990	0.995	0.995	0.92-0.87	0.985	0.992

To determine the fuel used in the aircraft's flight, the fuel fraction chart provided in Roskam's textbook will be used. From the mission requirements of the blended wing body airliner, the cruise velocity of a 500-passenger airliner will be approximated to be 565 MPH (909 km/hr). The lift-to-drag ratio will be assumed to be 22 from the assumption earlier in the literature review. The range of the aircraft, 6,000 nmi, comes from the mission requirements which will allow the aircraft to perform intercontinental flights. The thrust fuel consumption is also approximated through a literature review.

Table 2.3. Fuel ratios of the 500 - BWB airliner

Stage	Description	W_i/W_{i-1}	
1	Engine Start and Warm-up	W_1/W_0	0.990
2	Taxi	W_2/W_1	0.990
3	Take-off	W_3/W_2	0.995
4	Climb	W_4/W_3	0.980
5	Cruise to Full Range	W_5/W_4	$\exp[-R \cdot c_j / V(L/D)] = 0.680$
6	Loiter	W_6/W_5	$\exp[-E \cdot c_j / (L/D)] = 0.985$
7	Descent	W_7/W_6	0.990
8	Landing	W_8/W_7	0.992

Assumptions:

- Cruise Velocity: $V = 460$ kts (852 km/hr)
- Endurance: $E = 0.5$ hours (approx.)
- Range: $R = 6,000$ nmi (11,112 km)
- L/D Ratio: 22
- Thrust Fuel Consumption $C_j = 0.65$ lbs/lbs/hr

$$\frac{W_F}{W_0} = 1.06 * \left(1 - \frac{W_8}{W_0}\right) \quad (2.1)$$

$$\frac{W_F}{W_0} = 1.06 * \left(1 - \frac{W_8}{W_7} \frac{W_7}{W_6} \frac{W_6}{W_5} \frac{W_5}{W_4} \frac{W_4}{W_3} \frac{W_3}{W_2} \frac{W_2}{W_1} \frac{W_1}{W_0}\right) = 1.06 * (1 - 0.65) = 0.393 \quad (2.2)$$

Plugging the values of the guessed maximum takeoff weight gives a W_F of 374,000 lbs (169,643 kg).

The weight distribution of the aircraft is as follows:

- $W_P = 127,800$ lbs
- $W_E = 440,300$ lbs
- $W_F = 374,000$ lbs

Adding these values will give a maximum weight takeoff of $W_{MTOW} = 938,800$ lbs. The initial estimate of the maximum gross takeoff weight was 950,000 lbs. The error between the initial weight estimate and the hand calculated weight estimate is 0.11%. This is within a reasonable margin of error and appropriate for the aircraft design.

2.2.3.2 Calculation of Mission Weights using RDS Program

The RDS program is not equipped to handle unconventional aircraft configurations, such as a blended wing body. One solution is to change some of the input values to reflect a blended wing body design. In the RDS quick sizing tool, the “bomber” W_E/W_0 option reflects the current blended winged body design due to the geometry. Other parameters in this quick initial sizing tool were retrieved from the literature review.

- Initial Takeoff Weight Guess = 950,000 lbs (453,592 kg)
- $W_{crew} = 2,800$ lbs (1,270 kg), $W_{cargo} = 25,000$ lbs (11,340 kg), $W_{passengers} = 100,000$ lbs (45,359 kg),
- $W_{misUL} = 0$
- Select Best $W_E/W_0 =$ Bomber
- Empty Weight Fudge Factor = 1.0
- Select Best $C_{fe} =$ Civil Transport
- $S_{WET} / S_{REF} = 2.8$
- Parasite Drag Factor = 1.0
- Wing Aspect Ratio = 8.5
- Oswald Span Efficiency Factor (e) = 0.85

- Wing Loading = 105 lbf/ft²
- Select Propulsion Type = Jet Propulsion
- T/W = 0.175, cruise thrust SFC (1/hr) = 0.65
- Number of Engines = 2
- Range = 6,000 nmi (11,112 km)
- Cruise Velocity = 460 kts (852 km/h)
- Cruise Altitude = 35,000 ft (10,668 m)

Table 2.4. RDS screenshot of weight distributions

MISSION SIZING OR RANGE									
Seg.	4	CRUISE :	412.7	kts at	30000.0	ft	RANGE =	6545.4	nmi
Seg.	5	LOITER :	324.9	kts at	10000.0	ft	ENDURANCE =	0.50	hrs
TOTAL RANGE =			6545.4		TOTAL LOITER TIME =			0.50	
FUEL WEIGHT =			400699.9		EMPTY WEIGHT =			424300.1	
USEFUL LOAD (-wf) =			125000.0		AIRCRAFT GROSS WEIGHT =			950000.0	
Speed Correction or Possible Error! Check Sizing printout for Error Messages If OK in Mission Segments, error was corrected during iterations									

2.3 Takeoff Weight Sensitivities

2.3.1 Manual Calculation of Takeoff Weight Sensitivities

Using Roskam’s equations [14], the sensitivities for takeoff weight can be calculated; however, several variables must be calculated first before obtaining takeoff weight sensitivities. Various variables are used in the following equations and will be referred to as “C”, “D”, and “F”. The regression coefficients that were approximated earlier will also be used in these calculations.

Maximum Fuel Fraction:

$$M_{FF} = \left(\frac{W_8}{W_7} \frac{W_7}{W_6} \frac{W_6}{W_5} \frac{W_5}{W_4} \frac{W_4}{W_3} \frac{W_3}{W_2} \frac{W_2}{W_1} \frac{W_1}{W_0} \right) = 0.61 \quad (2.3)$$

For W_{FRES} , or fuel reserve weight, 6% of the total fuel will be used as a rough estimate.

The value for M_{tfo} or trapped fuel will be approximated to be 0 in an ideal conceptual design.

In Roskam's textbook [14], the following constants are calculated using these equations:

- $A = 0.08$
- $B = 1.045$
- $C = 1 - (1 + M_{res}) * (1 - M_{FF}) - M_{tfo} = 1 - (1 + 0.06)(1 - 0.65) = 0.587$
- $D = W_p = 127,800 \text{ lbs}$
- $F = \frac{-BW_{T0}^2(1+M_{RES})M_{FF}}{(C*W_{T0}*(1-B)-D)} = \frac{-1.045*950000^2(1+0.06)*0.65}{(0.629*950000*(1-1.045)-127800)} = 4,250,000$

These constants can be used to calculate the following weight sensitivities:

$$\frac{\partial W_{T0}}{\partial W_p} = \frac{BW_{T0}}{D - C(1 - B)W_{T0}} = 6.493 \frac{lb}{lb} \quad (2.4)$$

$$\frac{\partial W_{T0}}{\partial W_E} = \frac{BW_{T0}}{\text{invlog}_{10}\{(\log_{10}W_{T0} - A)/B\}} = 2.255 \frac{lb}{lb} \quad (2.5)$$

$$\frac{\partial W_{T0}}{\partial R} = \frac{FC_j}{V * \left(\frac{L}{D}\right)} = 273.0 \frac{lb}{mi} \quad (2.6)$$

$$\frac{\partial W_{T0}}{\partial E} = \frac{FC_j}{\left(\frac{L}{D}\right)} = 125,568 \frac{lb}{hr} \quad (2.7)$$

Maximum Weight Sensitivity to specific fuel consumption and lift to drag ratio:

$$\frac{\partial W_{T0}}{\partial C_j} = \frac{F * R}{V * \left(\frac{L}{D}\right)} = 2,519,762 \frac{\frac{lbs}{\frac{lbs}{hours}}}{\frac{lbs}{hours}} \quad (2.8)$$

$$\frac{\partial W_{T0}}{\partial \frac{L}{D}} = -\frac{F * R * C_j}{V * \left(\frac{L}{D}\right)^2} = -74,448 \quad (2.9)$$

2.3.2 Trade Studies

Trade Studies were performed to determine how payload weight affects the range of the aircraft, both of which are critical mission parameters as stated in chapter 1. Breguet's range equation can be used to establish a trendline to determine the impact of payload weight on the aircraft's range.

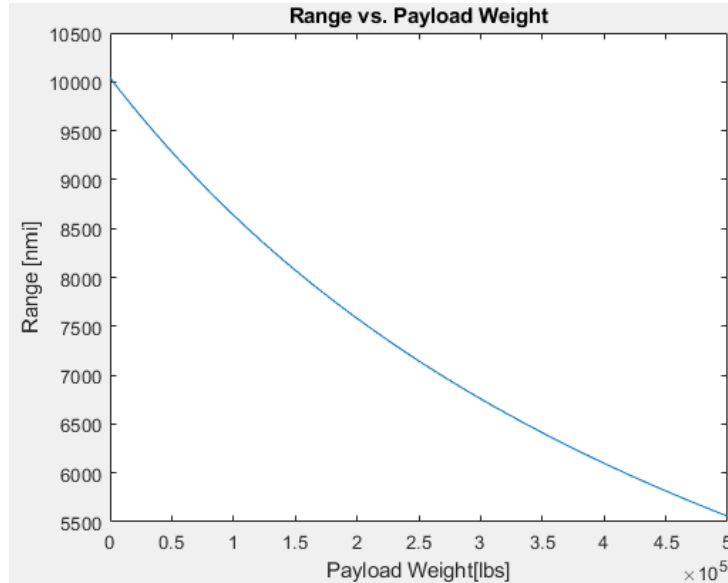


Figure 2.2. Range and payload trade study

2.4. Discussion

From the manual calculations, there is a reasonable margin of error between the estimated weight and the hand-calculated weight. The margin error is 0.4%. Many assumptions were made in the calculation of empty weight and fuel weight. Specific thrust fuel consumption and lift to drag ratio were key parameters that played a significant contribution to these calculations and were estimated to be 0.65 lbs/lbs/hr and 22 respectively. These values were approximated through a literature review. An L/D ratio of 22 is certainly above average than the conventional tube and wing configuration.

A takeoff weight sensitivity analysis was also conducted to determine how certain parameters would fluctuate regarding changes in key mission requirements. Specifically, maximum takeoff weight and its impact on the aircraft were studied. In addition, a trade study analysis using Breguet's range equation was used to determine a rough estimate of the performance of payload weight concerning the range. It should be noted that the graph does not consider changes in fuel weight. The graph indicates that this aircraft can carry a payload of 127,800 lbs and cover the 6,000 nmi mission range.

The takeoff weight sensitivity calculations can be summarized as follows:

- Takeoff Weight will increase 6.493 lbs for every additional pound increase in payload
- Takeoff Weight will increase 2.225 lbs for every additional pound increase in empty weight
- Takeoff Weight will increase by 270.3 lbs for every additional nautical mile increase in range.
- Takeoff Weight will increase 125,568 lbs for every additional hour increase in endurance.
- Takeoff weight will change by 2,519,762 lbs for every unit change in specific thrust fuel consumption
- Takeoff weight will decrease by 74,447 lbs for every unit change in the lift to drag ratio.

2.5. Conclusion

The calculations showed weight estimates and takeoff sensitivities based on Roskam's textbook [14]. Although this method is used for conventional tube and wing aircraft, the process should be similar for a blended winged body aircraft with changes for certain parameters to reflect the improved aerodynamics of a blended winged body. The initial weight estimates are within an agreeable margin of error and will be used for the rest of this project.

3. Performance Constraint Analysis

3.1 Introduction

Airliners, throughout history, always had specific performance constraints and regulations since failure will result in the deaths of hundreds of people. Many of these requirements are derived from conventional tube and wing aircraft. The blended wing body aircraft must be able to satisfy these requirements to be able to be used as an airliner for practical usage.

- Payload: 500 passengers and their luggage, 125,000 lbs if each person weights approximately 200 lbs and 50 lbs luggage
- 12 Crew members, gear (200 lbs x 12 + 400 lbs = 2,800 lbs of crew)
- Range: 6,000+ nmi (11,120 km)
- Cruise velocity: 460+ kts (0.80 Mach)
- Cruise altitude: 35,000 ft (10,668 m)
- Takeoff field length: < 13,000 ft (3,962 m)
- Landing field length: < 8,500 ft (2,591 m)

3.2. Manual Calculation of Performance Constraints

3.2.1 Stall Speed

The stall speed of the aircraft is when there is a loss of lift which is caused by boundary layer separation from the surface of the airfoil. This is very important for an airliner as a stalled aircraft will have the potential to end many lives. Many of the manual calculations will be referenced from Roskam's Aircraft Design Part 1 [14]. For transport jets, the C_{LMAX} will range anywhere from 1.2 to 1.8. The C_{LMAXTO} ranges from 1.6 – 2.2 The C_{LMAXL} will range from 1.8 – 2.8. The wing loading will be approximated to be 105 lb/ft². By plugging the values into the below equation, the approximate stall speed can be calculated.

$$V_s = \sqrt{\frac{2 * \frac{W}{S}}{\rho C_{LMAX}}} = \sqrt{\frac{2 * 105}{0.002378 * 1.5}} = 242 \frac{ft}{s} = 143 \text{ kts} \quad (3.1)$$

By assuming that the wing loading is 105 lb/ft², the airliner must fly at least 143 kts to break the stall speed. A C_{LMAX} of 1.5 was used because of the known fact that a blended winged body has great aerodynamic efficiency when compared to the conventional tube and wing configuration.

3.2.2 Takeoff Distance

The takeoff distance will determine the necessary distance needed for the aircraft to safely ascend from the airport. This is important for determining how long the runway should be and how large the airports should be for that specific aircraft. This blended wing body must follow FAR 25 regulations as it is a large airliner.

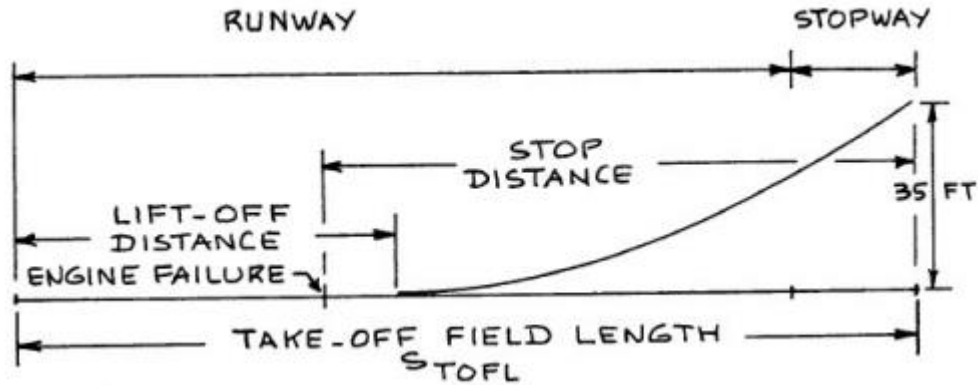


Figure 3.1. FAR 25 take-off distances [14]

The equation below can determine the thrust to weight ratio necessary that meets FAR 25 requirements.

$$S_{TOFL} = \frac{37.5 \frac{W}{S_{TO}}}{\sigma C_{LMAXTO} \frac{T}{W_{TO}}} \rightarrow \frac{T}{W_{TO}} = \frac{37.5 \frac{W}{S_{TO}}}{\sigma C_{LMAXTO} S_{TOFL}} \quad (3.2)$$

Using this equation, an assumed 13,000 ft of takeoff distance from the mission requirements will be used to calculate the thrust to weight ratio at takeoff.

$$\frac{T}{W_{TO}} = \frac{37.5 \frac{W}{S_{TO}}}{\sigma C_{LMAXTO} S_{TOFL}} = \frac{37.5 * 105}{0.786 * 1.9 * 13000} = 0.200 \quad (3.3)$$

In this example, σ is approximated to be 0.786 at 8,000 ft which was obtained from Roskam's textbook [14], and C_{LMAXTO} is approximated as 1.9. This was determined by using the highest value for the C_{LMAXTO} range. S_{TOFL} will be approximated as 13,000 ft from the mission requirements. W/S_{TO} has been assumed to be 105 lb/ft². Using these variables, T/W_{TO} is approximately 0.200.

3.2.3 Landing Distance

In contrast to takeoff distance, landing distance is necessary to determine the safety of the arrival of the aircraft. Generally, the landing distance is shorter, and a runway distance certified for takeoff is suitable for landing.

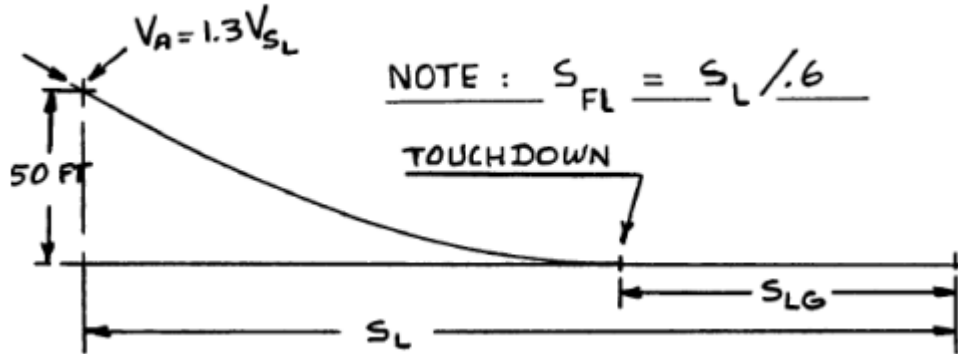


Figure 3.2. FAR 25 landing distances [14]

To determine the wing loading scenario when landing, the landing distance must adhere to FAR 25 requirements. As stated in the mission requirement, the landing distance within FAR 25 requirements should be 8,500 feet. This can be used to determine the approach velocity.

$$S_{FL} = 0.3V_A^2 \rightarrow V_A = \sqrt{\frac{S_{FL}}{.3}} = \sqrt{\frac{8500}{.3}} = 168 \text{ kts} \quad (3.4)$$

The approach velocity can be used to determine the velocity that will be used when landing with this equation.

$$V_A = 1.3 V_{SL} \rightarrow V_{SL} = \frac{V_A}{1.3} = \frac{168}{1.3} = 129 \text{ kts} \quad (3.5)$$

Using this next equation, the wing loading at landing can be determined.

$$\frac{W}{S_L} = \frac{(V_{SL} * 1.688)^2 \rho}{2} * C_{LMAXL} = \frac{(129 * 1.688)^2 * 0.002378}{2} * 2.1 = 118.4 \frac{lb}{ft^2} \quad (3.6)$$

To determine a minimum wing area size, the takeoff wing loading, and the maximum takeoff weight estimate can be used.

- $W/S_{TO} = 105 \text{ lbf/ft}^2$
- $W_0 = 950,000 \text{ lbf}$
- $S = 950,000/105 \sim 9,050 \text{ ft}^2$

With first order calculations, the minimum wing area size needs to be more than 9,050 ft². Similarly, the propulsion sizing can be calculated by using the takeoff thrust to weight ratio to determine the necessary force needed for flight.

- $T/W_{TO} = 0.200$
- $W_0 = 950,000 \text{ lbf}$
- $T = 0.200(950,000) \sim 190,000 \text{ lbf}$

3.2.4 Drag Polar Estimation

To determine an estimation for drag, an estimated wetted area must be used. Roskam's textbook contains several coefficients between parasitic area and wetted area. These can be used and put into an equation to determine an estimate of the parasitic area. The parasitic area value can be used to determine the parasitic drag that the blended wing body will have. Below listed are the correlation coefficient used to determine the parasitic area and wetted area for a jet transport aircraft.

- $a = -2.522$
- $b = 1$
- $c = 0.0199$
- $d = 0.7531$

$$\log_{10}(S_{wet}) = c + d * \log_{10} W_{TO} \quad (3.7)$$

$$\log_{10}(S_{wet}) = 0.0199 + 0.7531 * \log_{10} (950,000) \rightarrow S_{wet} = 33,200 \text{ ft}^2$$

$$\log_{10}(f) = a + b * \log_{10} S_{wet} \quad (3.8)$$

$$\log_{10}(f) = -2.522 + 1 * \log_{10} (33,200) \rightarrow f = 100 \text{ ft}^2$$

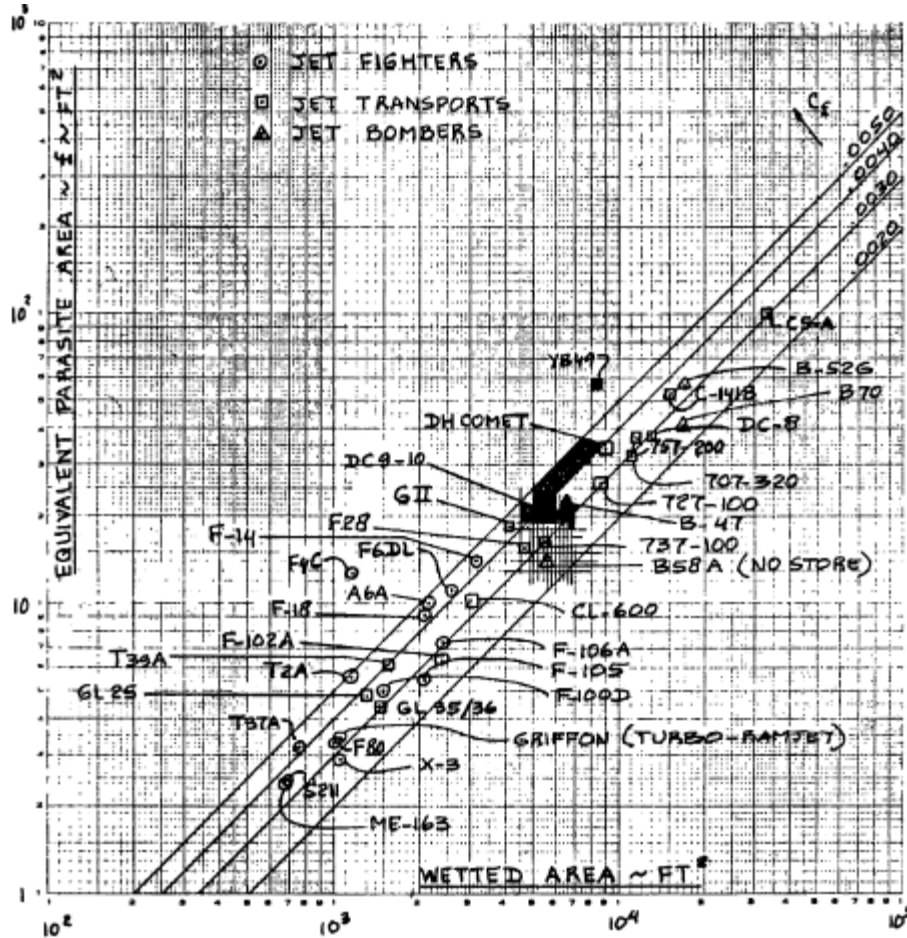


Figure 3.3. Equivalent parasitic area and wetted area in Roskam's textbook [14]

Using the value previously calculated for the estimated wetted area for the blended wing body design, an equivalent parasitic area of 100 ft² can be verified from the graph above. This in turn will give a $c_r = 100/33,200 = 0.0030$. The wing area for this aircraft will be estimated to be about 14,000 ft². A parasitic drag coefficient and the total drag coefficient can then be calculated from Roskam's equations.

$$C_{D_0} = \frac{f}{S} = \frac{100}{14000} = 0.007 \quad (3.9)$$

Using an Oswald efficiency of 0.85 and an AR of 8.5, a drag polar graph can be roughly estimated using the equation below.

$$C_D = C_{D_0} + \frac{C_L^2}{\pi e AR} \rightarrow C_D = 0.007 + \frac{C_L^2}{\pi(0.85)(8.5)} \quad (3.10)$$

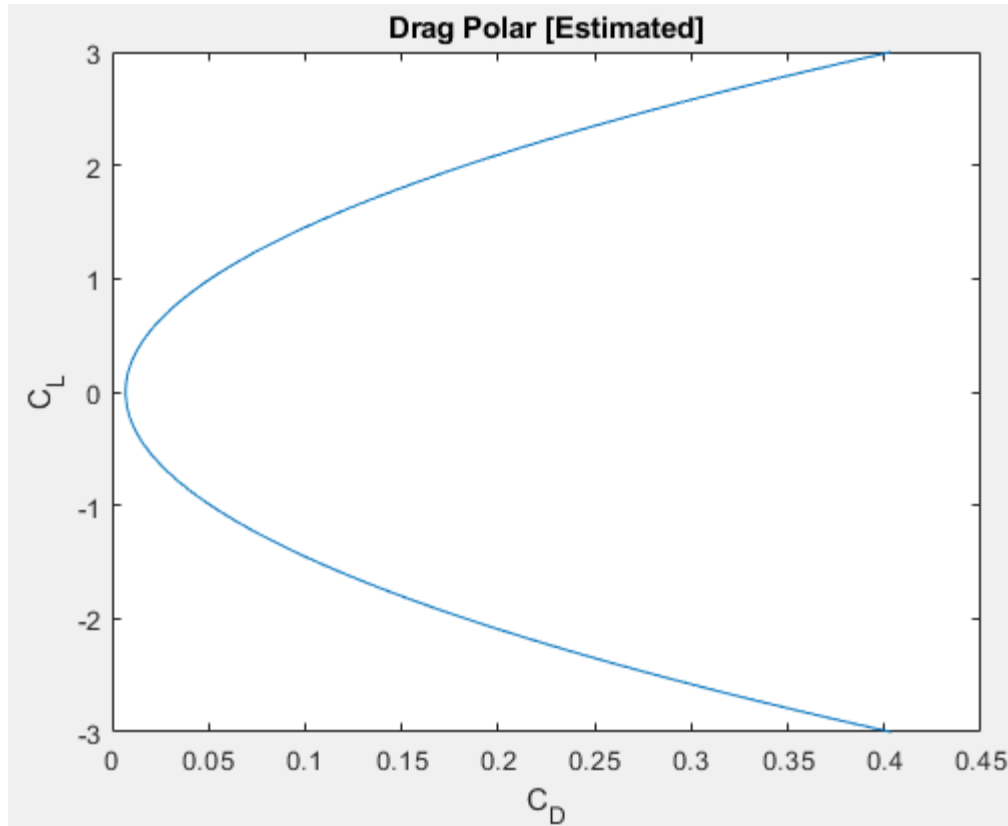


Figure 3.4. Estimated drag polar

Referring to Roskam's table for C_D increments of adding flaps and putting the gear down. A configuration table can be created.

Table 3.1. Roskam's estimate for C_D increments [14]

Table 3.6 First Estimates for ΔC_{D_0} and 'e'		
With Flaps and Gear Down		
Configuration	ΔC_{D_0}	e
Clean	0	0.80 - 0.85
Take-off flaps	0.010 - 0.020	0.75 - 0.80
Landing Flaps	0.055 - 0.075	0.70 - 0.75
Landing Gear	0.015 - 0.025	no effect

Table 3.2. Drag polar data for various configurations

Configuration	C_{D0}	AR	e	C_{Di}	C_{LMAX}
Clean	0.007	8.5	0.85	$0.044C_L^2$	1.5
Take-off Flaps, Gear up	0.017	8.5	0.80	$0.047C_L^2$	1.9
Take-off Flaps, Gear down	0.032	8.5	0.80	$0.047C_L^2$	1.9
Landing Flaps, Gear Up	0.067	8.5	0.75	$0.050C_L^2$	2.1
Landing Flaps, Gear Down	0.084	8.5	0.75	$0.050C_L^2$	2.1

3.2.5 Climb Sizing Estimation for FAR 25 Regulations

Using Roskam's equations, a T/W_{TO} can be designed for various configurations for different takeoff and landing methods. Table 3.1 will be used to determine L/D ratio values for these equations.

FAR 25.111 (OEI):

- Clean
- $1.2 V_{STO}$
- 50°F Temperature Effect
- $CGR > 0.012$
- $C_{LMAXTO} = 1.9$

$$C_L = \frac{C_{LMAXTO}}{1.44} \rightarrow C_L = 1.32 \quad (3.11)$$

$$C_D = 0.007 + 0.044C_L^2 \rightarrow C_D = 0.0837 \rightarrow \frac{L}{D} = 15.77 \quad (3.12)$$

$$\frac{T}{W_{TO}} = 2 * \frac{\left(\frac{1}{L/D} + 0.012 \right)}{0.8} = 0.19 \quad (3.13)$$

FAR 25.121 (OEI) (gear down, takeoff flaps):

- Gear Down, takeoff flaps
- Between V_{LOF} and V_2
- 50°F Temperature Effect
- $CGR > 0.00$
- $C_{LMAXTO} = 1.9$

V_{LOF}:

$$C_{LLOF} = \frac{C_{LMAXTO}}{1.1^2} \rightarrow C_L = 1.57 \quad (3.14)$$

$$C_D = 0.032 + 0.047C_L^2 \rightarrow C_{LMAX} = 0.15 \rightarrow \frac{L}{D} = 10.6 \quad (3.15)$$

$$\frac{T}{W_{T0}} = 2 * \frac{1}{\frac{L}{D}} = 0.19 \quad (3.16)$$

V₂:

$$C_L = \frac{C_{LMAXTO}}{1.44} \rightarrow C_L = 1.32 \quad (3.17)$$

$$C_D = 0.032 + 0.047C_L^2 \rightarrow C_D = 0.11 \rightarrow \frac{L}{D} = 12.0 \quad (3.18)$$

$$\frac{T}{W_{T0}} = 2 * \frac{1}{\frac{L}{D}} = 0.17 \quad (3.19)$$

Since V_{LOF} is more critical, the (T/W)_{T0} = 0.19/0.8 = 0.24

FAR 25.121 (OEI) (gear up, takeoff flaps):

- Gear Up, takeoff flaps
- 1.2 V_{STO}
- 50°F Temperature Effect
- CGR > 0.024
- C_{LMAXTO} = 1.9

$$C_L = \frac{C_{LMAXTO}}{1.44} \rightarrow C_L = 1.32 \quad (3.20)$$

$$C_D = 0.017 + 0.047C_L^2 \rightarrow C_D = 0.098 \rightarrow \frac{L}{D} = 13.40 \quad (3.21)$$

$$\frac{T}{W_{T0}} = 2 * \frac{\left(\frac{1}{\frac{L}{D}} + 0.024\right)}{0.8} = 0.246 \quad (3.22)$$

FAR 25.121 (OEI) (gear up, flaps):

- Gear up
- 1.2 V_{STO}
- 50°F Temperature Effect
- $CGR > 0.012$
- $C_{LMAXTO} = 1.7$

$$C_L = \frac{C_{LMAXTO}}{1.25^2} \rightarrow C_L = 1.01 \quad (3.23)$$

$$C_D = 0.017 + 0.044C_L^2 \rightarrow C_D = 0.063 \rightarrow \frac{L}{D} = 16.30 \quad (3.24)$$

$$\frac{T}{W_{T0}} = 2 * \frac{\left(\frac{1}{\frac{L}{D}} + 0.012\right)}{0.8} = 0.18 \quad (3.25)$$

FAR 25.119 (AEO) (balked landing):

- Landing Flaps, gear down
- 1.3 V_{SL}
- 50°F Temperature Effect
- $CGR > 0.032$
- $C_{LMAXL} = 2.1$

$$C_L = \frac{C_{LMAXL}}{1.3^2} \rightarrow C_L = 1.24 \quad (3.26)$$

$$C_D = 0.084 + 0.050C_L^2 \rightarrow C_D = 0.160 \rightarrow \frac{L}{D} = 7.75 \quad (3.27)$$

$$\frac{T}{W_L} = \frac{\left(\frac{1}{\frac{L}{D}} + 0.032\right)}{0.8} = 0.20 \quad (3.28)$$

FAR 25.121 (OEI) (balked landing):

- Landing Flaps, gear up
- 1.5 V_{SA}
- 50°F Temperature Effect
- CGR > 0.021
- C_{LMAXA} = 2.0

$$C_L = \frac{C_{LMAXA}}{1.5^2} \rightarrow C_L = 0.89 \quad (3.29)$$

$$C_D = 0.067 + 0.050C_L^2 \rightarrow C_D = 0.107 \rightarrow \frac{L}{D} = 8.35 \quad (3.30)$$

$$\frac{T}{W_L} = 2 * \frac{\left(\frac{1}{\frac{L}{D}} + 0.021\right)}{0.8} \left(\frac{W_L}{W_{T0}}\right) = 2 * \frac{\left(\frac{1}{8.49} + 0.021\right)}{0.8} \left(\frac{597,835}{950,000}\right) = 0.22 \quad (3.31)$$

The most critical requirement would be the one engine inoperative with takeoff flaps and the gear up during takeoff. The T/W_{T0} is about 0.25. Doing the math will give a needed thrust of about:

- T = 0.246(950,000) ~ 233,700 lbf

This means that the twin-engine configuration must be able to produce around 233,700 lbf. The propulsion engine selected is the GE-90, which can produce 115,540 lbf. Using a twin-engine propulsion system, this provides the blended wing body with a thrust force of about 231,080 lbf. There is about a 1.1% error between the thrust that can be provided and the necessary thrust to meet the most critical requirement.

3.3. Calculation of Performance Constraints with RDS Software

Table 3.3. RDS inputs of performance module

1 TAKEOFF		2 LANDING	
Wi/Wo or Wi	1.	Wi/Wo or Wi	1.
Altitude	0.0	Altitude	0.0
Obstacle Height	50.	Obstacle Height	50.
Rolling Coeff	0.03	Braking Coeff	0.3
CL-ground *	0.2	CL-ground *	0.3
CLmax-T.O. *	1.9	CLmax-Landing *	2.1
Time to Rotate	1.	Braking Delay	1.
GEAR Cd *	0.00294	Gear Cd *	0.04294
Thrust Setting	100.	Braking Cd *	0.0
Braking Coeff	0.3	T-rollout/fwd	0.0
Braking Cd *	0.0	Vtd/Vstall	1.1
#DropExtStores	0.0	#DropExtStores	0.0
(n/a)	0.0	(n/a)	0.0
(n/a)	0.0	(n/a)	0.0
AlternatePolar#	0.0	AlternatePolar#	0.0

Table 3.4. Performance analysis summary

 Data Column #1 TAKEOFF

TAKEOFF SUMMARY - MAX PERFORMANCE, ALL ENGINES OPERATING
 GROUND ROLL DISTANCE = 5863.9 ft
 ROTATE DISTANCE = 237.83
 TOTAL GROUND ROLL DISTANCE = 6101.8
 TRANSITION DISTANCE = 974.38
 CLIMB DISTANCE = 3.268
 TOTAL TAKEOFF DISTANCE = 7079.4
 FAR-25 ALL-ENGINES TAKEOFF DIST = 8141.3

TAKEOFF SUMMARY - BALANCED FIELD LENGTH
 DECISION SPEED = 146.42 kts
 DECISION POINT = 6363.1 ft
 TAKEOFF SPEED = 152.41 kts
 BALANCED FIELD LENGTH = 10156 ft

 Data Column #2 LANDING

 APPROACH DISTANCE = 725.97
 FLARE DISTANCE = 456.63
 TOTAL IN-FLIGHT DISTANCE = 1182.6
 FREE GROUND ROLL DIST = 226.22
 BRAKING DISTANCE = 2760.1
 TOTAL GROUND ROLL DISTANCE = 2986.3
 NO-FLARE LANDING DISTANCE = 3940.4
 TOTAL LANDING DISTANCE = 4168.9
 FAR PART 25 LANDING DISTANCE = 6948.1

 Data Column #1 TAKEOFF

AIRCRAFT OPERATING WEIGHT (wi) = 950000
 AIRCRAFT OPERATING WEIGHT RATIO (wi/w0) = 1.
 TAKEOFF THRUST-TO-WEIGHT RATIO (T/W) = 0.1989
 THRUST (START OF TAKEOFF) = 189000
 TAKEOFF WINGLOADING (W/S) = 105.56
 Vstall = 128.1 kts
 Vtakeoff (max perf) = 140.91 kts
 MAX PERFORMANCE TAKEOFF - GROUND ROLL
 Analysis Data for segment with ending Velocity = 140.91 kts
 Thrust =171272 Rolling/Braking Force =26685.5
 T/W =0.18029
 CL = 0.2 CD0 = 0.0066 K = 0.024
 Lift = 60482 Cd = 0.0075 Drag = 2276.7
 Incremental distance = 5863.9 Total distance = 5863.9
 Incremental time = 49.346 Total time = 49.346
 MAX PERFORMANCE TAKEOFF - ROTATE
 Average Rotate Velocity = 140.91 kts
 Incremental distance = 237.83 Total distance = 6101.8
 Incremental time = 1. Total time = 50.346
 MAX PERFORMANCE TAKEOFF - TRANSITION
 Average Transition Velocity 147.32 kts
 Incremental distance = 974.38 Total distance = 7076.2
 Incremental time = 3.919 Total time = 54.264
 MAX PERFORMANCE TAKEOFF - CLIMB
 Average Climb Velocity = 153.72 kts
 Obstacle Height = 50. ft
 Incremental distance = 3.268 Total distance = 7079.4
 Incremental time = 0.0126 Total time = 54.277
 Climb Angle = 5.836 (deg)

 TAKEOFF SUMMARY - MAX PERFORMANCE, ALL ENGINES OPERATING
 GROUND ROLL DISTANCE = 5863.9 ft
 ROTATE DISTANCE = 237.83
 TOTAL GROUND ROLL DISTANCE = 6101.8
 TRANSITION DISTANCE = 974.38
 CLIMB DISTANCE = 3.268
 TOTAL TAKEOFF DISTANCE = 7079.4
 FAR-25 ALL-ENGINES TAKEOFF DIST = 8141.3

 TAKEOFF SUMMARY - BALANCED FIELD LENGTH
 DECISION SPEED = 146.42 kts
 DECISION POINT = 6363.1 ft
 TAKEOFF SPEED = 152.41 kts
 BALANCED FIELD LENGTH = 10156 ft

Figure 3.5. RDS takeoff analysis part 1

```

BALANCED FIELD LENGTH CALCULATION DETAILS
GROUND ROLL: START TO DECISION SPEED (Vdecision=      146.31 kts)
Thrust =170592      Rolling/Braking Force =26541.
  T/W =0.17957
  CL = 0.2          CD0 = 0.0066          K = 0.024
  Lift = 65300      Cd = 0.0075          Drag = 2458.1
  Incremental distance = 6363.1    Total distance = 6363.1
  Incremental time = 51.498    Total time = 51.498
GROUND ROLL: DECISION SPEED TO OEI TAKEOFF (Vtakeoff=      152.41 kts)
Thrust =81095.5      Rolling/Braking Force =24344.8
Effective T/W (net of stopped engine drag) =0.08323
  CL = 0.2          CD0 = 0.0065          K = 0.024
  Lift = 138506     Cd = 0.0075          Drag = 5198.7
  Incremental distance = 1547.1    Total distance = 7910.2
  Incremental time = 6.131    Total time = 57.629
ROTATE & TRANSITION WITH OEI (Vtransition=      159.34 kts)
Thrust =79706.5
Effective T/W (net of stopped engine drag) =0.0818
  CL = 1.228        CD0 = 0.0065          K = 0.0433
  Lift = 951345     Cd = 0.0718          Drag = 55597
  Incremental distance = 562.45    Total distance = 8472.7
  Incremental time = 2.134    Total time = 59.763
CLIMB WITH OEI      (Vclimb=      166.26 kts)
                   Climb Angle = 1.56 (deg)
Thrust =79706.5
Effective T/W (net of stopped engine drag) =0.0818
  CL = 1.128        CD0 = 0.0065          K = 0.0433
  Lift = 951345     Cd = 0.0616          Drag = 51922
  Incremental distance = 1683.2    Total distance = 10156
  Incremental time = 5.994    Total time = 65.757
ABORTED STOP FROM DECISION SPEED
  Stopping distance = 3409.8    Stopping time = 27.577

```

Figure 3.6. RDS takeoff analysis part 2

Data Column #2 LANDING

```

AIRCRAFT OPERATING WEIGHT (Wi) = 950000
AIRCRAFT OPERATING WEIGHT RATIO (Wi/W0) = 1.
ROLLOUT THRUST-TO-WEIGHT RATIO (T/W) = 0.0
LANDING WINGLOADING (W/S) = 105.56
Vstall = 121.85 kts
Vtouchdown = 134.03 kts
Vapproach = 140.13 kts
Approach Angle = -3. (deg)
APPROACH DISTANCE = 725.97
FLARE DISTANCE = 456.63
TOTAL IN-FLIGHT DISTANCE = 1182.6
FREE GROUND ROLL DIST = 226.22
BRAKING DISTANCE = 2760.1
TOTAL GROUND ROLL DISTANCE = 2986.3
NO-FLARE LANDING DISTANCE = 3940.4
TOTAL LANDING DISTANCE = 4168.9
FAR PART 25 LANDING DISTANCE = 6948.1

```

LANDING CALCULATION DETAILS:

APPROACH & FLARE

```

Vapproach = 140.13 kts
Obstacle Ht = 50. ft
Thrust =85568.4
Effective T/W (net of stopped engine drag) =0.0
CL = 1.89                      CD0 = 0.0466                      K = 0.0503
Lift = 1130738                      Cd = 0.2261                      Drag = 135284
Incremental distance = 1182.6                      Total distance = 1182.6
Incremental time = 5.043                      Total time = 5.043

```

TOUCHDOWN BRAKING DELAY

```

Vtd = 134.03 kts
Incremental distance = 226.22                      Total distance = 1408.8
Incremental time = 1.                      Total time = 6.043

```

GROUND ROLL

```

V-average = 67.017 kts
Thrust =83120.4                      Rolling/Braking Force =272684
Effective T/W (net of stopped engine drag) =0.0
CL = 0.3                      CD0 = 0.0466                      K = 0.024
Lift = 41054                      Cd = 0.0487                      Drag = 6668.5
Incremental distance = 2760.1                      Total distance = 4168.9
Incremental time = 24.402                      Total time = 30.445

```

----- RDS-Student Version win10.3 -----

Figure 3.7. RDS landing analysis

3.4. Discussion

Table 3.5. Wing and propulsion sizing comparison analysis with RDS

PARAMETER	MISSION REQUIREMENT	CALCULATED VALUE	RDS VALUE
Stall Speed	143 kts (264 km/h)	143 kts (264 km/h)	156.45 kts (290 km/h)
CLMAX	N/A	1.7	1.7
Landing Distance	8,500 ft (2,591 m)	8,500 ft (2,591 m)	8,511 ft (2,594 m)
CLMAXL	N/A	2.1	2.1
Takeoff Distance	13,000 ft (3,962 m)	13,000 ft (3,962 m)	6,128 ft (1,868 m)
CLMAXTO	N/A	1.9	1.9
Balanced Field Length	15,000 ft (4,572 m)	15,000 ft (4,572 m)	5,461 ft (1,665 m)
Cruise Speed	491+ kt1 (909 km/h)	504 kts (933 km/h)	600 kts (1,111 km/h)

From Table 3.1, many of the RDS calculations when applied to a blended wing body have a significant difference when compared to the manually calculated values. The RDS software was originally designed for a conventional tube and wing aircraft and therefore some of the equations used to calculate the performance constraints can be inaccurate. Because of this inconsistency, using values from RDS may not be reliable.

From this chapter, preliminary sizing of the wing and propulsion were calculated. The blended wing body should have a reference wing area of greater than 9,050 ft². According to the literature review [2], the blended wing body's reference wing is approximately 60% greater than the conventional tube and wing-body. According to the initial estimate, the blended wing body's reference wing area is 14,500 ft²; however, in chapter 6, the wing area was determined to be 16,284 ft². The engines must be able to produce a minimum of 83,125 lbf because of the assumption of a twin-engine aircraft; however, in a one-engine inoperative condition, the engines must be able to produce 116,850 lbf each. The GE90 can provide 115,000 lbf which is within 1.1% error. This should be sufficient for a rough estimate for the propulsion sizing.

3.5. Conclusion

The values calculated from the RDS software are accurate for a tube and wing aircraft configuration; however, for a blended wing body, the calculations seemed to be inconsistent with calculated values. Certain values like approach velocity, stall velocity, and thrust-to-weight ratio at takeoff were relatively close to calculated values. Other values, such as field length and C_L seemed to be a bit too small for a larger airliner.

From the manual calculations, the preliminary reference wing area and propulsion sizing were estimated. A preliminary reference wing area of 14,500 ft² and a twin-engine that can provide 233,700 lbf were approximated for this design. In chapter 6, the geometry of the blended wing body was finalized to be 16,284 ft². In addition, a first order drag polar estimation of the blended wing body was made from Roskam's method and empirical data. Most future design requirements will be determined from manually calculated values and might require some readjustments for accuracy improvements.

4. Configuration Selection

4.1 Introduction

The configuration of an aircraft is vital to the aircraft's performance and its ability to perform its mission effectively. The configuration selection includes the design of the wings, the fuselage size, geometry, and placement, the empennage design, the propulsion system, and the landing gear. Generally, a configuration selection can be well described using an isometric view of the aircraft to provide a clear understanding of the proposed aircraft design. This chapter will discuss similar aircraft mission profile and their configuration, the design of the various parts of the blended wing body, and a visual of the CAD model of the aircraft.

4.2 Discussion of Items which have Major Impact on Design

4.2.1. List of Items with Major Impact on the Design

- Cabin Sizing
 - Maximum Passenger Weight
 - Allotted Cabin Space for the Fuselage
- Aerodynamic Performance
 - Lift-to-Drag Ratio
 - C_{LMAX} at various conditions
 - Wing Loading
 - Thrust to Weight Ratio
- Weight & Stability
 - Location of Aircraft Components
 - Yaw Control
 - Landing Gear Size and Placement
 - Fuel Storage

4.2.2 Discussion

Three major design items that can heavily affect the design of the aircraft are cabin sizing, necessary aerodynamic performance, and weight & stability. Because the design aircraft is a blended wing body, the cabin inside the fuselage will play a critical component due to the passenger's safety and the pressure concentration in that location.

4.3. Comparative Study of Airplanes with Similar Mission Performance

4.3.1 Recap of Similar Aircraft Studies

Table 4.1. Similar conventional aircraft study [12]

	Boeing 747-400	Airbus A340-600	Boeing 777-300
Configuration	Conventional TAW configuration with 4 turbofan jet engines	Conventional TAW configuration with 4 turbofan jet engines	Conventional TAW configuration with 2 turbofan jet engines
Payload Weight	Maximum Structural Payload: 165,082 lbs (74,880 kg) Max number of passengers: 416	Maximum payload weight: 148,150 lbs (67,200 kg) Max number of passengers: 380	Maximum payload weight: 157,145 lbs (71,280 kg) Max number of passengers: 398
Crew Member Weight	Crew Members: 12 Gear: 400 lbs Total Crew Weight: 2,800 lbs	Crew Members: 12 Gear: 400 lbs Total Crew Weight: 2,800 lbs	Crew Members: 12 Gear: 400 lbs Total Crew Weight: 2,800 lbs
Empty Weight	402,300 lbs (182,480 kg)	391,760 lbs (177,700 kg)	353,800 lbs (160,500 kg)
Gross Takeoff Weight	Maximum Take-off Weight: 800,000 lbs (362,870 kg)	Maximum Take-off Weight: 804,690 lbs (365,000 kg)	Maximum Take-off Weight: 666,000 lbs (299,370 kg)
Maximum Fuel Weight	203,520 Liters of Jet A-1 (360,742 lbs)	194,897 Liters of Jet A-1 (345,364 lbs)	171,176 Liters of Jet A-1 (303,411 lbs)
Wing Loading	137 lbf/ft ² (670 kg/m ²)	171 lbf/ft ² (835 kg/m ²)	143 lbf/ft ² (700 kg/m ²)
Thrust-to-Weight Ratio	0.270 (lbf/lbf) 4 GE CF6-80C2B5F Engines (Manufactured	0.298 (lbf/lbf) 4 Rolls-Royce Trent 500 (Manufactured	0.350 (lbf/lbf) 2 General Electric GE90 Engines

	by General Electric)	by Rolls-Royce)	(Manufactured by General Electric)
Engine Maximum Thrust	62,100 lbf (276.23 kN)	60,000 lbf (267 kN)	115,540 lbf (514 kN)
Thrust Specific Fuel Consumption	0.344 lbs/lbf/h (1.24 g/kN/s)	0.542 lbs/lbf/h (1.95 g/kN/s)	0.545 lbs/lbf/h (1.96 g/kN/s)
Engine Weight	9,854 lbs(4,470 kg)	11,000 lbs(4,990 kg)	19,316 lbs (8,762 kg)
Engine Length	168 in (4.27 m)	184.6 in (4.69 m)	286.67 in (7.281 m)
Engine Diameter	106 in (2.69 m)	97.4 in (2.47 m)	128 in (3.30 m)
Range	7,262 nmi (13,450) km at maximum take-off weight	7,500 nmi (13,890 km)	6,006 nmi (11,120 km)
Cruise Velocity	Mach 0.855 (495 kts) [917 km/h]	Mach 0.83 (475 kts) [880 km/h]	Mach 0.84 (488 kts) [904 km/h]
Cruise Altitude	35,000 ft (11,000 meters)	41,100 ft (12,525 m)	35,000 ft (11,000 m)
Maximum Velocity	Mach 0.92 (533 kts) [987 km/h]	Mach 0.86 (493 kts) [913 km/h]	Mach 0.89 (513 kts) [950 km/h]
Cruise Lift-to-drag Ratio	15.5	19.0	19.3
Landing Stall Velocity	160 kts (296 km/h)	156 kts (290 km/h)	149 kts (276 km/h)
Maximum Rate of Climb	3600 ft/min (1100 m/min)	2300 ft/min (700 m/min)	3,500 ft/min (1067m/min)
Maximum Service Ceiling	45,069 ft (13,747 m)	41,000 ft (12,500 m)	43,100 ft (13,140 m)
Takeoff Distance	9,236 ft (2,815 m)	10,300 ft (3,140 m)	11,120 ft (3,380 m)
Landing Distance	6,250 ft (1,905 m)	6,200 ft (1,890 m)	6,050 ft (1844 m)
Wing Area	5,825 ft ² (541.2 m ²)	4,704.8 ft ² (437 m ²)	4,604.8 ft ² (427.80 m ²)
Wing Span	211.3 ft (64.4 m)	198 ft (60.40m)	200 ft (60.9 m)

Wing Chord	48 ft (14.63 m)	40 ft (12.20 m)	45.4 ft (13.85 m)
Wing Aspect Ratio	7.7	9.3	8.7
Fuselage Length	225.2 ft (68.63 m)	246 ft (74.96 m)	206 ft (62.74 m)
Fuselage Width	21.3 ft (6.50 m)	18.5 ft (5.64 m)	20 ft (6.20 m)

Table 4.2. Similar winged body aircraft study [2][12]

	Boeing X-48B	Northrop Grumman B-2 Spirit
Configuration	Blended Winged Body Design with 3 turbojet engines	Flying Wing Design with 4 turbofan jet engines
Payload Weight	N/A	Bomb weight capacity: 40,000 lbs (18,143 kg)
Crew Member Weight	N/A	Crew Members: 12 Gear: 400 lbs Total Crew Weight: 2,800lbs
Gross Takeoff Weight	523 lbs (227 kg)	335,600 lbs (152,633 kg)
Engine	3 JetCat USA P200 Gas Turbine Engine	4F118-GE-100 Engines
Engine Thrust	54 lbf (0.24 kN)	60,000 lbf (267 kN)
Engine Weight	5.53 lbs (2.51 kg)	19,000 lbs (1,500 kg)
Engine Diameter	5.12 in (0.130 m)	46.5 in (1.18 m)

Engine Length	N/A	101 in. (2.60 m)
Range	N/A (Endurance of 30 minutes)	6,000 nmi (11,100 km)
Cruise Velocity	118 kts [219 km/h]	486 kts 900 km/h
Cruise Altitude	9,843 ft (3,000 meters)	49,900 ft (15,200 m) (Service Ceiling)
Cruise Lift-to-drag Ratio	N/A	21.5 (at 35,000 ft)
Landing Distance	6,250 ft (1,905 m)	6,200 ft (1,890 m)
Wing Area	100.5 ft ²	4,704.8 ft ² (437 m ²)
Wing Span	20.4 ft	198 ft (60.40m)
Wing Chord	48 ft (14.63 m)	40 ft (12.20 m)
Wing Aspect Ratio	5.1	5.87

4.3.2. Configuration Comparison of Similar Airplanes



Figure 4.1. Boeing 747-400 [8]



Figure 4.2. Airbus 340-600 [9]



Figure 4.3. Boeing 777-300 [10]



Figure 4.4. X-48B [5]



Figure 4.5. Airbus MAVERIC [6]



Figure 4.6. Northrop Grumman B-2 Spirit [11]

4.3.3. Discussion

Most of the airliners use a low-wing configuration for various reasons. A low-wing design makes it easy for aircraft to retract their landing gear as well as have a favorable ground effect. This favorable ground effect will help allow the aircraft to take off earlier and provide stability when landing. Conventional airliners have one large vertical stabilizer for yaw control and to help provide a balance of the weight in the aircraft. The X-48B does not have any yaw control mechanisms and relies on winglets. The Airbus MAVERIC has a twin vertical stabilizer to help provide yaw control. Engines are placed on the back for a blended wing body design to help provide weight distribution due to the lack of one large vertical stabilizer. Many of these aircraft designs have the conventional retractable tricycle gear and will be used for this aircraft.

4.4 Selection of Propulsion System

4.4.1 Selection of the Propulsion System Type

A turbofan jet engine will be used as the main propulsion for the blended wing body aircraft. Turbofan jet engines have high thrust and are fuel-efficient, making them the most suitable for airliners. A turbofan jet engine is a variation of a gas turbine engine. Air is captured by the inlet and part of it is distributed to the engine's core where it is mixed with fuel and combusts onto the nozzle. Another portion of the air goes into a fan and bypasses the engine. Essentially, the engine produces thrust from both the fan and the core. This type of engine seems to be most suitable for the blended wing body airliner mission profile.

4.4.2 Selection of the Number of Engines

A twin-engine configuration will be used for this design. In case of a one-engine inoperative failure, the aircraft should still be able to take off and land safely, assuming the engines have enough thrust. The symmetrical design also provides a more even weight distribution throughout the aircraft. In addition, differential thrusting could potentially be used to help perform yaw maneuvers due to the lack of a full empennage in a blended wing body aircraft. The GE-90 specification that will be used is listed below.

Table 4.3. Engine specifications [17]

	Units
Number of Engines	2
Maximum Thrust (sea level)	127,900 lbf (569 kN)
Maximum Sustained Power	115,300 lbf (513 kN)
Specific Fuel Consumption	0.547 lb/lbf/h (15.4 g/kN/s)
Bypass Ratio	8.4-9
Weight	17,400 lb (7,893 kg)
Length	286.9 in (7.29 m)
Diameter	123 in. (3.1m)
Height	155.6 in (3.95 m)

4.5 Configuration Selection

4.5.1 Overall Configuration

Most airliners have a conventional configuration with most being symmetrical and having backward swept low-wings, retractable landing gear, and a horizontal and vertical stabilizer. The high-bypass ratio on their engines is used to achieve transonic speeds and allow the aircraft to have an efficient specific fuel consumption. Large wings are generally used because of the large payload from all the passengers while also having a sizable range. Concerning the mission requirements of the blended wing body airliner, the wings of this aircraft will contain a backward swept low-wing configuration that will be blended into the fuselage. Two high-bypass ratio turbofan engines will be placed towards the aft of the fuselage for more even weight distribution. A twin-tail vertical stabilizer configuration will be used for the empennage. Retractable landing gear will be used during landing and takeoff. The fuselage will be blended into the aircraft's wing.

4.5.2 Wing Configuration

A low-wing conventional backward sweep will be used for this design. The low wing design will provide easy retraction for the landing gear and optimize efficiency for transonic cruise flight. This configuration will also create favorable ground effects, decreasing takeoff distance for the aircraft. A low-wing design will also provide structural stability for the aircraft during landing. All of these are important considerations for a large airliner.

4.5.3 Empennage Configuration

The empennage will only have vertical stabilizers to control and provide pitch & yaw stability. In a paper [17], inclined twin vertical stabilizers for blended wing bodies were found to be a feasible option for directional stability. These vertical stabilizers will provide yaw-roll coupling moments and control systems will need to be designed with that in mind. The volume coefficient for the vertical stabilizers in the case study revealed that it could be as low as 0.02417. This means that these vertical stabilizers will not produce that much drag due to their smaller size, but still provide the aircraft with directional stability it lacks.

4.5.4 Integration of the Propulsion System

Twin turbofan jet engines will be integrated into the aircraft. They will be installed toward the aft of the aircraft for weight distribution. In a CFD research study [16], 2 engines aft of the aircraft provided the highest lift-to-drag ratio, making this the most efficient placement of the propulsion system. Subsonic inlets and nozzles will be implemented because the aircraft's cruise speed is assumed to be under sonic speeds.

4.5.5 Landing Gear Disposition

The aircraft will use a tricycle retractable landing gear. This will allow easy and convenient takeoff and landing procedures while minimizing drag during the cruise. This gear is inherently stable due to the three contact points of the landing gear, providing passenger safety during landing and takeoff. In addition, the landing gear will allow the pilot to see well when taxiing.

4.5.6 Configuration Proposal

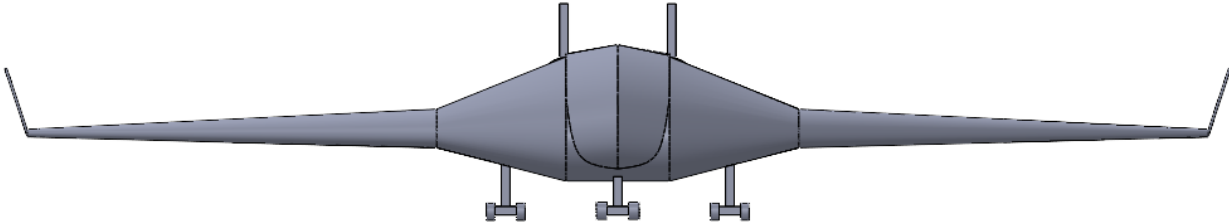


Figure 4.7. Proposed configuration front view

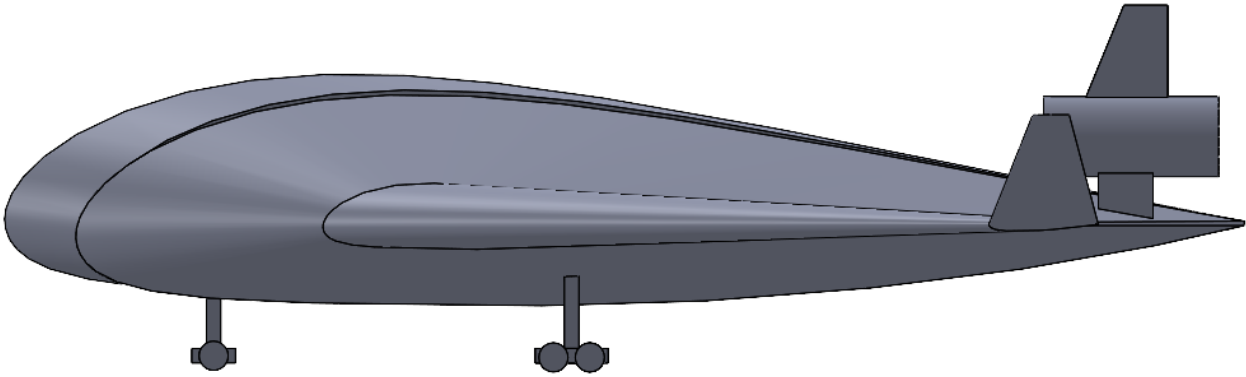


Figure 4.8. Proposed configuration side view

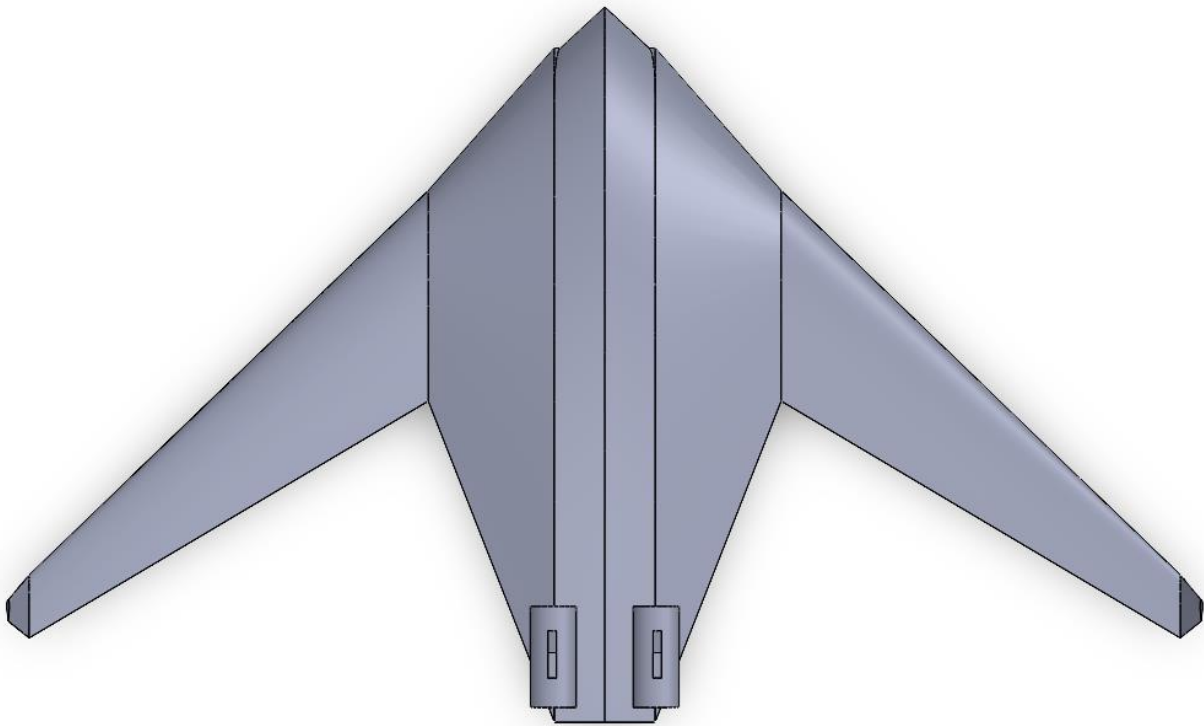


Figure 4.9. Proposed configuration top view

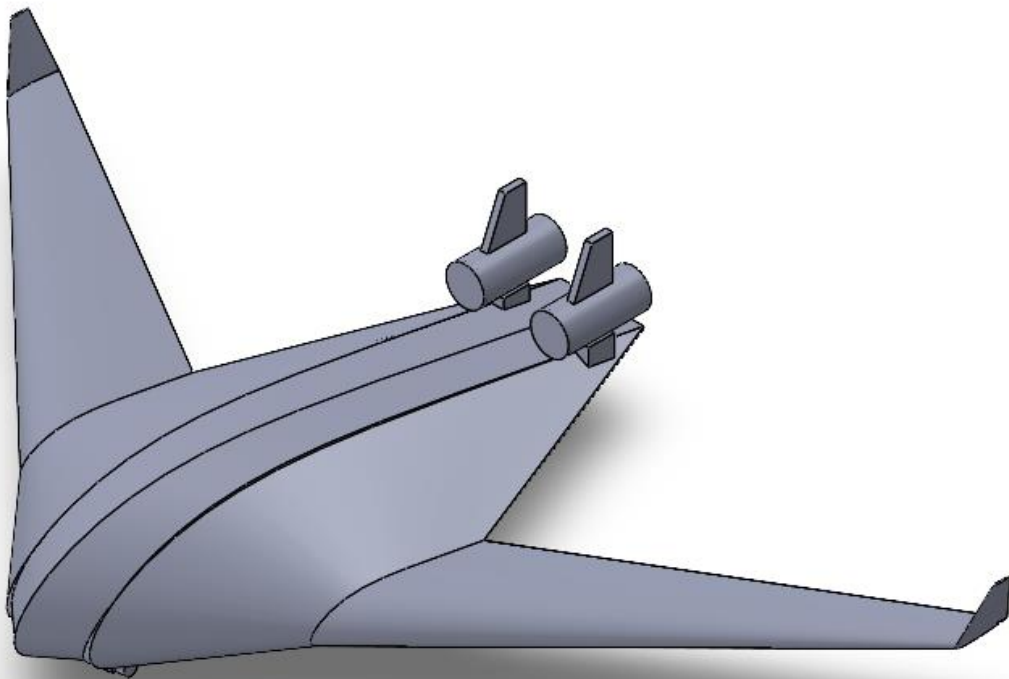


Figure 4.10. Proposed configuration isometric view

5. Fuselage Design

5.1 Introduction

The fuselage is the main body of the aircraft and contains the cargo, passenger, fuel, and crew members. In a blended wing body, the wings and the fuselage are blended so the fuselage includes the wing. This airliner will have a conventional, two-crew-glass cockpit in the front of the engine to allow the pilot to have a good view of the environment. The pilot needs to be able to see the wings as well as what is ahead of the aircraft. The crew's sleeping quarters are adjacent to the cockpit room. Passengers will be seated in the cabin and carry-on luggage will be stored in a compartment underneath the chair seat. Most of the seats are towards the front of the aircraft as the blended winged body design allows the most space towards the front. The cabin will be in an "auditorium" room where many passengers will be seated next to each other. Restrooms and galleys will be located throughout the airliner. Emergency doors will be on the stairs next to the restroom. Ideally, the cabins would be pressurized and have a "bubble" shape to reduce the stress in the areas with edges. Business-class and economy class seats will be on the main floor and more business class seats can be found on the second floor of the aircraft. Emergency exits will be located upstairs on top of the wings and under the cabin if the aircraft happens to fail.

5.2 Layout Design of the Cockpit

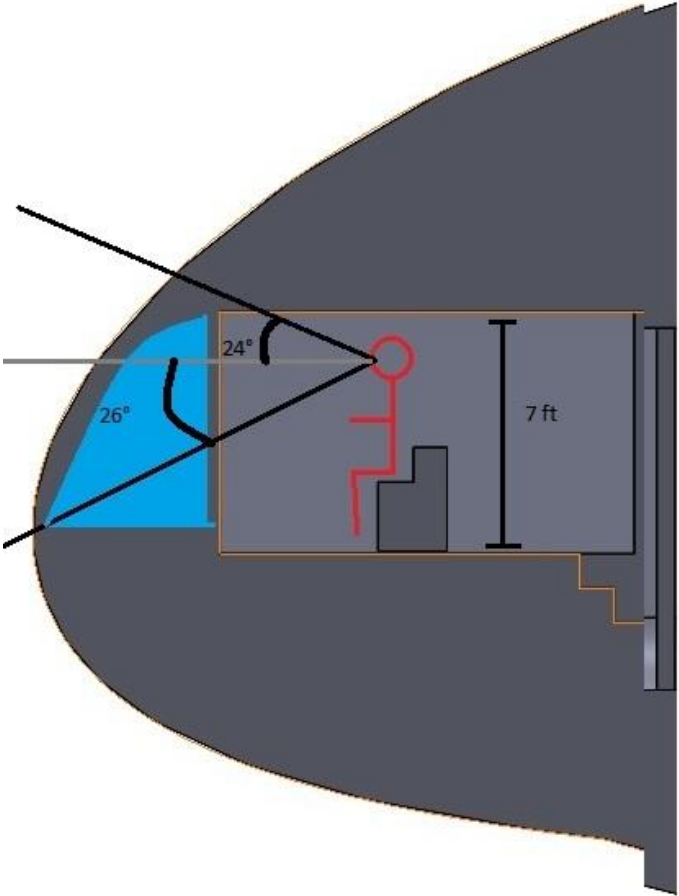


Figure 5.1. Side cockpit view for the blended wing body design

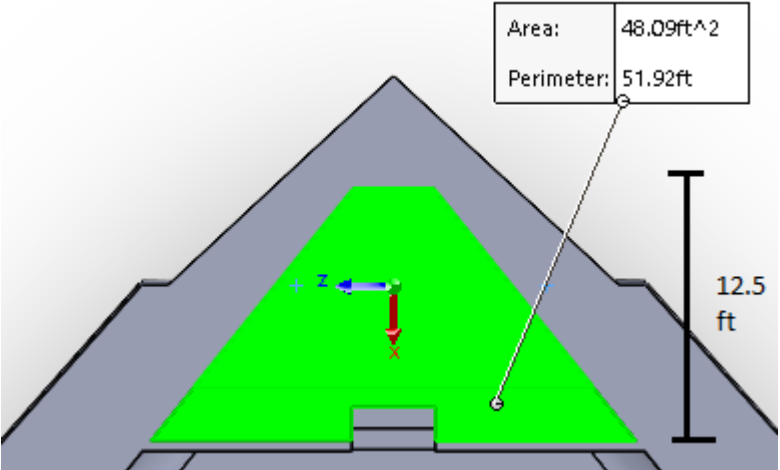


Figure 5.2. Top cockpit view for the blended wing body design

5.3 Layout Design of the Fuselage

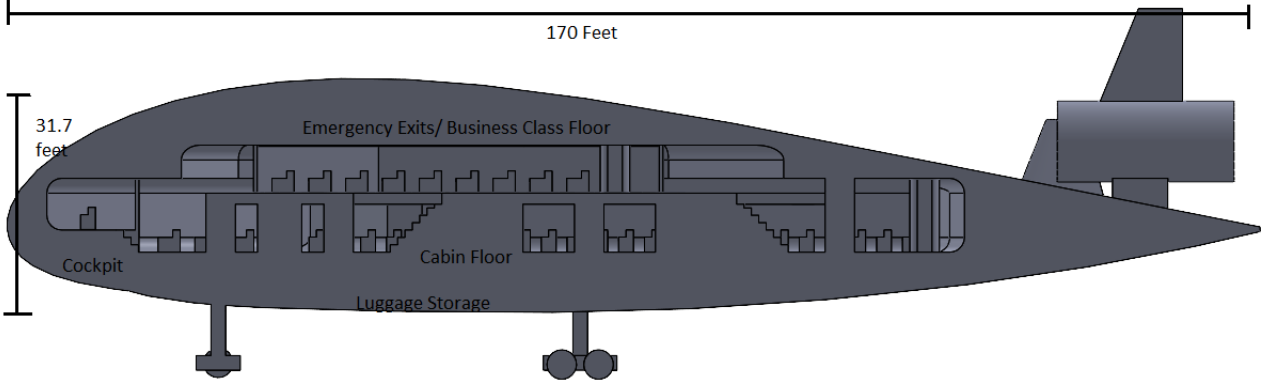


Figure 5.3. Side fuselage view for the blended wing body design

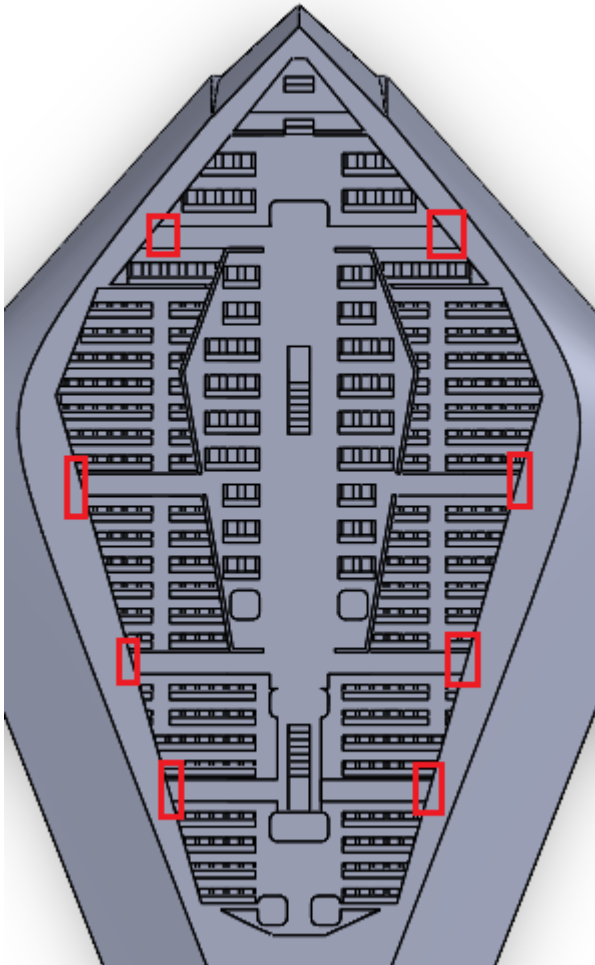


Figure 5.4. Top fuselage view for the emergency exits

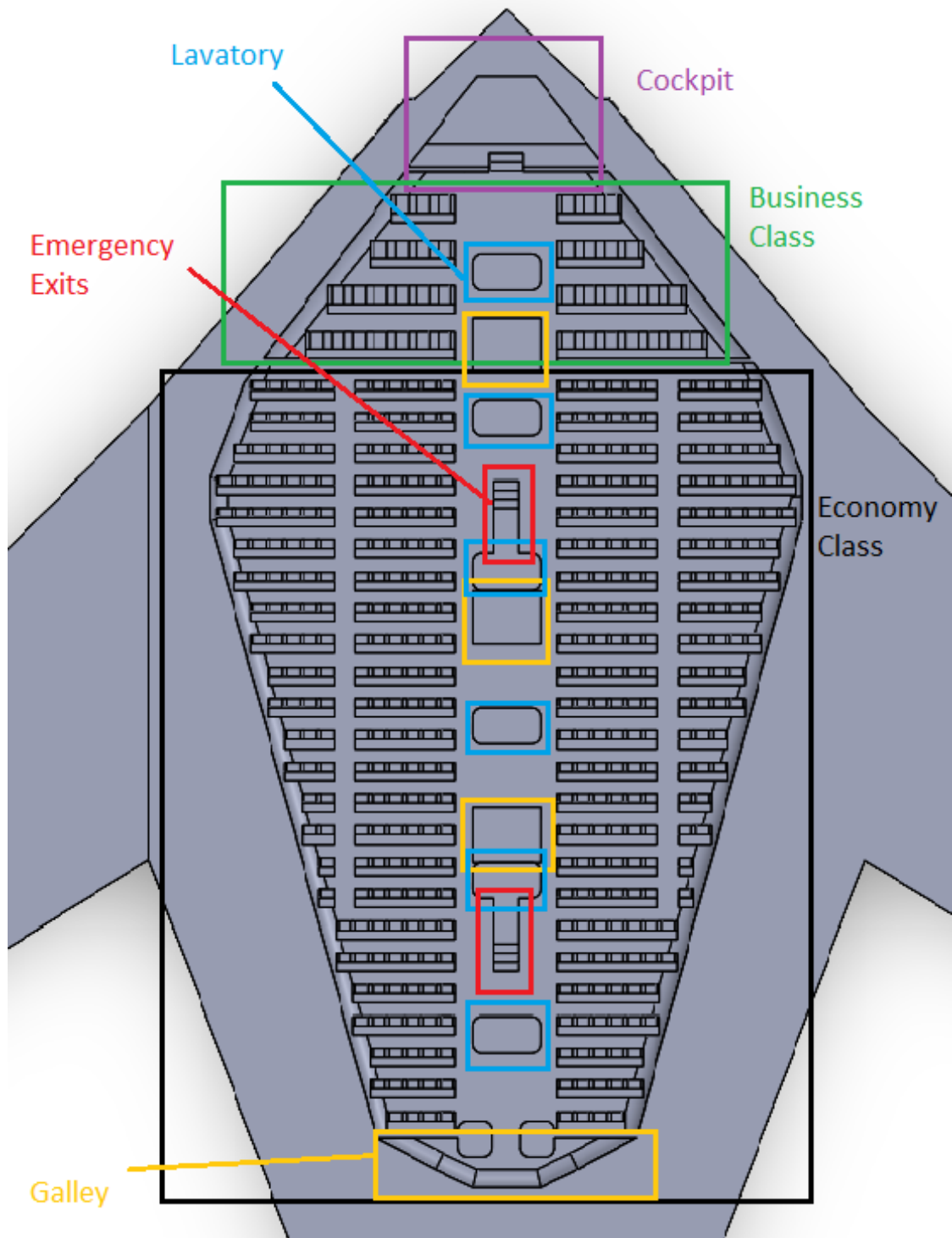


Figure 5.5. Top fuselage view for the blended wing body design

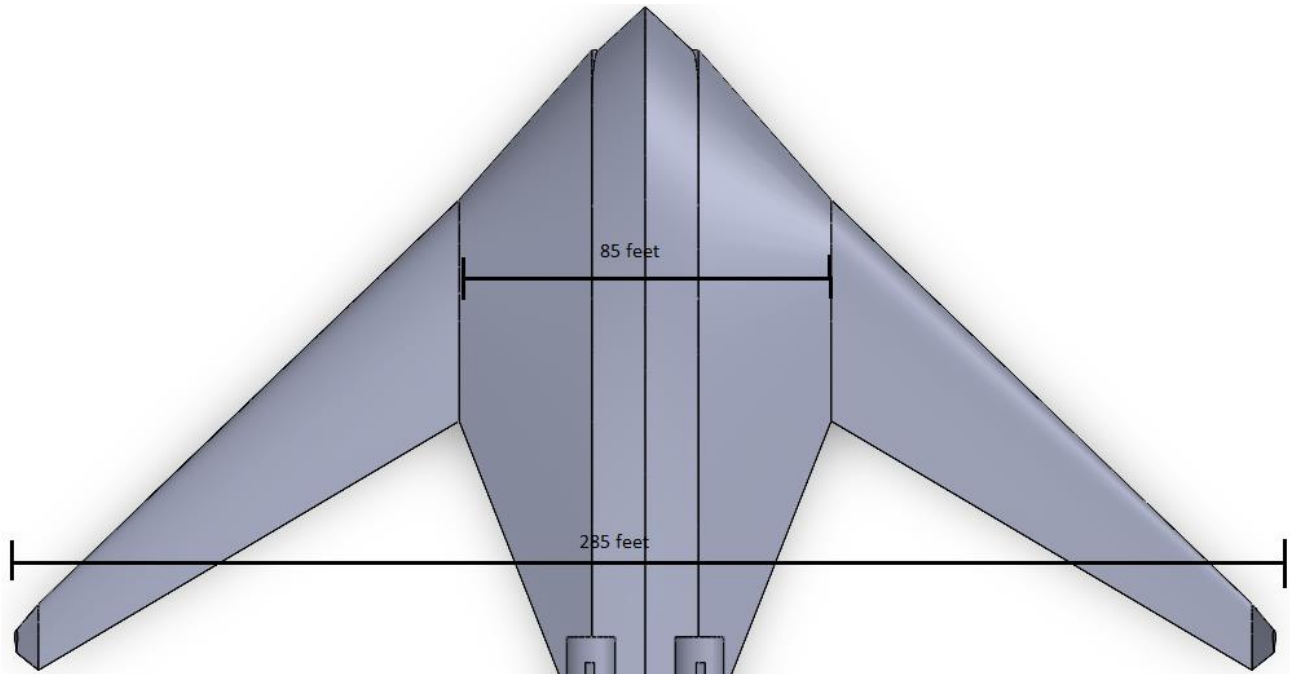


Figure 5.6. Top fuselage dimensions for the blended wing body design

5.4 Discussion

The fuselage is quite large due to the nature of the blended wing body. This allows for a “theatre-like” configuration of seats allowing the aircraft to hold more people. The emergency exits are located on the top floor and stairs are used to access them. Stairs are used because the cabin is located mid-wing, which means that the only exits are above or below the wing. Above the wing, exits are used to make space for fuel and luggage that are in the bottom of the aircraft. There are galleys and lavatories throughout the aircraft for passenger convenience. There are about 80 business class seats and 420 economy class seats for this aircraft. The aircraft has a length of 160 feet and a width of 285 feet; however, only 85 feet of the entire aircraft’s width will be used for the fuselage. Landing gear and most of the luggage will be on the bottom of the aircraft. Fuel will be stored in the wings and any extra space underneath the cabin. The cockpit is located towards the most forward region of the aircraft to provide the best view for the pilot.

6. Wing, High-lift System & Lateral Control Design

6.1 Introduction

This chapter will discuss the details of the wing for the blended wing body. The wing planform, high-lift system, and lateral control system of the wing are dependent on several parameters such as:

- Gross Area, S
- Aspect Ratio, A
- Taper ratio, $\lambda = c_t/c_r$ (ratio of tip chord to root chord)
- Dihedral angle, Γ
- Sweep angle, Λ
- Thickness Ratio, t/c
- Incidence angle, i
- Geometric twist
- Airfoil selection

The aircraft wings are separated into multiple sections that have a certain functionality during various parts of the flight. The wing planform is vital to the aerodynamic efficiency of the aircraft, such as providing the necessary lift for the aircraft while also minimizing the drag the aircraft must overcome. In addition, because of the nature of a blended wing body, the airfoil thickness for the “fuselage” must be large enough to house the passengers, luggage, aircraft structure, engines, and fuel tanks. The geometric parameters are calculated through XFLR5’s CAD feature, which can create a realistic model with values for the parameters listed earlier.

The high lift devices and lateral control surfaces will be determined using Roskam’s textbook as well as using a literature review. The literature review will also be used to determine a rough estimation for several geometric parameters of the wings.

6.2 Wing Planform Design

The critical criteria that determine the geometry of the wing planform are the following:

- Gross Area
- Taper Ratio
- Aspect Ratio

The aspect ratio was roughly approximated from various conventional large airliners and blended wing body concepts in the past. The wing planform area was determined by multiplying the estimated gross takeoff weight with the necessary wing loading determined in chapter 3; however, it should be noted that this does not include the “fuselage” area of the wing. The calculations in chapter 3 assumed 9,500 ft² referenced wing area with a total area of approximately 14,500 ft².

The fact that the body is an airfoil allows a more accurate CFD analysis when determining aerodynamic coefficients for the blended wing body since the entire aircraft can be modeled in XFLR5. A modeled wing in XFLR5 means that many of the wing’s geometry may seem significantly off than a conventional wing due to the “wing-fuselage” section. In the XFLR5 model, an area of 16,284 ft² was determined. Because the analysis will be done using XFLR5, this value will be used. The taper ratio of the entire blended wing body was 0.028. This taper ratio is extremely low because the center portion of the aircraft has a large chord when compared to the small chord length of the winglets at the ends of the wings. The aspect ratio of the blended wing body was approximated to be 4.9 by XFLR5. The smaller aspect ratio considers the airfoil-like fuselage to the end of the thinner wings on the side of the aircraft.

- Aspect Ratio = 4.91
- Wing Area = 16,284 ft²
- Taper Ratio = 0.028

A top view of the XFLR5 wing planform with dimensions of the fuselage, wings, and winglet is shown below. Furthermore, the mean aerodynamic chord, or MAC, is shown at its approximate location.

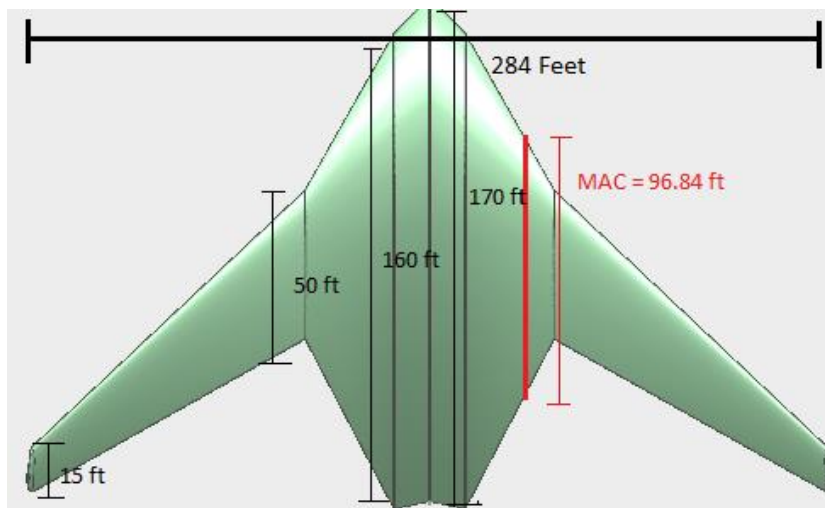


Figure 6.1. Top view of wing planform from XFLR5

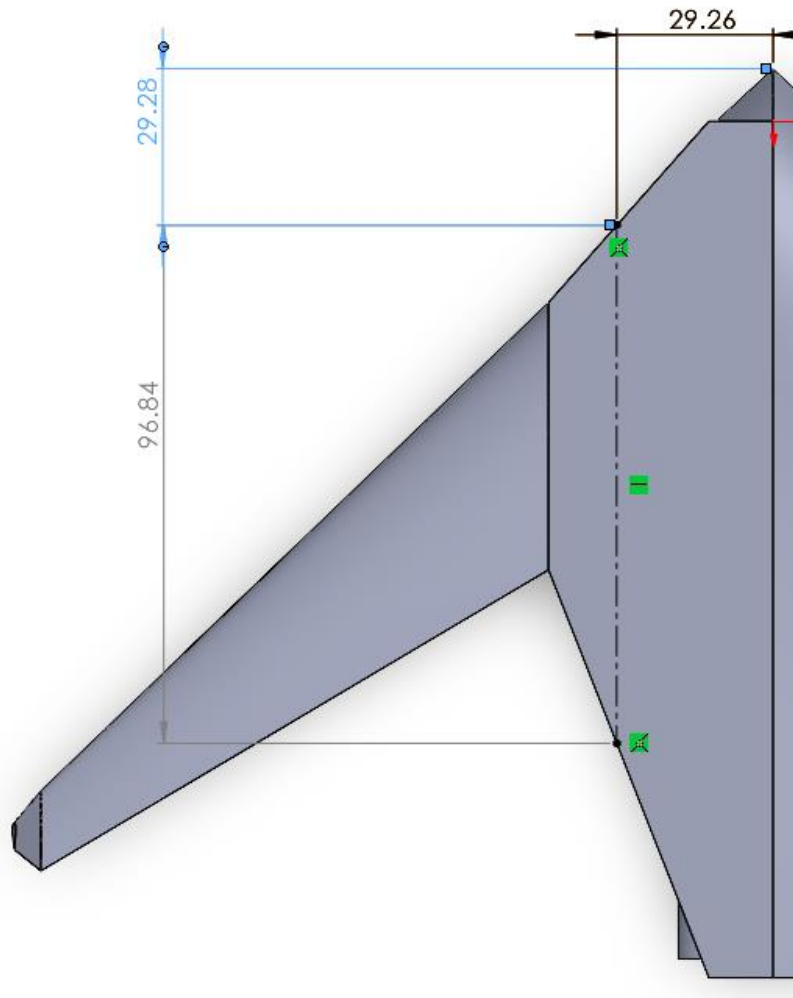


Figure 6.2. Mean aerodynamic center and location

Figure 6.2. is used to determine the exact location of the mean aerodynamic center. This was done by locating where the chord length is exactly 96.84 ft and then locating that exact chord length relative to the nose and center of the aircraft.

Another method that was used to calculate values relating to the mean aerodynamic chord was the trapezoidal estimation method. Using, appendix D from Gudmundsson's General Aviation Aircraft Design textbook [20], the location and the mean aerodynamic center can be calculated.

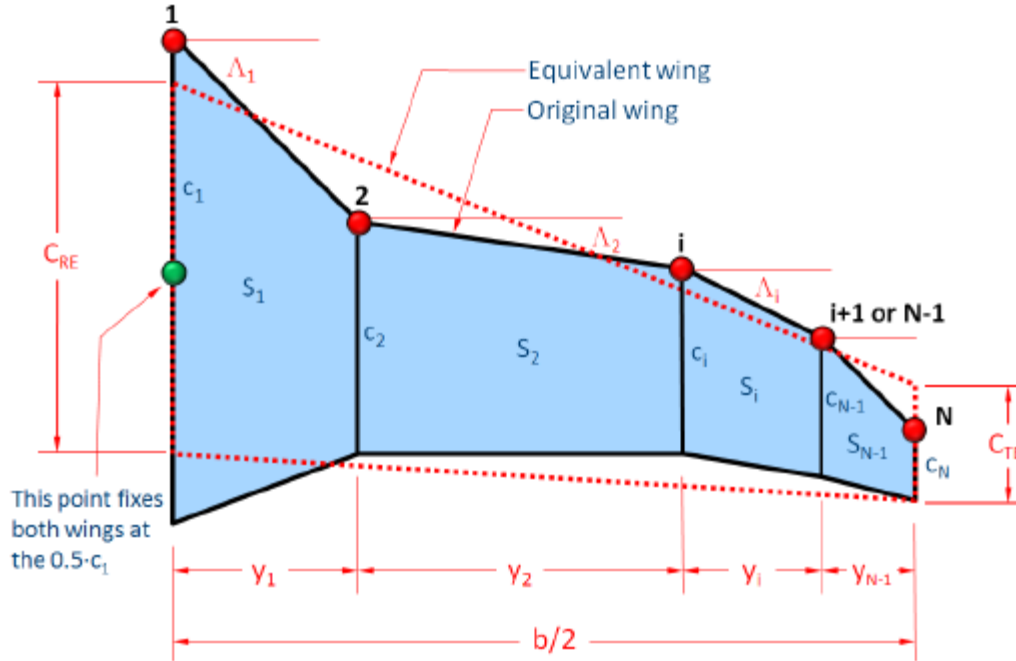


Figure 6.3. Trapezoidal area of wing planform [20]

According to Gudmundsson, the trapezoidal area of each section can be calculated with the following equation.

$$S_i = \frac{y_i(c_i + c_{i+1})}{2} \quad (6.1)$$

After summing every section, the hypothetical weighted wing area can be calculated with the following equation:

$$S_W = \frac{b}{S} \left(\sum_{i=1}^{N-1} c_i S_i + \sum_{i=1}^{N-1} c_{i+1} S_i \right) = 13,308 \text{ ft}^2 \quad (6.2)$$

Using the weighted wing area, the weighted chord root can be determined:

$$C_{WRE} = \frac{2}{S_W} \left(\sum_{i=1}^{N-1} c_i S_i \right) = 150.7 \text{ ft} \quad (6.3)$$

Lastly, the mean aerodynamic center of a multi-trapezoidal wing planform can be determined once the weighted chord root and taper ratio has been determined.

$$MGC = \frac{2C_r}{3} \frac{1 + \lambda + \lambda^2}{1 + \lambda} = 101.6 \text{ ft} \quad (6.4)$$

Hand calculations and XFLR5 calculations were 5 ft apart. Since the hand calculations are an approximation using trapezoidal area estimates, XFLR5 calculations should be used in wing planform analysis and design.

The lateral location can be calculated with this equation provided from the textbook.

$$y_{MGC} = \frac{b(1 + 2\lambda)}{6(1 + \lambda)} = 25.42 \text{ ft} \quad (6.5)$$

Although the hand calculations provide an estimated value for the lateral location, the modeled dimensions from SolidWorks will be used because the geometry used is closer to the exact value modeled in XFLR5.

Table 6.1. Wing planform design

Parameter	Value
Reference Wing Area (S)	16,284 ft ² (1,512.83 m ²)
Aspect Ratio (AR)	4.91
Wingspan (b)	284 ft (86.56 m)
Mean Geometric/ Aerodynamic Center Longitudinal Location (\bar{x})	29.28 ft (8.92 m)
Aerodynamic Center Lateral Location (\bar{y})	29.26 ft (8.92 m)
Taper Ratio(λ) Excluding Winglets	0.088
Quarter Chord Sweep Angle ($\Lambda_{c/4}$)	36.81°
Dihedral Angle (Γ_w)	6°
Incidence Angle (i_w)	0°
Geometric Twist Angle	0°

The dihedral angle was approximated with Elsevier’s datasets [18] which contains dihedral angles of various conventional airliners. Because the aircraft is essentially one wing, the fuselage and wing are aligned with each other, which means that the incidence angle can be assumed to be about 0°. The quarter chord sweep angle was determined by using an equation from Roskam’s [19] listed below, which shows the relationship between M_{cc} , t/c , C_L , and Λ .

$$\begin{aligned}
& \frac{M_{\infty}^2 * \cos^2 \Lambda}{\sqrt{(1 - M_{cc}^2 * \cos^2 \Lambda)}} * \left[\left(\frac{\gamma + 1}{2} \right) * \frac{2.64 * \left(\frac{t}{c} \right)}{\cos \Lambda} + \left(\frac{\gamma + 1}{2} \right) * \frac{2.64 * \left(\frac{t}{c} \right) * (0.34 * C_L)}{\cos^3 \Lambda} \right] \\
& + \frac{M_{\infty}^2 * \cos^2 \Lambda}{1 - M_{cc}^2 * \cos^2 \Lambda} \left[\left(\frac{\gamma + 1}{2} \right) * \frac{1.32 * \left(\frac{t}{c} \right)^2}{\cos \Lambda} \right] + \\
& M_{\infty}^2 * \cos^2 \Lambda * \left[1 + \left(\frac{\gamma + 1}{2} \right) * \frac{0.68 * C_L}{\cos^2 \Lambda} + \left(\frac{\gamma + 1}{2} \right) * \left(\frac{0.34 * C_L}{\cos^2 \Lambda} \right)^2 \right] - 1 = 0 \quad (6.6)
\end{aligned}$$

- $M_{\text{cruise}} = M_{\text{div}}$
- $M_{\text{div}} = 1.02M_{\text{cc}}$
- $t/c =$ thickness ratio
- $\gamma =$ isentropic expansion factor for air
- $C_L =$ coefficient of lift during cruise
- $\Lambda =$ sweep angle

The thickness ratio used was 0.18 since the airfoil, NACA 25118, has a t/c of 18%. The isentropic expansion factor of air is 1.4. M_{cruise} is the Mach number that was used in the mission requirements which is 0.80. C_L was determined by using the weight of the aircraft, the air density at 35,000 ft, the velocity when Mach number is 0.80, and the estimated gross area of the aircraft.

- $W = 950,000$ lbf
- $V = 663$ mph
- $\rho = 7.38 * 10^{-4}$ slugs/ft³
- $S = 16,284$ ft²

Using the coefficient of lift equation, C_L can be determined.

$$C_L = \frac{2W}{\rho V^2 S} \quad (6.7)$$

Once C_L is determined, the equations in Roskam's textbook [19] can be solved. Plugging the equation into MATLAB, the sweep angle for the wing was determined to be 36.8 degrees.

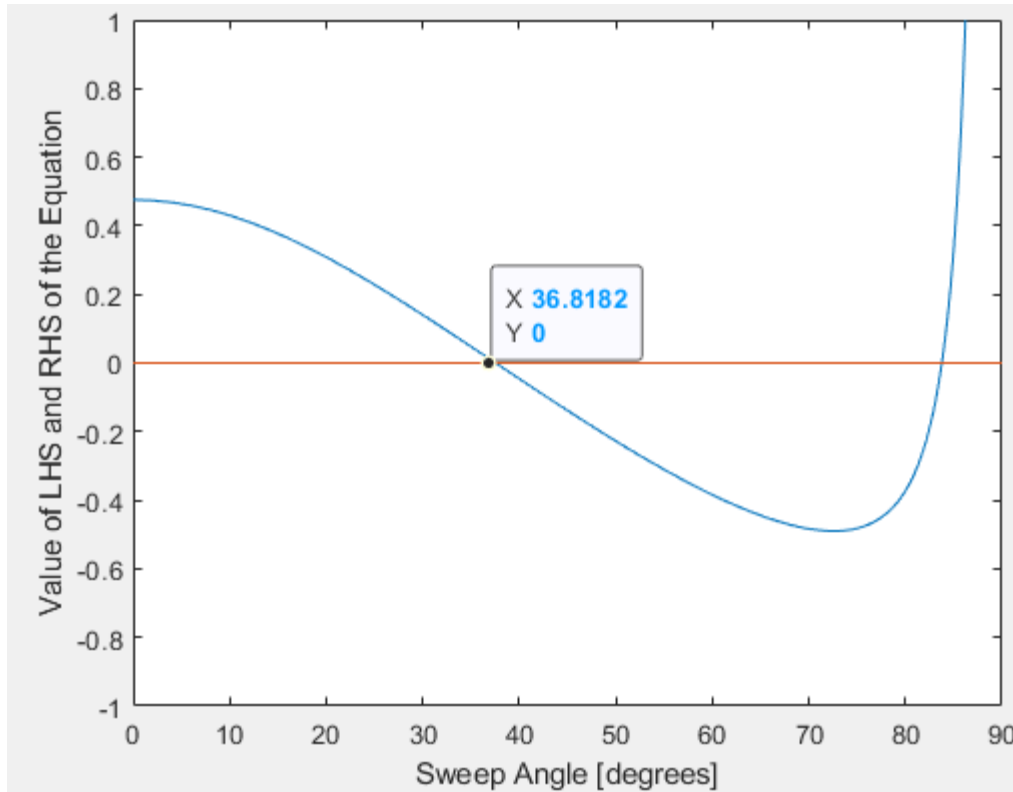


Figure 6.4. The sweep angle combinations curve from 0° to 90° for current aircraft parameters

6.3 Airfoil Selection

Two airfoils will be used in this blended wing body design. One for the fuselage and the other for the wing itself. Airfoil selection was determined by the geometric thickness for housing as well as optimizing for aerodynamic efficiency. Through literature research, multiple sources have used the NACA 25112 for the fuselage airfoil. This is due to its capability of generating high lift when compared to other airfoils [20]; however, the chord thickness ratio would simply be too small for a large airliner. The NACA 25118 was chosen for the 6% increase in thickness. The NASA SC (2) 0412 airfoil was used for the wings. Due to the airliners reaching transonic speeds, the airfoils should be supercritical to account for shocks along the cross-section of the wing.



Figure 6.5. NASA SC (2) 0412 airfoil profile

Table 6.2. NASA SC (2) 0412 airfoil profile parameters

Parameter	Value
Airfoil Camber	1.02%
Airfoil Thickness (t/c)	12.00%

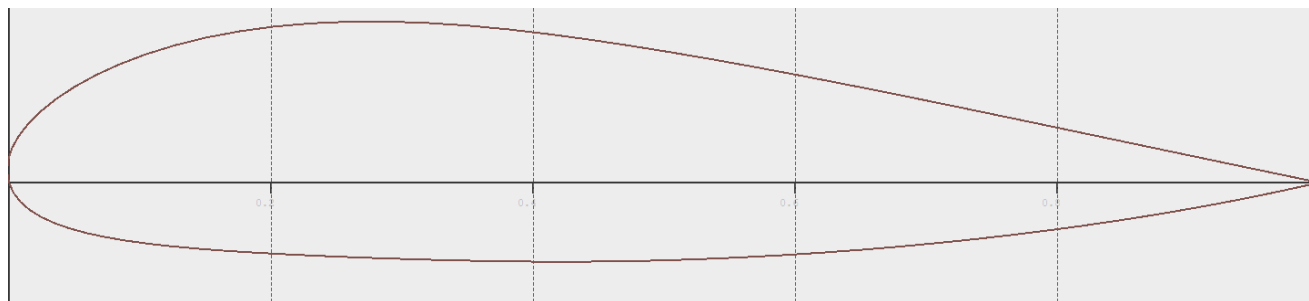


Figure 6.6. NACA 25118 airfoil profile

Table 6.3. NACA 25118 airfoil profile parameters

Parameter	Value
Airfoil Camber	3.28%
Airfoil Thickness (t/c)	18.00%

6.4 Wing Design Evaluation

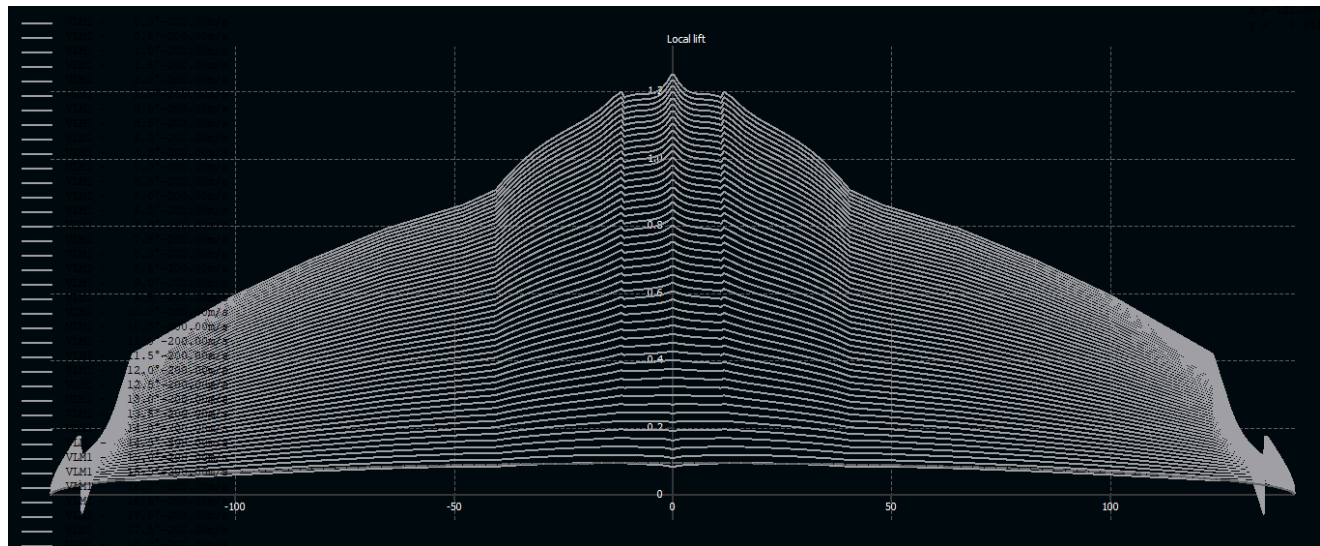


Figure 6.7. Local lift coefficient normalized to the mean aerodynamic chord with XFLR5

XLFR5 was used to determine the lift coefficient across the wing. As expected, the lift towards the wing root is greater than the rest of the blended wing body. The local C_{LMAX} seems to peak at about 1.25, which is a bit off than the desired lift that was assumed; however, this high lift coefficient was only reached after a 25 degrees angle of attack. Realistically, a 25-degree angle of attack would cause passengers safety concerns and discomfort and therefore would not be feasible.

6.5 Design of High-Lift Devices

Using the design parameters from chapter 3, C_{LMAX} for clean, takeoff, and landing were approximated. Wing design geometry was determined earlier in this chapter.

- $C_{LMAX} = 1.5$
- $C_{LMAXTO} = 1.9$
- $C_{LMAXL} = 2.1$
- $A = 4.91$
- $S = 16,284 \text{ ft}^2$
- $b = 284 \text{ ft}$
- $\Lambda_{c/4} = 36.8^\circ$
- $\lambda = 0.088$
- $c_r = 170.0 \text{ ft}$
- $c_t = 15.0 \text{ ft}$

Using the known data, the Reynolds number at the root and tip of the wing can be determined using the equations from Roskam's [19].

$$Rn_r = \frac{\rho V C_r}{\mu} = \frac{0.002378 * 242 * 170}{3.737 * 10^{-7}} = 261.8 * 10^6 \quad (6.8)$$

$$Rn_t = \frac{\rho V C_t}{\mu} = \frac{0.002378 * 242 * 15}{3.737 * 10^{-7}} = 23.1 * 10^6 \quad (6.9)$$

Using the matching graphs from Roskam's a clean C_{LMAX} for the root and tip can be approximated.

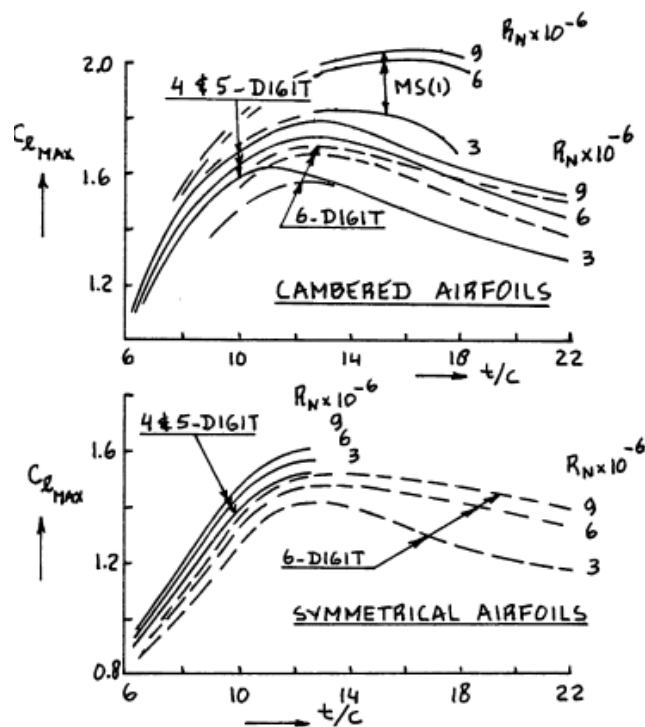


Figure 6.8. Effect of airfoil thickness on C_{LMAX} [19]

From the graphs, above C_{LMAX} of the root and tip of the wings are as follows:

- Inboard $C_{LMAX} = 2.1$
- Outboard $C_{LMAX} = 2.0$

Using the equation from Roskam's [19], the C_{LMAX} of the determined sweep angle for the blended wing body can be calculated.

$$C_{Lmax_{uw}} = 0.95 * \frac{2.1 + 2.0}{2} = 1.948$$

$$C_{Lmax_w} = 1.81(\cos 36.8) = 1.55$$

Since the value is within a 5% error of the expected $C_{LMAX} = 1.5$, the C_{LMAX} is deemed acceptable for this design. The next step would be to calculate the change in C_{LMAX} in takeoff and landing scenarios.

$$\Delta C_{L_{maxTO}} = 1.05(1.9 - 1.5) = 0.42$$

$$\Delta C_{L_{maxL}} = 1.05(2.1 - 1.5) = 0.63$$

A local change in C_{IMAX} can be calculated if an approximated surface area of the flaps is assumed.

$$\Delta C_{L_{MAX}} = \Delta C_{L_{MAX}} \left(\frac{S}{S_{wf}} \right) K_{\Lambda} \tag{6.10}$$

$$K_{\Lambda} = \left(1 - 0.08 \cos^2(\Lambda) \cos^{\frac{3}{4}}(\Lambda) \right) = 0.9565 \tag{6.11}$$

Table 6.4. Approximated change in local section lift coefficient with arbitrary S_{wf}/S values

	Landing Flaps		Take-Off Flaps	
S_{wf}/S	0.3	0.6	0.3	0.6
$\Delta C_{L_{MAX}}$	2.009	1.004	1.339	0.669

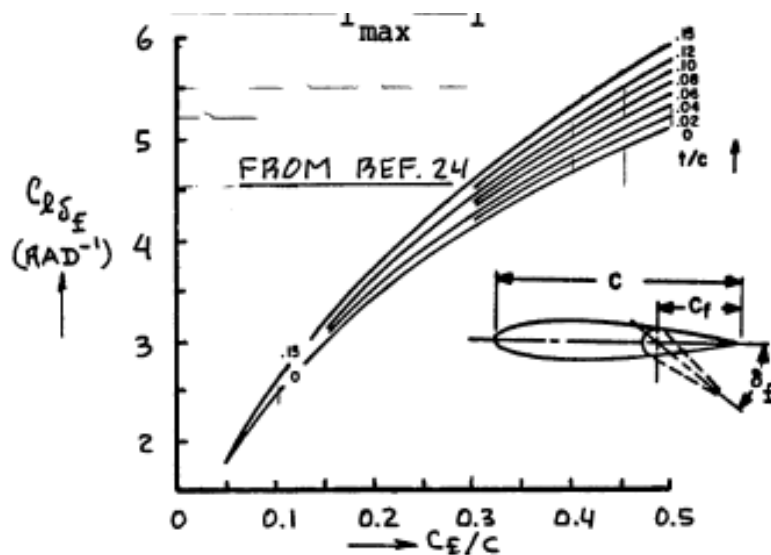


Figure 6.9. Flap length concerning chord length and its impact on the flap deflection angle [19]

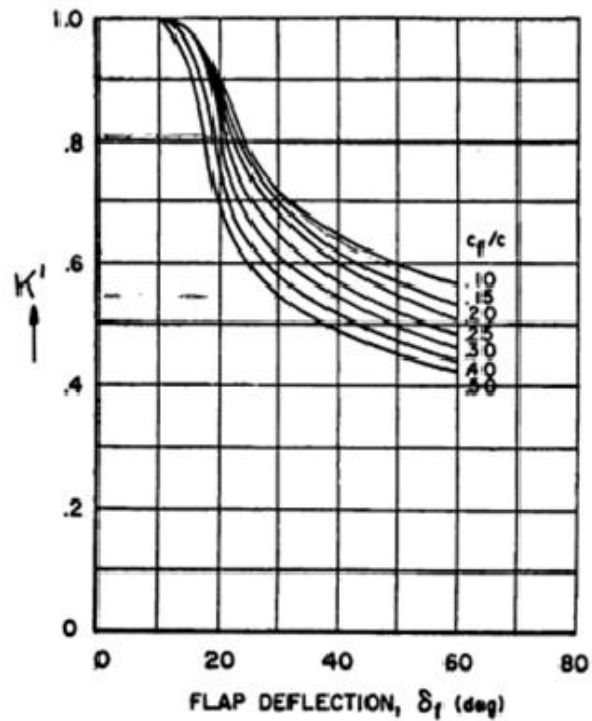


Figure 6.10. Flap deflection angle and its impact on variable K' [19]

A type of flap must be determined for this aircraft. From the literature review [1], a simple flap is the only feasible option since other flap designs provide too much pitching moment. The blended wing body does not have enough control authority to compensate for the large pitching moment generated from the flaps.

The following equations are used by Roskam [19] to determine a more accurate area for the flaps on the aircraft. The change in local coefficient of lift can be determined by the following equation:

$$\Delta C_l = C_{L\delta_f} \delta_f K' \quad (6.12)$$

Takeoff:

$$C_{L\delta_f} = 5.25/\text{rad}$$

$$\delta_{fTO} = 15 \text{ deg.} = 0.266 \text{ rad}$$

$$K' = 1$$

$$c_f/c = 0.35$$

$$\Delta C_l = C_{L\delta_f} \delta_f K' = 1.064$$

$$\Delta C_{l_{MAX}} = \Delta C_{L_{MAXTO}} \left(\frac{S}{S_{wf}} \right) K_\Lambda$$

$$1.39 = 0.42 \left(\frac{S}{S_{wf}} \right) 0.9565$$

$$\left(\frac{S_{wf}}{S} \right) = 0.287$$

$$\delta_{fL} = 40 \text{ deg.} = 0.698 \text{ rad}$$

$$K' = 0.55$$

$$\Delta C_l = C_{L\delta_f} \delta_f K' = 1.536$$

$$\Delta C_{l_{MAX}} = \Delta C_{L_{MAXL}} \left(\frac{S}{S_{wf}} \right) K_\Lambda$$

$$2.015 = 0.63 \left(\frac{S}{S_{wf}} \right) 0.9565$$

$$\left(\frac{S_{wf}}{S} \right) = 0.30$$

Summary of leading flap geometry:

- $S_{wf} / S = 0.30$
- $c_f/c = 0.35$
- Simple flap
- Take-off $\delta_f = 15$ deg.
- Landing $\delta_f = 40$ deg.

By multiplying S_{wf}/S and c_f/c , the total control surface area is approximately 0.105 or 10.5% of the wing. The “wing” portion of the aircraft is approximately 6,291 ft² from the SolidWorks model, which equates to 627 ft² of control surface area.

In addition, $C_{L_{MAX}}$ during clean, landing and takeoff are as follows:

- $C_{L_{max}} = 1.55$
- $C_{L_{maxTO}} = 1.55 + 0.42 = 1.97$
- $C_{L_{maxL}} = 1.55 + 0.63 = 2.18$

6.6 Design of the Lateral Control Surfaces

The lack of a horizontal stabilizer means that a blended wing body needs another alternative for lateral control authority. Elevons, which are a combination of elevators and ailerons, will be implemented on the trailing edge of the wing. This will help provide the necessary longitudinal control during take-off and landing. The elevons will run from 0.05 fraction of the outboard section of the thinner wing to the 0.90 fraction of the inboard section of the inner wing.

6.7 Wing Drawings

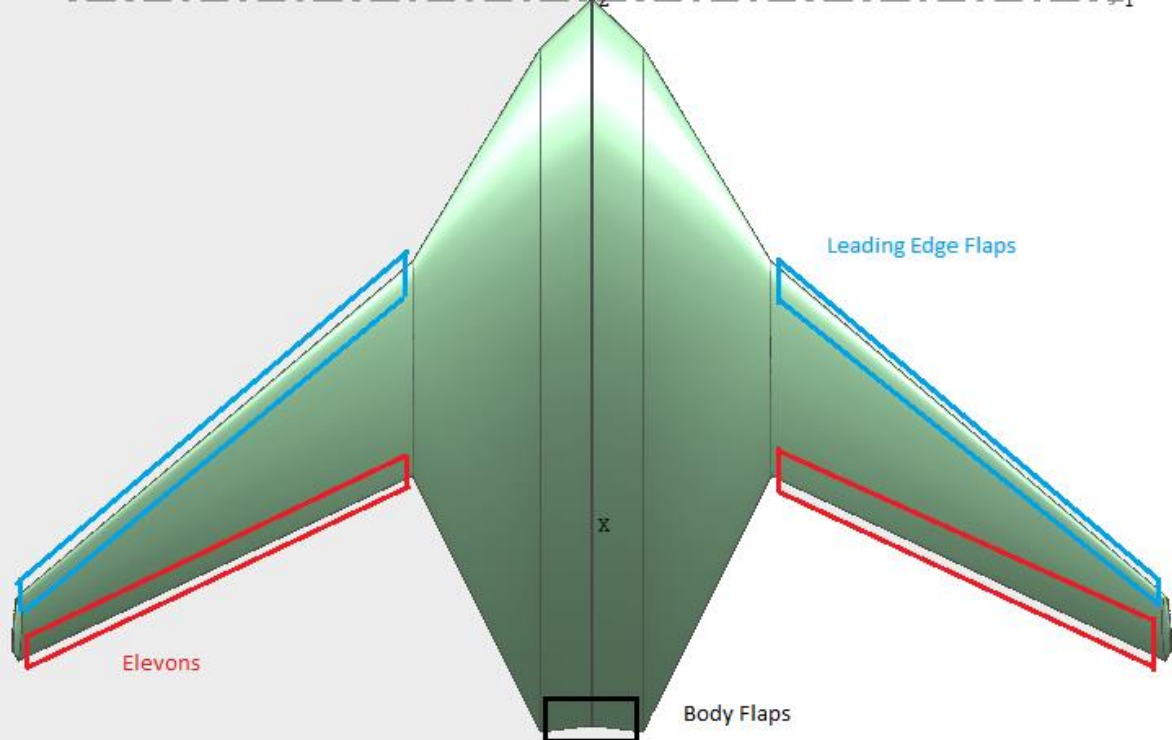


Figure 6.11. High-lift device placement

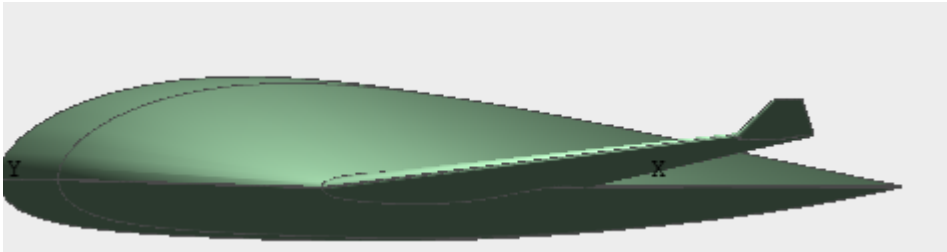


Figure 6.12. Side view of aircraft wing

6.8. Discussion

Because the wing and the fuselage are blended, the analysis consists of almost the entire aircraft. The body of the aircraft uses a NACA 25118 airfoil for high lift performance. A NACA 25118 is used instead of a NACA 25112 for the increase in volume which is needed for the passengers, fuel, structure, and other important components of the aircraft. The NASA SC (2)-0412 is used for its high performance during transonic cruise speeds. Supercritical airfoils are needed for higher critical Mach numbers and their flat surface is useful for storage.

This wing configuration allows for only a small portion of the trailing edge to be used for flaps because of the high pitching moment it generates. Further analysis would be needed to determine if flaps are feasible for this aircraft design. The feasibility of flaps in this design are still questionable due to a lack of research in the pitching moment of this aircraft. Instead, elevons are used to help control the longitudinal and lateral direction of the aircraft. Most of the trailing edges are used for the elevons to compensate for the lack of a horizontal stabilizer. Thus, the elevons are the only longitudinal and lateral control authority on this wing. Leading-edge flaps are used to increase the lift that is needed during take-off and landing while minimizing the increase of pitching moment. The leading-edge flaps will be able to extend up to 30% from the wing. This will give 627 ft² of control surface area. Similarly, body flaps at the rear of the fuselage can also be used to increase lift and support longitudinal stability and will also be able to extend the same amount.

7. Design of the Empennage & Control Surfaces

7.1 Introduction

This chapter will go into the depth of the empennage design. In most empennage designs, there are horizontal and vertical stabilizers. The empennage's main purpose is to provide the aircraft stability during flight akin to feathers on an arrow. The horizontal stabilizer provides pitch stability whereas the vertical stabilizer helps to control yaw. The horizontal stabilizer has a control surface called the elevator which allows the pilot or flight control system to change pitch when necessary and is needed during takeoff and landing. The vertical stabilizer has rudders toward the rear section, and this allows the aircraft to turn left or right. Generally, empennage design consists of the following parameters:

- Aspect Ratio
- Taper ratio
- Thickness ratio
- Sweep angle
- Airfoil(s)
- Dihedral angle
- Control surface areas

Because the aircraft is a blended wing body, a horizontal stabilizer will not be used. Instead, only a vertical stabilizer will be used for yaw control support. This chapter will discuss the location of the vertical stabilizer, the geometry of the vertical stabilizer, and its overall impact on the aircraft.

7.2 Overall Empennage Design

The empennage design as explained in chapter 4 consists of a twin vertical tail for yaw control and stability. This design will help provide the necessary yaw authority needed to control a blended wing body aircraft while also minimizing the amount of total drag that the vertical stabilizers will provide the aircraft. A blended wing body configuration does not use a traditional horizontal empennage because of its flying wing geometry. Instead, trailing edge elevons throughout the wingspan are used for longitudinal and lateral control authority.

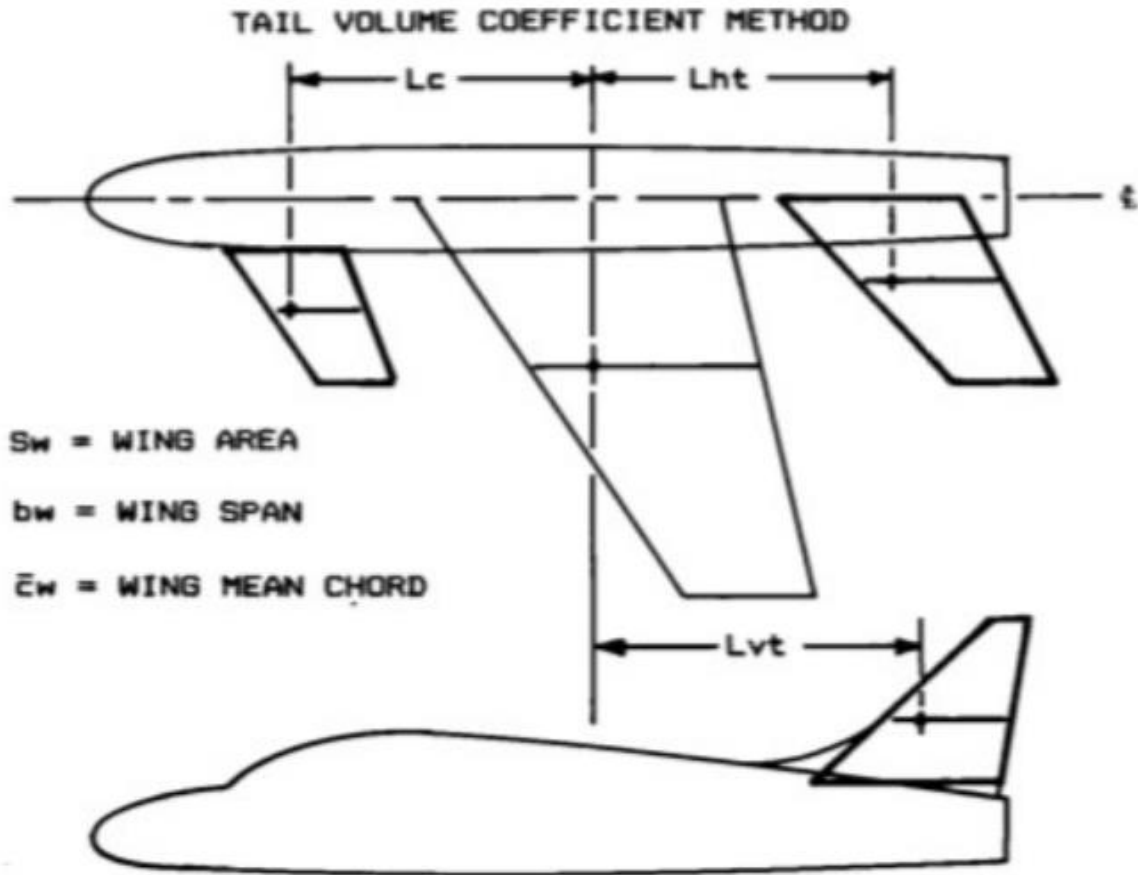


Figure 7.1. Location estimates of empennage parts [14]

To determine the location of the vertical stabilizers for this aircraft, the moment arm of the aircraft must be estimated which is about 45% to 50% of the fuselage length. The x-location of the vertical empennage is approximated to be 154.62 ft from the cockpit of the aircraft. Using this information L_{VT} can be approximated to be about 84.93 ft. Since the mean aerodynamic center is 69.69 ft and the x-location of the vertical stabilizer is 154.62 ft, the difference between the two values will give L_{VT} . To calculate the surface area of the vertical stabilizer, the following equation can be used:

$$S_{VT} = \frac{C_{VT} b_w S_w}{L_{VT}} \quad (7.1)$$

$C_{VT} = 0.09$ and this value can be found from Roskam's aircraft design textbook [14].

$$S_{VT} = \frac{(0.09)(284)(6291)}{84.93(2)} = 1,236 \text{ ft}^2$$

It should be noted that since this is a twin fin configuration, the surface area is divided by 2. In addition, the surface area of the wing does not include the fuselage portion of the BWB configuration.

7.3 Design of the Vertical Stabilizer

The following dimensions are for the twin tail vertical stabilizers that will be on the blended wing body configuration.

Table 7.1. Vertical stabilizer parameters

Parameter	Value
Reference Wing Area (S)	1236 ft ² (114.82 m ²) *For both fins
Aspect Ratio (AR)	2.55
Wingspan (b)	56.0 ft (17.07 m)
Mean Geometric/ Aerodynamic Center Longitudinal Location (\bar{x})	154.62 ft (47.13 m)
Taper Ratio(λ)	0.42
Quarter Chord Sweep Angle ($\Lambda_c/4$)	25.74°
Dihedral Angle (Γ_w)	90 °
Incidence Angle	0 °
Airfoil	NACA-0012

Table 7.2. Roskam's table for vertical tail design parameters [19]

Table 8.14 Planform Design Parameters for Vertical Tails

Type	Dihedral Angle, Γ_v deg.	Incidence Angle, i_v deg.	Aspect Ratio, A_v	Sweep Angle, $\Delta_c/4_v$ deg.	Taper Ratio, λ_v
Homebuilts	90	0	0.4 - 1.4	0 - 47	0.26 - 0.71
Single Engine Prop. Driven	90	0	0.9 - 2.2	12 - 42	0.32 - 0.58
Twin Engine Prop Driven	90	0	0.7 - 1.8	18 - 45	0.33 - 0.74
Agricultural	90	0	0.6 - 1.4	0 - 32	0.43 - 0.74
Business Jets	90	0	0.8 - 1.6	28 - 55	0.30 - 0.74
Regional Turbo-Props.	90	0	0.8 - 1.7	0 - 45	0.32 - 1.0
Jet Transports	90	0	0.7 - 2.0	33 - 53	0.26 - 0.73
Military Trainers	90	0	1.0 - 2.9	0 - 45	0.32 - 0.74
Fighters	75 - 90	0	0.4 - 2.0	9 - 60	0.19 - 0.57
Mil. Patrol, Bomb and Transports	90	0	0.9 - 1.9	0 - 37	0.28 - 1.0
Flying Boats, Amph. and Float Airplanes	90	0	1.2 - 2.4	0 - 32	0.37 - 1.0
Supersonic Cruise Airplanes	75 - 90	0	0.5 - 1.8	37 - 65	0.20 - 0.43

Many of the design parameters from Table 7.1 correlates with many of the generalization in table 7.2. Dihedral angle and incidence angle should be 90 degrees and 0 degrees respectively for maximum yaw control authority. The aspect ratio, sweep angle, and taper ratio fall within jet transports and transport aircraft type parameters. The NACA 0012 was used for its simple geometry and symmetry.

7.4 Empennage Design Evaluation

Table 7.3. XFLR5 empennage inputs

	y 0	chord 0	offset 0	dihedral(°)	twist(°)	foil	X-panels	X-dist	Y-panels	Y-dist
1	0.000	31.000	0.000	0.0		0.00NACA 0012		7Uniform		7Cosine
2	28.000	13.000	18.000			0.00NACA 0012				

Table 7.4. XFLR5 empennage outputs

Wing Span	56.00 ft
Area	1232.00 ft ²
Projected Span	56.00 ft
Projected Area	1232.00 ft ²
Mean Geom. Chord	22.00 ft
Mean Aero Chord	23.23 ft
Aspect ratio	2.55
Taper Ratio	0.42
Root to Tip Sweep	25.74 °
Number of Flaps	0
Number of VLM Panels	49
Number of 3D Panels	112

7.5 Design of the Longitudinal and Directional Controls

Rudders are used to control the direction of the aircraft through the twin fins. The rudders will run 90% of the vertical stabilizers' span to have maximum control authority. This translates to about 26 feet of the vertical stabilizer with the wing root chord being 31 ft and the tip chord being 13 ft.

7.6 CAD Drawings

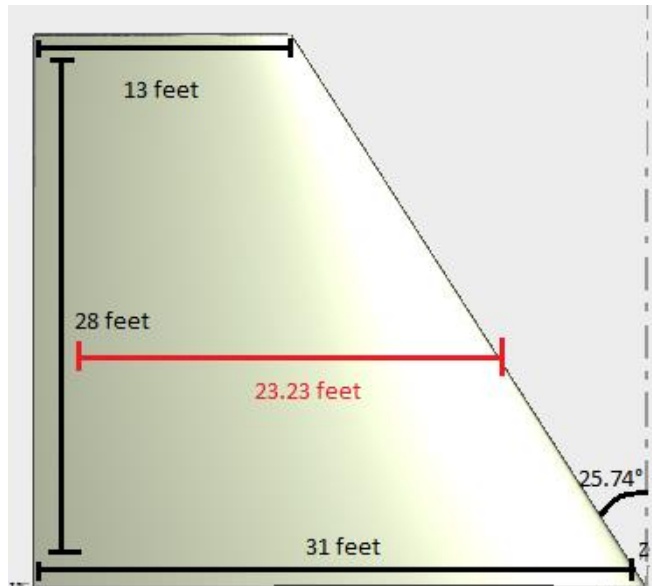


Figure 7.2. XFLR5 CAD of the vertical tail

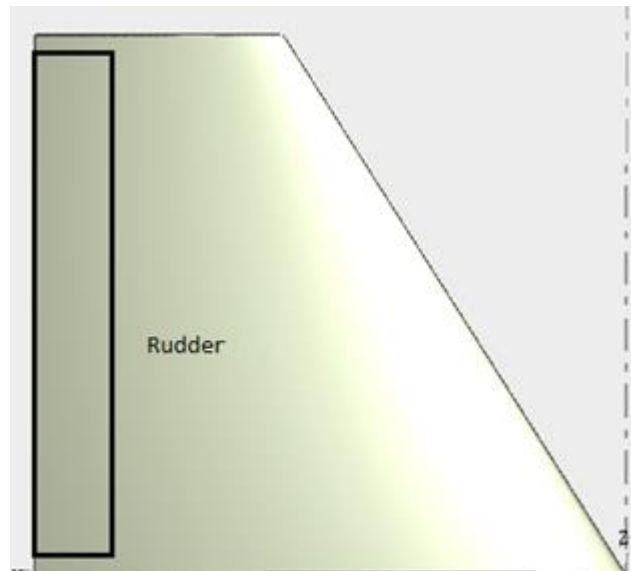


Figure 7.3. XFLR5 rudder placement of the vertical tail

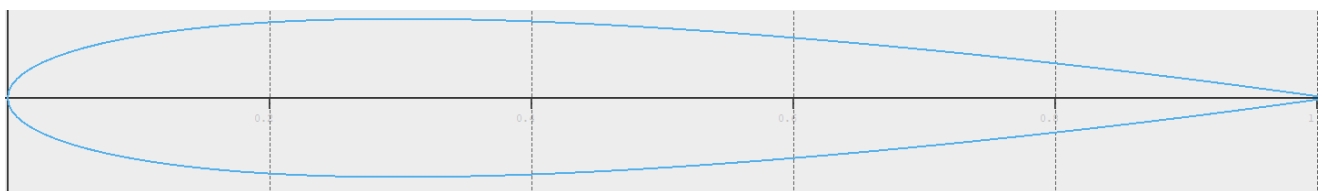


Figure 7.4. NACA 0012 rudder airfoil

7.7 Discussion

Blended wing body aircraft suffer from their lack of control authority due to the lack of a dedicated horizontal empennage. Control surfaces must be placed on the wing to emulate elevator-like functionalities. This is one of the main reasons why blended wing body aircraft have not been introduced into the commercial industry. The lack of control authority can be detrimental to the performance of the aircraft and can easily cause severe injuries to the passengers. The twin tail configuration attempts to minimize the drag by minimizing the surface area of the vertical stabilizers while still maintaining the necessary control authority needed to perform yaw and pitch maneuvers.

8. Landing Gear Design

8.1 Introduction

This chapter will discuss the preliminary design of the landing gear of the aircraft. The landing gear is vital to the takeoff, landing, and aerodynamic aspects of the aircraft. The center of gravity of this aircraft is generally used to determine the size and location of the landing gear. In this blended wing body design, a retractable tricycle gear will be used for its inherent stability as well as for aerodynamic efficiency. The tricycle gear also provides a flat surface and provides excellent load distribution throughout the landing gear. The following parameters of the landing gear will be discussed:

- Number, type, and size of tires
- Length and diameter of the struts
- Preliminary Arrangement
- Tip-over criteria
- Retraction Feasibility
- CAD model

Many design choices used in the conventional tube and wing airliners can be applied to blended wing bodies. The location of the landing gear will be determined based on the aircraft's center of gravity. The length and diameter of the landing gear can be determined based on the tip-over criteria and ground clearance needed for takeoff and landing. Loading of the landing gear can be determined using Roskam's method [19].

8.2 Estimation of the Center of Gravity Location

Table 8.1. CG location at critical loading scenarios

Weight Scenarios	Weight	CG Location (x, z)
Max Gross Takeoff Weight	950,000 lb	X: 77.8 ft Z: 15.8 ft
Full Payload Weight (No Fuel)	603,860 lb	X: 76.6 ft Z: 16.7 ft
Empty Weight	476,060 lb	X: 78.9 ft Z: 17.3 ft

8.3 Landing Gear Design

8.3.1. Tire Design Choices

Roskam's Part II Aircraft design textbook has rough estimates of tire design choices for a large jet transport. The table from Roskam will be used as a reference to determine tire size, number, and pressure.

Table 8.2. Roskam's tire size reference table [19]

Table 9.2 Typical Landing Gear Wheel Data ($n_s = 2$ unless otherwise noted)

Type	W_{TO} lbs	Main Gear				Nose Gear			
		$D_t \times b_t$ in. x in.	$n_s P_m / W_{TO}$	PSI	n_{mt}	$D_t \times b_t$ in. x in.	P_n / W_{TO}	PSI	n_{nt}
Transport Jets	44,000	34x12	0.89	75	2	24x7.7	0.11	68	2
	73,000	40x14	0.92	77	2	29.5x6.75	0.08	68	2
	116,000	40x14	0.94	170	2	24x7.7	0.06	150	2
	220,000	40x14	0.94	180	4	29x7.7	0.06	180	2
	330,000	46x16	0.93	206	4	40x14	0.07	131	2
	572,000	52x20.5	0.93	200	4*	40x15.5	0.07	190	2
	775,000	49x17	0.94	205	4**	46x16	0.06	190	2
Military Trainers	2,500	17x6	0.82	36	1	13.5x5	0.18	28	1
	5,500	20.3x6.5	0.91	60	1	14x5	0.09	40	1
	7,500	20.25x6	0.92	65	1	17.2x5.0	0.08	45	1
	11,000	23.3x6.5	0.90	143	1	17x4.4	0.10	120	1
Fighters	9,000	20x5.25	0.86	135	1	17x3.25	0.14	82	1
	14,000	18.5x7	0.87	110	1	18x6	0.13	37	1
	25,000	24x8	0.91	210	1	18x6.5	0.09	120	1
	35,000	24x8	0.90	85	2	21.5x9.8	0.10	57	1
	60,000	35.3x9.3	0.88	210	1	21.6x7.5	0.12	120	2
	92,000	42x13	0.93	150	1	20x6.5	0.07	120	2

For Flying Boats, Amphibious and Float Airplanes as well as for Supersonic cruise airplanes, use jet transport data.

*three main gear struts: $n_s = 3$ ** four main gear struts: $n_s = 4$

Note: all other airplanes have $n_s = 2$: two main gear struts.

From the reference table, any airliner that weighs more than 775,000 lbf should require 4 struts for the main landing gear and 2 struts for the nose landing gear. Assuming the main landing gears' struts have 4 wheels each and the nose landing gear has 2 wheels, it is recommended that the landing gear should have 18 wheels in total. The data above can be used to extrapolate values for a 950,000 lbf aircraft.

Table 8.3. Main landing gear tires

Number of Wheels	16
Maximum Diameter	52 in.
Maximum Width	18 in.
Pressure	215 psi

Table 8.4. Nose landing gear tires

Number of Wheels	2
Maximum Diameter	52 in.
Maximum Width	18 in.
Pressure	200 psi

8.3.2. Strut Design Choices

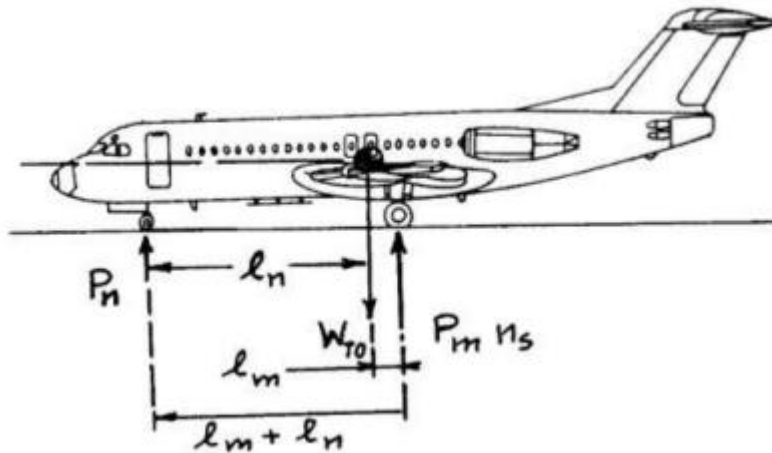


Figure 8.1. Geometric definition for static load on landing gear

Using these two equations from Roskam's, the static load for the main and nose landing gear can be determined. The load ratio for each landing gear can be approximated.

$$p_n = \frac{W_{TO} * l_m}{l_m + l_n} \quad (8.1)$$

$$p_n = \frac{W_{TO} * l_n}{\text{numbers of struts} * (l_m + l_n)} \quad (8.2)$$

Table 8.5. Main landing gear struts

Number of Struts	4
Length of Struts	11 ft.
Strut Loading	205,397 lbf
Load Ratio	0.84

Table 8.6. Nose landing gear struts

Number of Struts	1
Length of Struts	11 ft.
Strut Loading	128,412 lbf
Load Ratio	0.16

8.3.3. Preliminary Arrangement

During takeoff and landing, the aircraft must have sufficient ground clearance and satisfy the aircraft tip-over criteria. This is crucial for jet transports carrying many people to ensure a safe and smooth flight. Roskam's Aircraft Design textbook has a few figures demonstrating acceptable ground clearance and tip-over criteria.

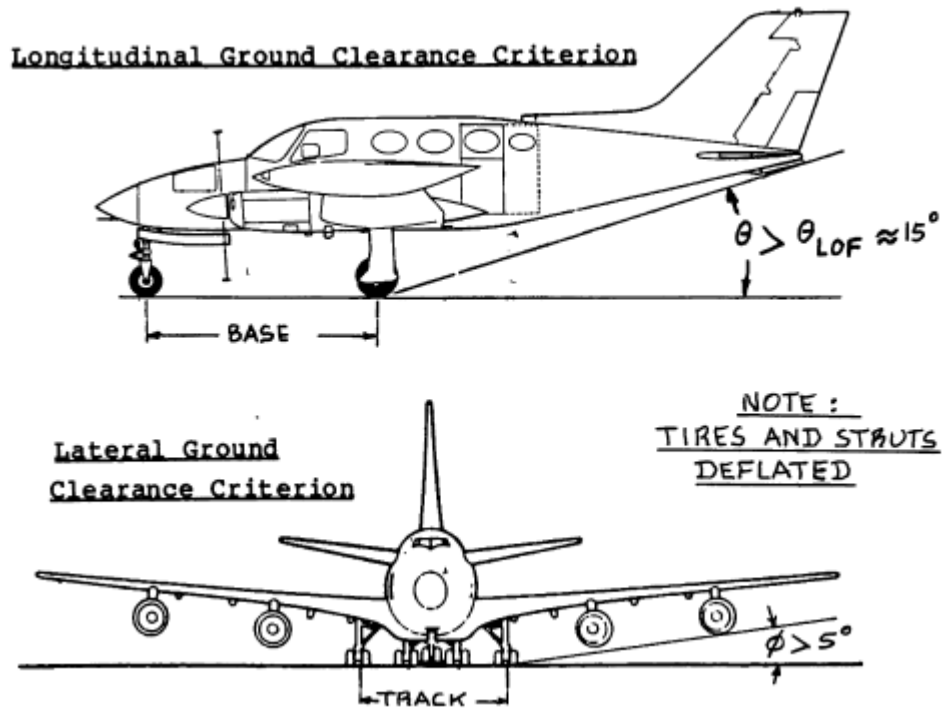


Figure 8.2. Longitudinal and lateral ground clearance criteria [19]

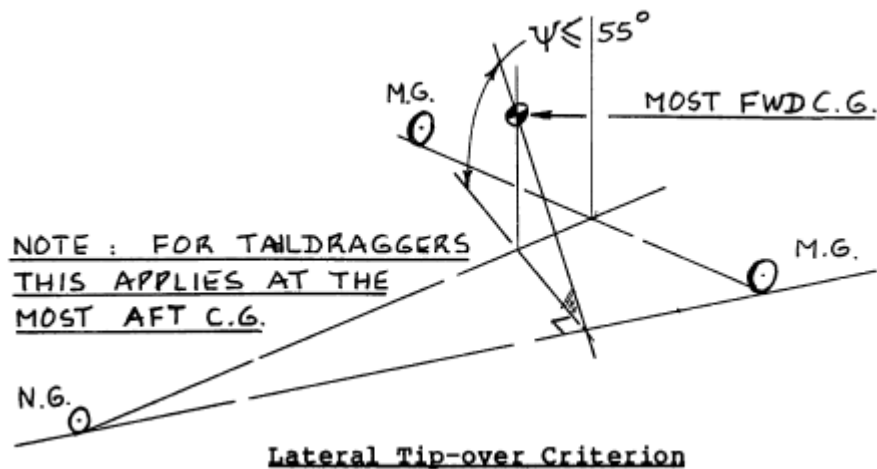


Figure 8.3. Lateral tip-over criteria [19]

Since the longitudinal ground clearance angle is greater than 15 degrees and the lateral ground clearance angle is greater than 5 degrees, the blended wing body design satisfies both the ground clearance criteria.

To determine the longitudinal tip over criteria, the most aft center of gravity will be used. In this case, it is when the blended wing body has no fuel or passengers. Trigonometry can be used to determine a rough angle needed to determine if the blended wing body satisfies this criterion. By using the distance from the center of gravity of the aircraft and the main landing gear as well as the center of gravity of the aircraft and ground, this angle can be calculated.

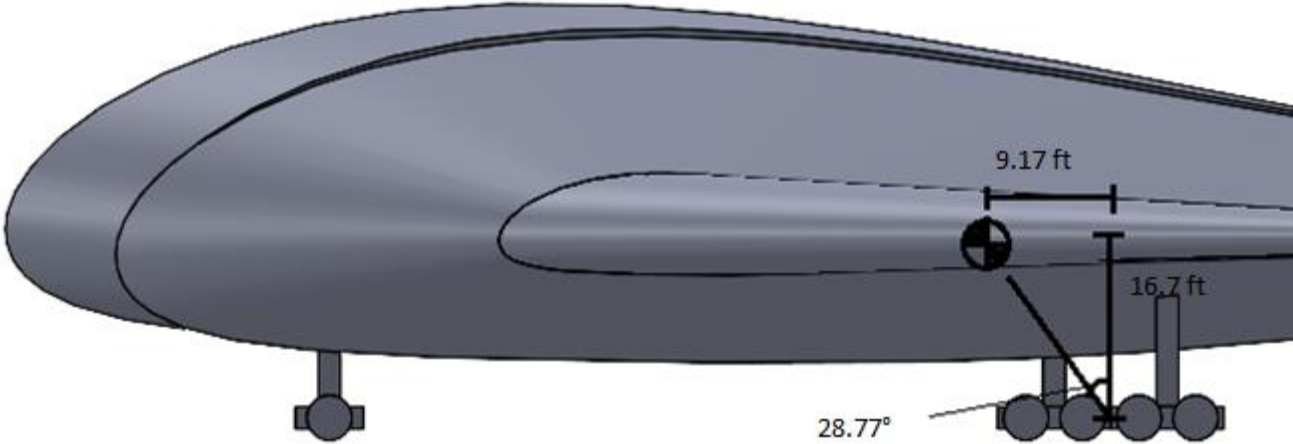


Figure 8.7. Longitudinal tip-over criterion at the most forward C.G.

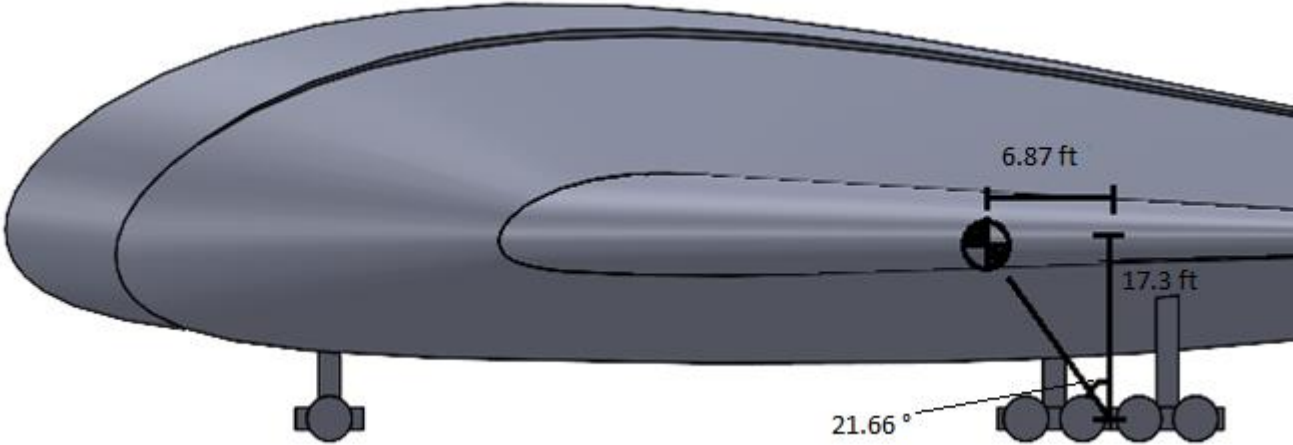


Figure 8.8. Longitudinal tip-over criterion at the most aft C.G.

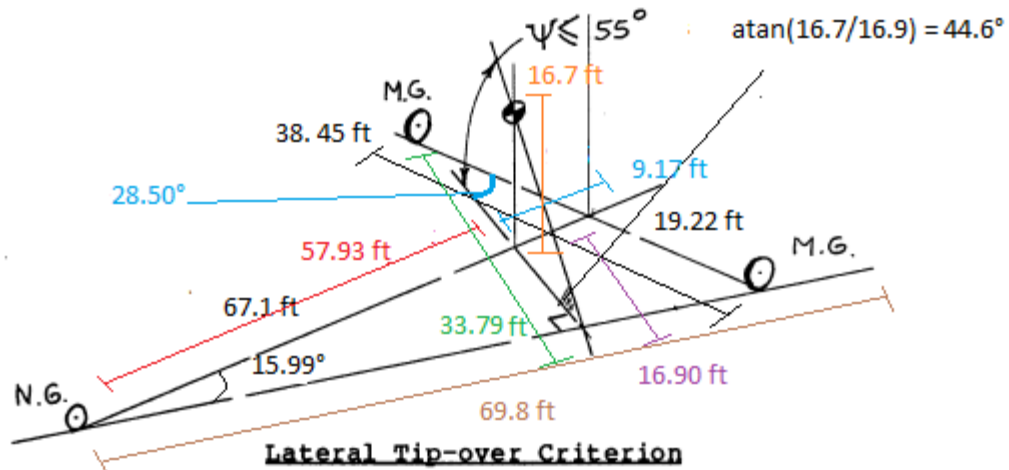


Figure 8.9. Lateral tip-over criterion at the most forward C.G.

The longitudinal tip-over criterion seems reasonable for the blended wing body, even though at the most forward center of gravity there is an angle of 28.77 degrees. Since the longitudinal tip-over angle is not above 40 degrees, the longitudinal placement of the main landing gear should be sufficient. The landing gear arrangement also meets the lateral tip-over criterion. The 44.6-degree angle meets the 55 degrees or less lateral tip over criterion.

8.3.4. Retraction Feasibility

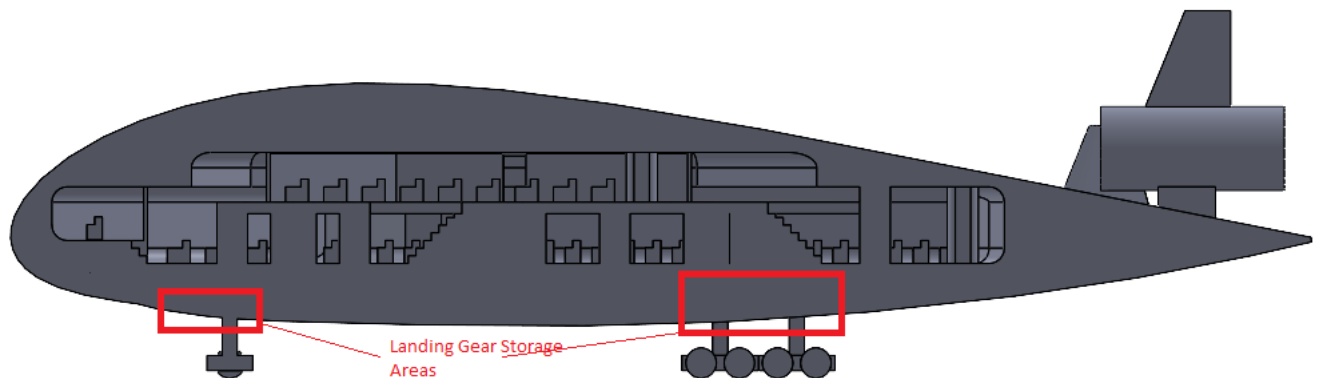


Figure 8.10. Retraction feasibility of landing gears

There is an ample amount of space underneath the cabin for the retraction of the landing gear. As a result, there should be no issues during retraction during takeoff and landing. Landing gear retraction should be used to improve the aerodynamic efficiency of the aircraft.

8.4 Discussion

This chapter discusses the methodology and engineering design choices concerning the landing gear. The tires sizes and specifications seem reasonable because other commercial large airliners like the Boeing 747-400 have comparable tire size and tire pressure. The nose landing gear will need to absorb an above-average amount of loading when compared to other airliners due to the distance between the center of gravity and the main landing gear. The main landing gear is designed to be 85.77 feet from the nose to meet the longitudinal ground clearance criterion. Ideally, the landing gear should be closer to the center of gravity to minimize the nose landing gear load ratio; however, the ground clearance criterion needs to be prioritized to ensure a safe takeoff and landing. The current landing gear arrangement satisfies all the ground clearance and tip-over criteria. The aircraft's fuselage also has an ample amount of room for the landing gear, making retraction a feasible option.

9. Weight & Balance Analysis

9.1 Introduction

This chapter discusses the weight breakdown of the various components in the aircraft. Understanding weight and balance are crucial in determining aircraft stability and landing. In addition, learning the change in center of gravity during cruise flight and other scenarios is important in understanding if the aircraft will be stable. The moment-arm will also need to be accounted for since a blended wing body will have issues with high downward pitching due to the lack of a horizontal stabilizer. Weight and balance will be analyzed using the methods below:

- Weight Breakdown in the X-Direction
- Weight Breakdown in the Z-Direction
- CG Excursion Diagram

9.2 Component Weight Breakdown

Weights of the individual components are calculated using Raymer's Aircraft Design textbook [22]. In chapter 15 of this textbook, a series of equations are provided to estimate the various individual component weights. In-depth calculations of these components are shown in the appendix.

The location of the center of gravity is approximated using the SolidWorks model in chapter 4; however, not every component is modeled. These values are approximated based on an assumed location in the SolidWorks model.

Both values are put into an Excel spreadsheet which approximates the center of gravity and calculates the moment arm. The center of gravity and moment-arm calculations uses equations from Raymer's Aircraft Design textbook. This spreadsheet can calculate these values for maximum gross takeoff weight, no payload scenario, no fuel scenario, and empty weight.

Table 9.1. CG inputs in Excel for the X-location

	Weight lbs or kg	X-Location ft or m	Moment ft-lbs or kg-m
STRUCTURES GROUP	421796	74.7	31493290.6
Wing	145241	79	11474039.0
Horiz. Tail	0	0	0.0
Vert. Tail	5984	140.33	839734.7
Fuselage	228158	66.39	15147409.6
Main Lndg Gear	29410	85.77	2522495.7
Nose Lndg Gear	2590	18.67	48355.3
Engine Mounts	10413	140.33	1461256.3
Firewall	0	0	0.0
Engine Section	0	0	0.0
Air Induction	0	0	0.0
			0.0
			0.0
PROPULSION GROUP	42837.0	134.1	5743933.6
Engine(s)	38632	140.33	5421228.6
Tailpipe	0	0	0.0
Engine Cooling	0	0	0.0
Oil Cooling	0	0	0.0
Engine Controls	148	15	2220.0
Starter	348	15	5220.0
Fuel System	3709	85	315265.0
			0.0
			0.0
EQUIPMENT GROUP	19362.0	57.9	1121720.0
Flight Controls	1924	20	38480.0
Instruments	763	20	15260.0
Hydraulics	578	20	11560.0
Electrical	541	20	10820.0
Avionics	2422	25	60550.0
Furnishings & Misc	7608	75	570600.0
Air Conditioning	5241	75	393075.0
Handling Gear	285	75	21375.0
APU installed	0	0	0.0
Misc Empty Weight	0	0	0.0
			0.0
			0.0
			0.0
			0.0

Table 9.2. CG outputs in Excel for the X-location

We-Allowance	0.0	79.3	0.0
EMPTY WEIGHT	483995.0	79.3	38358944.2
USEFUL LOAD GROUP	466005.0	76.7	35751400.0
Crew	2800	25	70000.0
Passengers			
Payload	125000	69	8625000.0
Fuel (weight available)	338205.0	80	27056400.0
Oil	0	0	0.0
			0.0
			0.0
			0.0
TAKEOFF GROSS WEIGHT	950000	78.0	74110344.2
	Fuel-Out CG	76.9	
	Payload-Out CG	79.4	

Table 9.3. CG inputs in Excel for the Z-location

	Weight lbs or kg	Z-Location ft or m	Moment ft-lbs or kg-m
STRUCTURES GROUP	421526	0.1	56083.1
Wing	145241	0.41	59548.8
Horiz. Tail	0	0	0.0
Vert. Tail	5984	16.33	97718.7
Fuselage	228158	1.04	237284.3
Main Lndg Gear	29140	-16	-466240.0
Nose Lndg Gear	2590	-16	-41440.0
Engine Mounts	10413	16.25	169211.3
Firewall	0	0	0.0
Engine Section	0	0	0.0
Air Induction	0	0	0.0
			0.0
			0.0
PROPULSION GROUP	42837.0	14.7	627770.0
Engine(s)	38632	16.25	627770.0
Tailpipe	0	0	0.0
Engine Cooling	0	0	0.0
Oil Cooling	0	0	0.0
Engine Controls	148	0	0.0
Starter	348	0	0.0
Fuel System	3709	0	0.0
			0.0
			0.0
EQUIPMENT GROUP	19362.0	0.0	0.0
Flight Controls	1924	0	0.0
Instruments	763	0	0.0
Hydraulics	578	0	0.0
Electrical	541	0	0.0
Avionics	2422	0	0.0
Furnishings & Misc	7608	0	0.0
Air Conditioning	5241	0	0.0
Handling Gear	285	0	0.0
APU installed	0	0	0.0
Misc Empty Weight	0	0	0.0
			0.0
			0.0
			0.0
			0.0

Table 9.4. CG outputs in Excel for the Z-location

We-Allowance	222513.5	1.4	314572.4
EMPTY WEIGHT	483725.0	1.4	683853.1
USEFUL LOAD GROUP	466275.0	-1.8	-855870.0
Crew	127800	-1.4	-178920.0
Passengers			
Payload	0	0	0.0
Fuel (weight available)	338475.0	-2	-676950.0
Oil	0	0	0.0
			0.0
			0.0
			0.0
TAKEOFF GROSS WEIGHT	950000	-0.2	-172016.9
	Fuel-Out CG	0.8	
	Payload-Out CG	-0.2	

9.3 Component Weight Breakdown

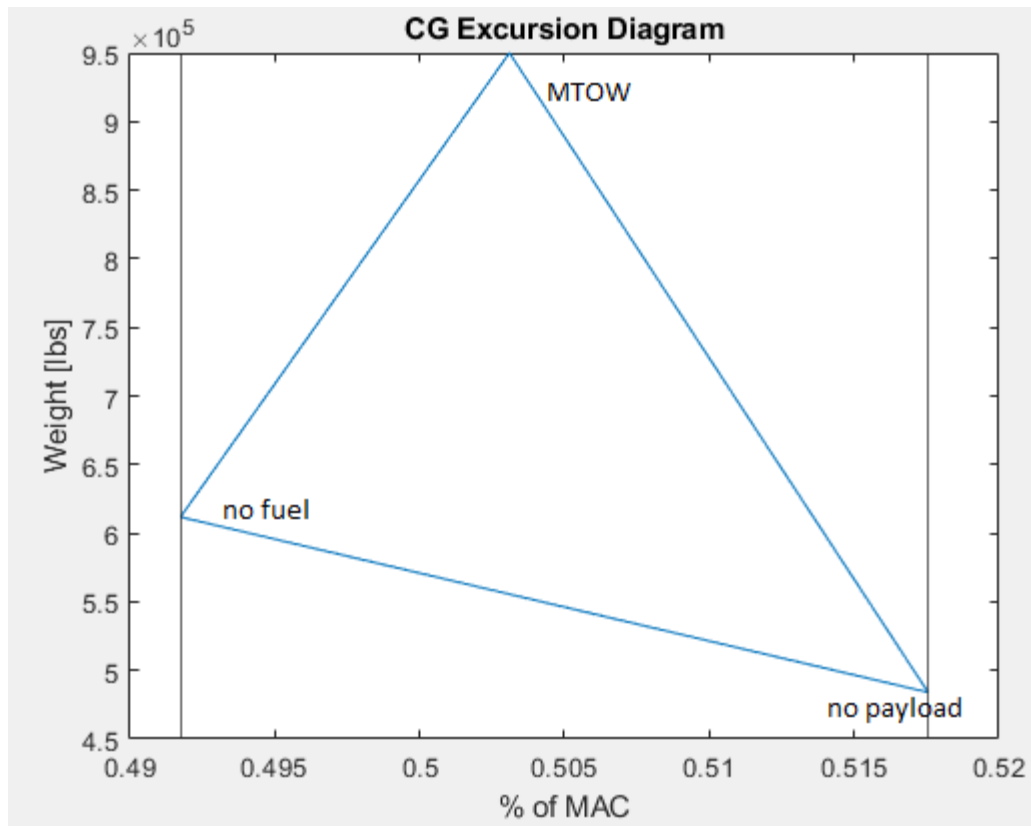


Figure 9.1. CG excursion diagram

9.4. Discussion

In chapter 2, the weight was approximated as below.

- $W_P = 127,800$ lbs
- $W_E = 440,300$ lbs
- $W_F = 374,000$ lbs

When calculating the individual components using Raymer's equations [22], the general weight distribution are as follows:

- $W_P = 127,800$ lbs
- $W_E = 483,995$ lbs
- $W_F = 338,205$ lbs

The empty weight of the aircraft is 40,000 lbs more than estimated, which means that the fuel weight is 40,000 lbs less. This will result in roughly a 10% decrease in range. The center of gravity of the aircraft tends to be around the 50% mean aerodynamic chord. This is because of the "airfoil" cross-section that the blended wing body aircraft possesses. Since an airfoil has more structure in the front, most of the weight will be distributed to the front. To counteract this extra weight, the engines are placed towards the rear of the aircraft instead of under the wing-like most conventional airliners.

10. Stability Analysis

10.1 Introduction

This chapter will briefly discuss the stability analysis performed on this aircraft. Specifically, the static margin and its feasibility for the blended wing body aircraft. Static margin is important for the stability of the aircraft since it allows the engineer to determine the center of gravity limits. If the center of gravity manages to fall out of these limits, then the engineer must re-evaluate the position of several aircraft components or develop a control system such that the center of gravity is within these limits.

10.2 Static Margin

The two most important center of gravity values is the most forward and aft center of gravity. These values were calculated in chapter 9. To calculate the static margin or SM, the following items are needed:

- Center of gravity
- Mean aerodynamic chord
- Neutral Point

The neutral point is calculated through XFLR5 which was determined to be 87.725 ft. The most forward and aft center of gravity points are 76.6 ft and 79.4 ft, which correlates to when the aircraft is out of fuel and the empty weight of the aircraft respectively. Using this equation, the most forward and most aft static margin values can be calculated.

$$\text{Static Margin} = (X_{NP} - X_{CG})/MAC \times 100 \quad (10.1)$$

For the most forward center of gravity:

$$\text{Static Margin} = \frac{87.725 - 76.9}{96.84} \times 100 = 11.18\%$$

For the most aft center of gravity:

$$\text{Static Margin} = \frac{87.725 - 79.4}{96.84} \times 100 = 8.60\%$$

10.3 Discussion

The static margin was calculated to be 11.18% of the aerodynamic mean chord for the most forward CG limit and 8.60% of the aerodynamic mean chord for the most aft CG limit. Both values seem reasonable for a blended wing body aircraft. These limits imply that the center of gravity of the aircraft makes it inherently stable. In addition, the relatively low static margin means that the inherent pitching moment caused by the aircraft is not high. This improves the stability of the blended wing body due to the blended wing body's lack of a horizontal stabilizer.

11. Drag Polar Estimation

11.1 Introduction

This chapter will briefly discuss the drag polar of this aircraft. Drag polar estimation is important to determine the predicted aerodynamic efficiency of an aircraft. The drag polar is determined by the wetted area of the aircraft. Using SolidWorks, the surface area of the aircraft can be calculated and used as the wetted area in many of the drag polar calculations. Using Roskam's method [19] for calculating the drag polar, graphs of the lift-drag ratio will be generated for the clean, takeoff, and landing scenarios. The airplane's wetted area will include the following:

- Wing
- Fuselage
- Vertical Tail
- Engine Nacelles

In chapter 3, the wetted area was estimated to be 33,000 ft². The SolidWorks model approximated it to be 37,854 ft².

11.2 Drag Polars

Judging from the Roskam's Equivalent Parasitic Area vs Wetted Area graph in figure 3.3, an equivalent parasitic area of 100 ft² was estimated; however, the wetted area through SolidWorks is larger. Through extrapolation, the parasitic area can be approximated to be 114 ft². The Parasitic drag can be calculated with:

- Equivalent parasitic area: 114 ft²
- Wing area: 16,284 ft²
- $c_r = \text{equivalent parasitic area/wetted area} = 114/37,854 = \mathbf{0.0030}$

Using this equation: $C_{D_0} = \frac{100}{16,284} = 0.0061$

In addition to calculating parasitic drag, compressibility drag will also be looked at. In Roskam's textbook, a Mach number vs. Zero Lift Drag rise is provided.

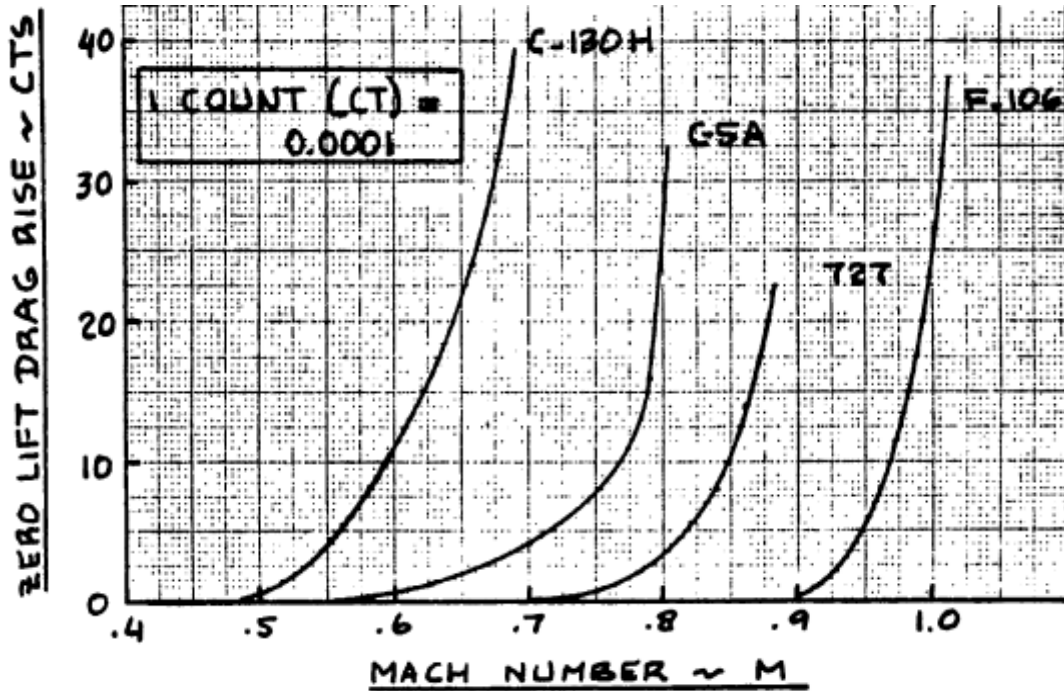


Figure 11.1. Typical compressibility drag behavior

From the graph, the compressible drag increment for Mach 0.80 approximates to be 0.0003. Drag compressibility is negligible for subsonic speeds, but since the blended wing body aircraft is expected to be traveling at transonic speeds, the drag compressibility needs to be analyzed.

$$C_D = C_{D_0} + \frac{C_L^2}{\pi e AR} \rightarrow C_D = 0.0061 + \frac{C_L^2}{\pi(0.85)(4.9)} \quad (11.1)$$

Referring to Roskam's table for C_D increments of adding flaps and putting the gear down. A configuration table can be created.

Table 11.1. Roskam's estimate for C_D increments [14]

Configuration	ΔC_{D_0}	e
Clean	0	0.80 - 0.85
Take-off flaps	0.010 - 0.020	0.75 - 0.80
Landing Flaps	0.055 - 0.075	0.70 - 0.75
Landing Gear	0.015 - 0.025	no effect

Table 11.2. Drag polar data for various configurations

Configuration	C_{D0}	AR	e	C_{Di}	C_{LMAX}	L/D_{max}
Clean	0.0061	4.9	0.85	$0.076C_L^2$	1.5	23.1
Take-off Flaps, Gear up	0.016	4.9	0.80	$0.081C_L^2$	1.9	13.87
Take-off Flaps, Gear down	0.031	4.9	0.80	$0.081C_L^2$	1.9	9.97
Landing Flaps, Gear Up	0.066	4.9	0.75	$0.086C_L^2$	2.1	6.61
Landing Flaps, Gear Down	0.083	4.9	0.75	$0.086C_L^2$	2.1	5.89

L/D_{max} was calculated using the following equation:

$$\frac{L}{D_{max}} = \sqrt{\frac{\pi(A)e}{4C_{D_0}}} \quad (11.2)$$

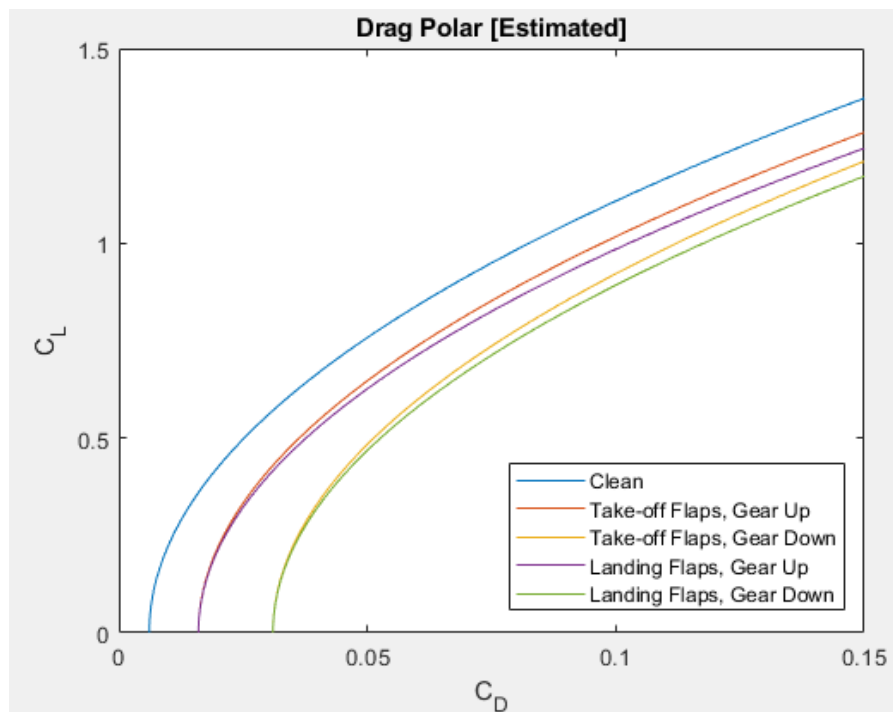


Figure 11.2. Manually calculated drag polar estimation for various configuration

11.3 XFLR5 Calculations

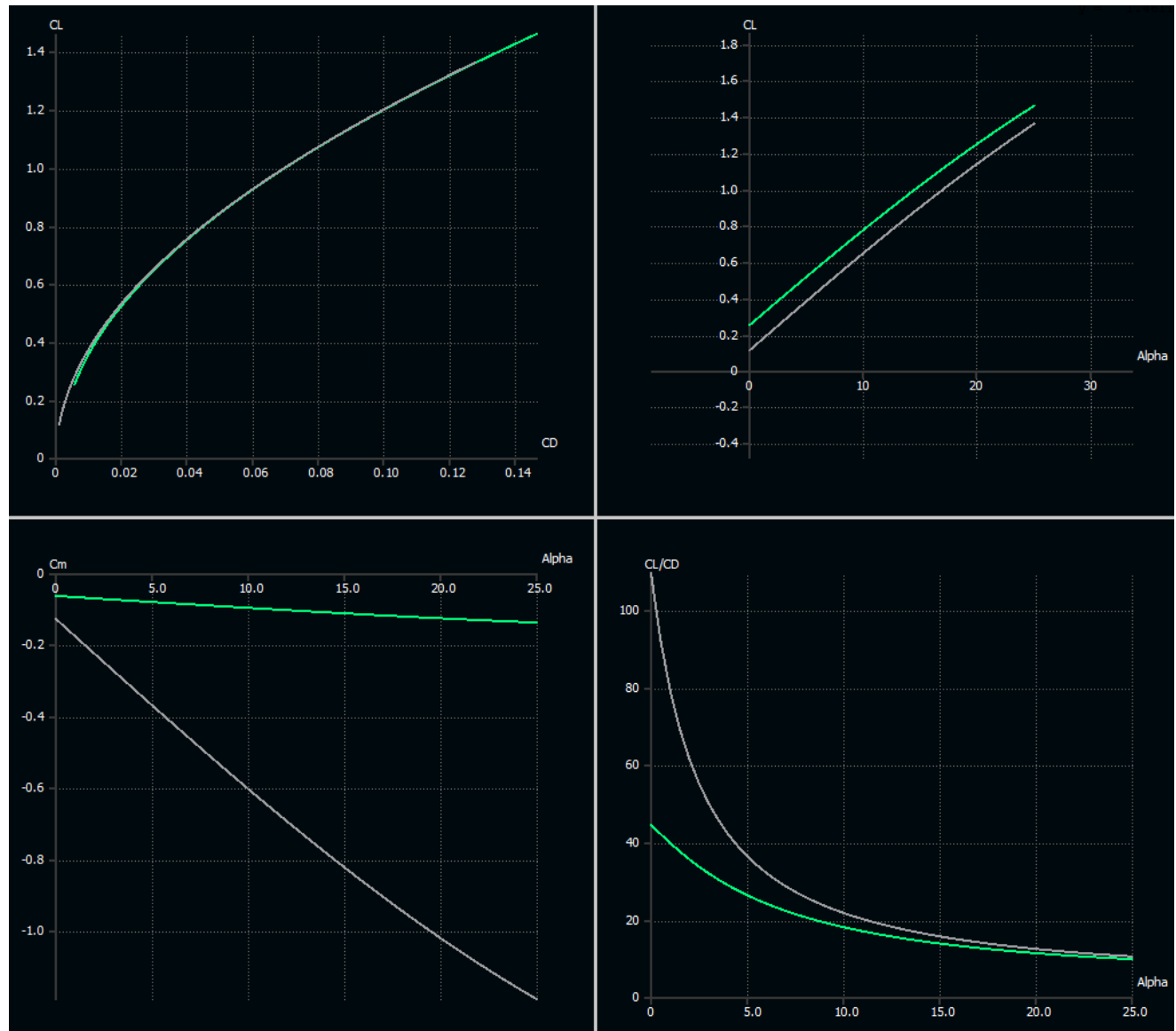


Figure 11.3. XFLR5 calculations for cruise clean (white) and takeoff (green) configurations

11.4 Discussion

The lift to drag ratio is noticeably lower during take-off and landing. In addition, having the landing gear retracted increases the lift to drag ratio as seen in figure 11.2. It should be noted that values in XFLR5 have some margin of error since XFLR5 tends to underestimate the impacts of drag during flight. The wetted area and total area of the aircraft were slightly above what was approximated in chapter 3.

12. Drawings, Environmental and Safety Considerations

12.1 Drawings

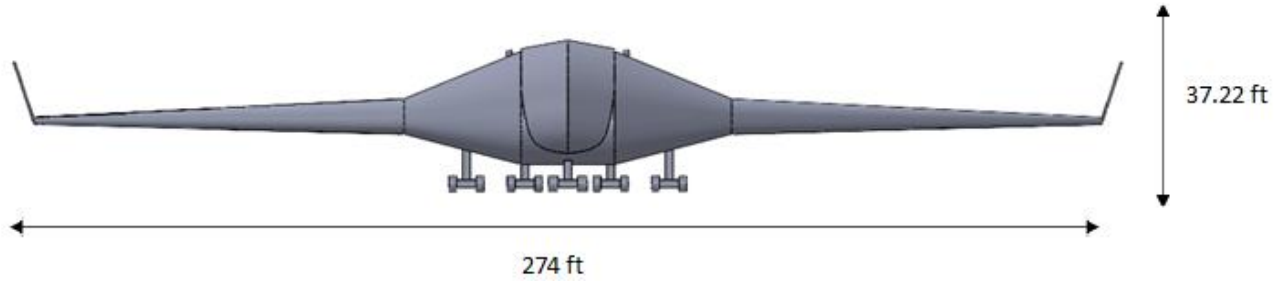


Figure 12.1. Front view of modeled blended wing body aircraft

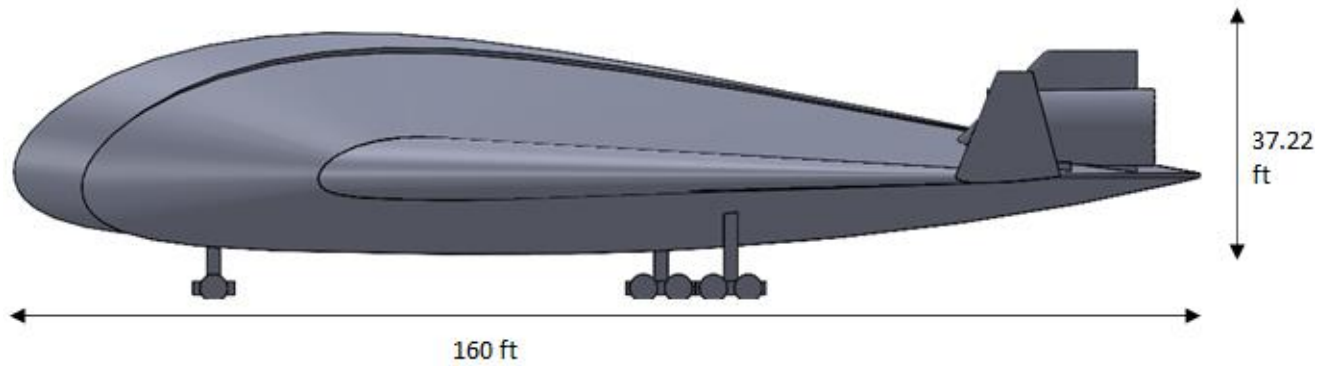


Figure 12.2. Side view of modeled blended wing body aircraft

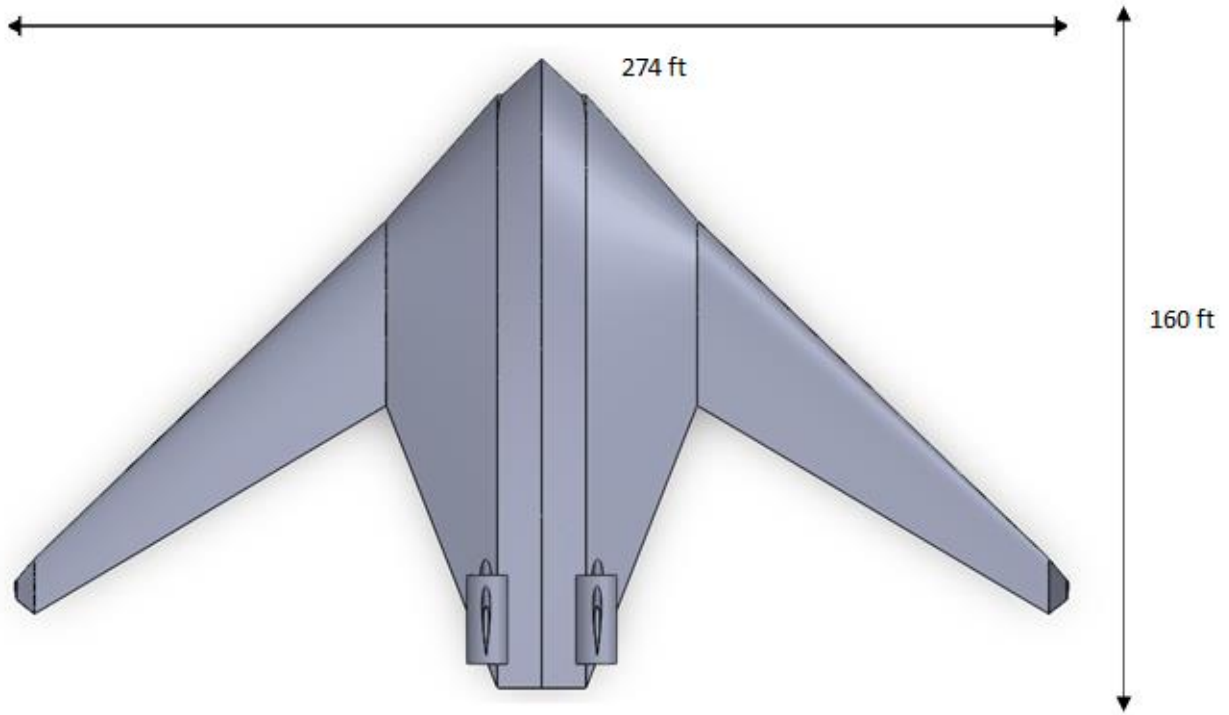


Figure 12.3. Top view of modeled blended wing body aircraft

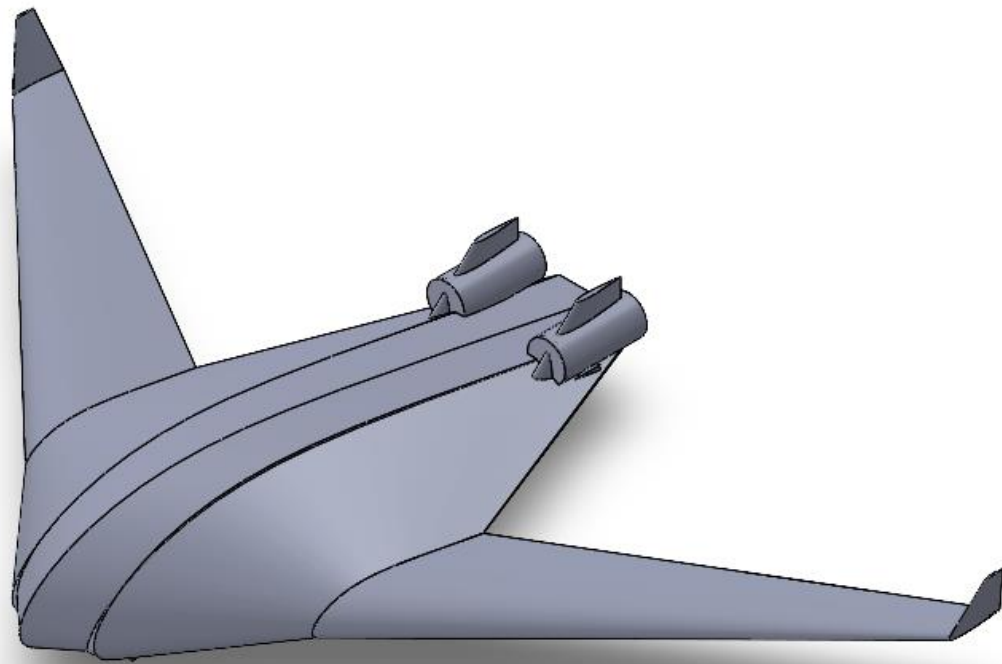


Figure 12.4. Iso view of modeled blended wing body aircraft

Table 12.1. Blended wing body aircraft parameters

	Wing-Fuselage	Vertical Stabilizer
Area	16,445 ft ²	1,232 ft ² =
Span	284 ft	28 ft
Mean Geometric Chord	96.84 ft	22.00 ft
Aspect Ratio	4.91	2.55
Sweep Angle	36.81°	25.74°
Taper Ratio	0.03	0.42
Airfoils	NACA 25118 for Fuselage SC-20412 for Wing	NACA 0012
Thickness Ratio	18% for Fuselage 12% for Wing	12%
Elevons Span	0.05 to 0.90 of Wing	N/A

12.2 Environmental Considerations

The main advantage of designing a blended wing body would be its improved aerodynamic efficiency. A research paper estimated that the geometric shape and configuration of a blended wing body aircraft could potentially burn 27% less fuel [4]. Fuel consumption would reduce with the use of a blended wing body aircraft and therefore reduce aircraft gas emissions. Many research papers have investigated a blended wing body design 10 years ago and it has been widely agreed upon that its aerodynamic efficiency would positively impact the aviation industry. In addition, the complex shape would increase costs in manufacturing the fuselage. A blended winged body is uniquely shaped as opposed to a tube and wing where the tube-like fuselage is a lot easier to manufacture due to its simplistic shape. In addition, more research and engineering would have to be put in due to the design being unconventional. Many large aircraft manufacturing companies like Boeing and Airbus would need to pour a lot of their manpower into developing these advanced aircraft designs; however, the auditorium-like cabin will allow more passenger capacity. Overall, this should environmentally benefit the world in the long run because of the reduction in gas emissions due to its efficiency in the next following decades.

12.3 Safety Considerations

One of the main reasons that blended wing body aircraft are not commercially available is due to their safety concerns. Their control authority and inherent low stability makes them less reliable than a conventional tube and wing aircraft. The lack of a horizontal stabilizer makes it difficult for the aircraft to be stable during flight. A NASA report also claims that passengers felt uncomfortable due to the aircraft landing at high angles of attack. The “auditorium-like” cabin for the passengers also makes it more difficult for people seated in the middle of the aircraft to evacuate during an emergency [2].

13. Drag Polar Estimation – Class II

13.1 Introduction

In chapter 11, an overall prediction of the drag that the aircraft will experience was analyzed at subsonic speeds due to the capabilities of XFLR5. This chapter will cover a more thorough analysis of various drag contributors to the aircraft during flight, such as the wings, empennage, and the nacelle. Since the blended wing body aircraft does not have a standard fuselage, the drag coefficient from the fuselage will not be considered. Instead, the drag coefficient of the fuselage and the wing will be modeled as one large wing. It should be noted that these drag polar calculations are calculated at transonic flight and are based on Roskam's textbook [23].

13.2 Wing Drag Estimation

Wing drag estimation can be determined by summing the zero-lift drag coefficient and the lift drag coefficient term. The zero-lift drag coefficient term is split into two terms: when Mach number is equal to 0.60, and the wave drag coefficient at the sweep angle.

$$C_{D_{wing}} = C_{D_{0W}} + C_{D_{LW}} \quad (13.1)$$

$$C_{D_{0W}} = C_{D_{0w@M=0.6}} + C_{D_{wwave}} \quad (13.2)$$

The following values are from chapter 6 of the report and from Roskam's [23] assumptions which will be used in the below equations.

- $\Lambda_c = 36.81^\circ$
- $L' = 1.2$
- $\frac{t}{c} = 0.18$
- $\frac{S_{wetw}}{S} = \frac{33,000}{16,284} = 2.027$

To determine the drag coefficient when Mach number is equal to 0.60 the following values must be defined.

- R_{wf} , the wing/fuselage interference factor
- R_{LS} , the lifting surface correction factor
- C_{fw} , turbulent flat plate friction coefficient of the wing

$$C_{D_{0w@M=0.6}} = (R_{wf}) * (R_{LS}) * (C_{fw}) \left(1 + L' \left(\frac{t}{c}\right) + 100 \left(\frac{t}{c}\right)^4 \frac{S_{wetw}}{S}\right) \quad (13.3)$$

$R_{wf} = 1$, the wing/fuselage interference factor will be assumed to be 1.0 because of the blended wing body shape.

$R_{LS} = 1.21$, which was determined by approximating the value using figure 13.1.

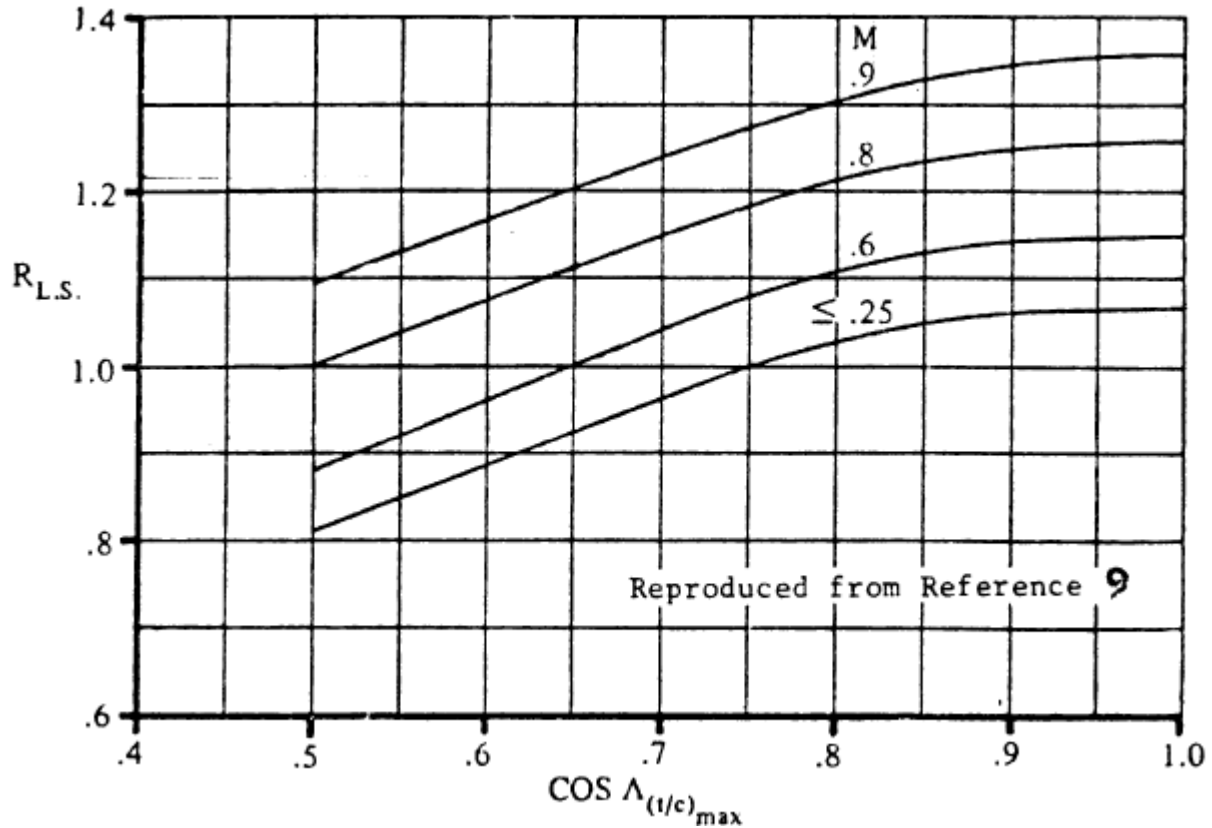


Figure 13.1. Lifting surface correction factor [23]

C_{fw} , can be determined by calculating the Reynolds number using equation 13.4 and using figure 13.2.

$$R_{Nw} = \frac{\rho U_1 c_{we}}{\mu} \quad (13.4)$$

$$R_{Nw} = \frac{\left(7.38 \times 10^{-4} \frac{\text{slugs}}{\text{ft}^3}\right) \left(778.08 \frac{\text{ft}}{\text{s}}\right) (29.28 \text{ ft})}{3.053 \times 10^{-7} \frac{\text{slugs}}{\text{ft}} * \text{sec}} = 5.50 \times 10^7$$

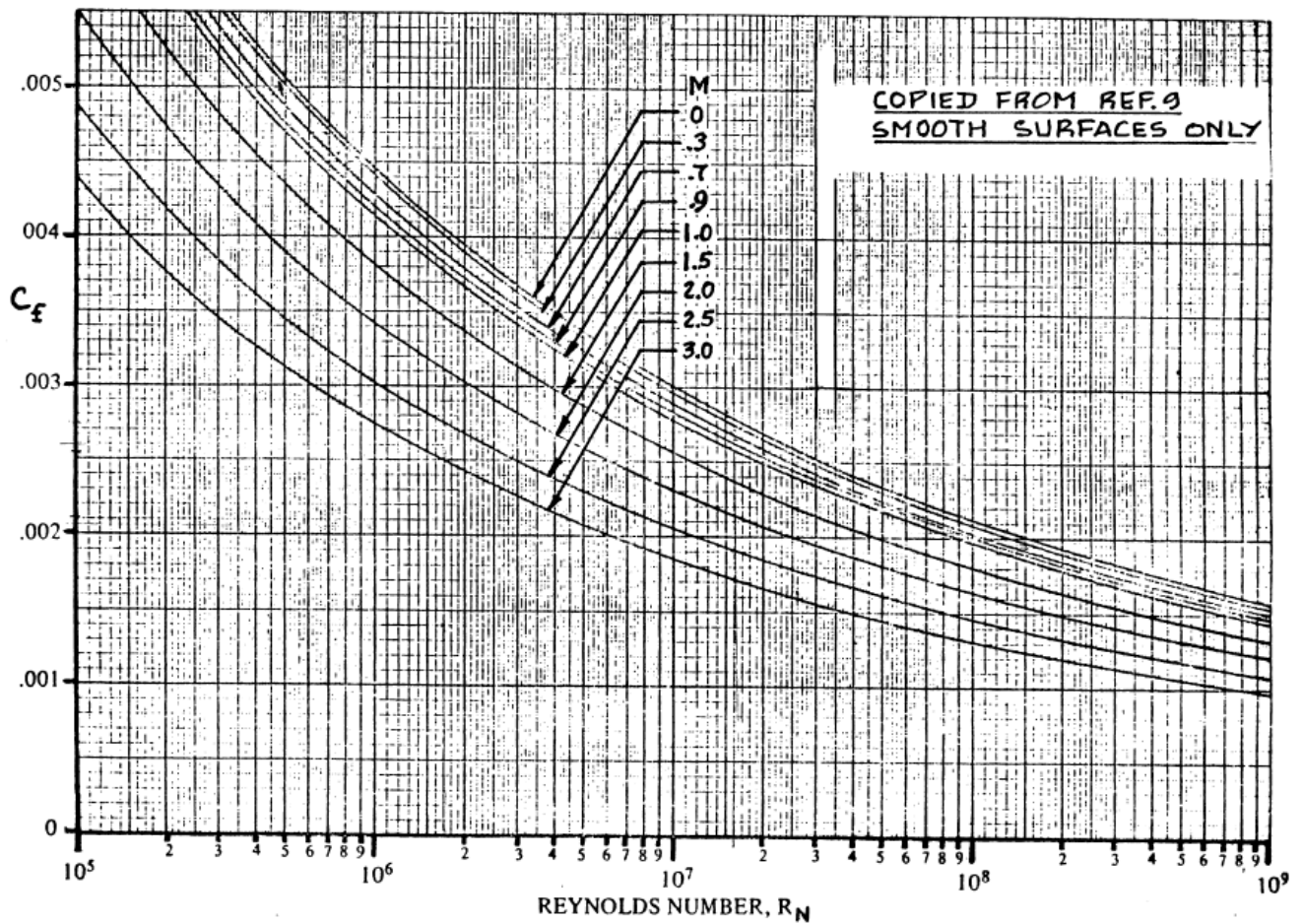


Figure 13.2. Turbulent mean skin-friction coefficient [23]

$$C_{f_w} = 0.0025$$

The zero-lift drag coefficient at Mach=0.60 can be determined, using the values that were approximated.

$$C_{D_{0w@M=0.6}} = (1) * (1.21) * (0.0025)(1 + 1.2(0.18) + 100(0.18)^4) * 2.027 = 8.10 * 10^{-3}$$

The wave drag coefficient at the sweep angle can be determined using figure 13.3 and the following parameters:

- $A \frac{t}{c}^{\frac{1}{3}} = 2.77$
- $M = 0.80$

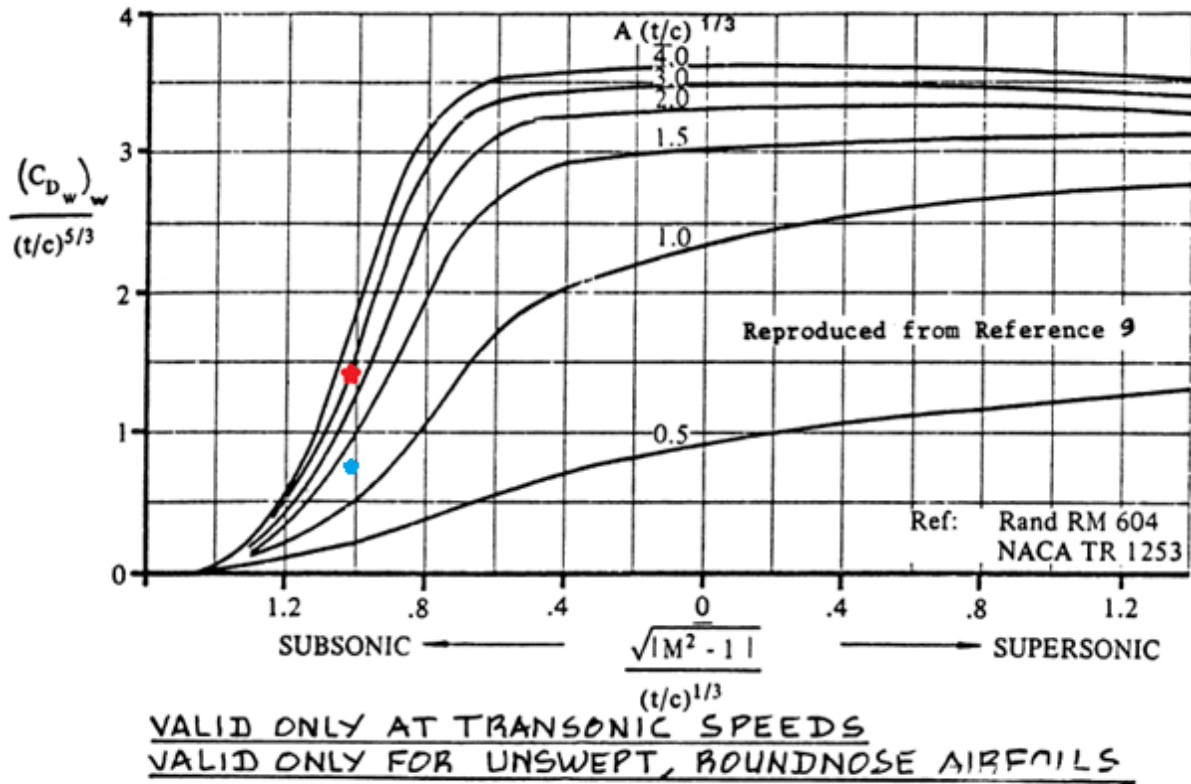


Figure 13.3. Zero-lift wave drag coefficient [23]

The approximated wave drag coefficient is located at the red marker in figure 13.3.

$$C_{D_{wwave}} = 0.0717$$

Using the sweep angle with equation 13.5 gives the wave drag coefficient at the sweep angle.

$$C_{D_{wwavesweep}} = C_{D_{wwave}} * \cos^{2.5} \left(\frac{\Lambda_c}{4} \right) \tag{13.5}$$

$$C_{D_{wwave_sweep}} = 0.0411$$

The summation of the zero-lift drag coefficient at Mach = 0.60 and the wave drag coefficient at the sweep angle is the zero lift drag of the wing.

$$C_{D_{0W}} = C_{D_{0W@M=0.6}} + C_{D_{wwave}} = 8.10 * 10^{-3} + 0.0411 = 0.0492$$

The drag coefficient caused by lift can be determined using a similar graph.

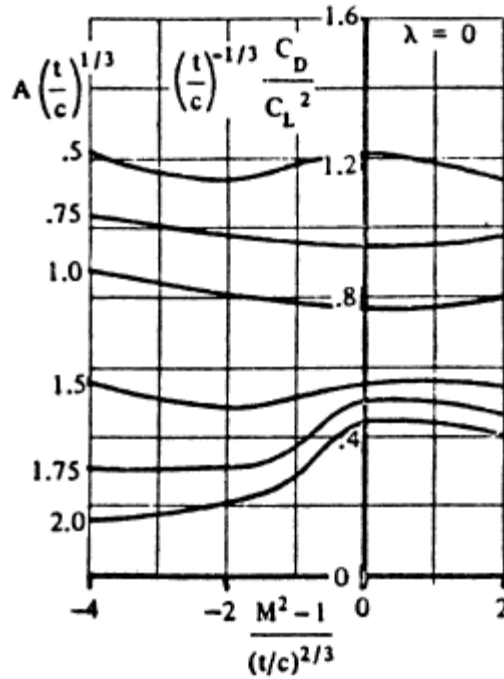


Figure 13.4. Transonic drag due to lift from the wing[23]

$$C_{D_{LW}} = \frac{C_D}{C_L^2} * C_L^2 \quad (13.6)$$

$$\frac{C_D}{C_L^2} = 0.169$$

The total drag coefficient from the wings is approximated to be:

$$C_{D_{wing}} = 0.0492 + 0.169C_L^2$$

13.3 Empennage Drag Estimation

Calculations for the empennage drag estimation are like the wing drag estimation; however, since the blended wing body configuration uses a twin tail empennage design, the coefficient of drag from the empennage is doubled.

$$C_{D_{emp}} = 2(C_{D_{0emp}} + C_{D_{Lemp}}) \quad (13.7)$$

$$C_{D_{0emp}} = C_{D_{0emp@M=0.6}} + C_{D_{empwave}} \quad (13.8)$$

$$C_{D_{0emp@M=0.6}} = (R_{empf}) * (R_{LS}) * (C_{f_{emp}}) \left(1 + L' \left(\frac{t}{c} \right) + \frac{100 \left(\frac{t}{c} \right)^4 S_{wetemp}}{S} \right) \quad (13.9)$$

Since the equations are almost identical, refer to equation 13.2 for a detailed explanation of how to calculate the zero-lift drag coefficient and drag coefficient from lift.

- $R_{empf} = 1$
- $\Lambda_{\frac{c}{4}} = 25.74^\circ$
- $R_{wf} = 1.25$
- $L' = 2$
- $\frac{t}{c} = 0.12$
- $\frac{S_{wetemp}}{S} = \frac{1236}{16284} = 0.0759$

$$R_{Nemp} = \frac{\rho U_1 c_{we}}{\mu} \quad (13.10)$$

$$R_{Nemp} = \frac{\left(7.38 * 10^{-4} \frac{slugs}{ft^3}\right) \left(778.08 \frac{ft}{s}\right) (154.62 ft)}{3.053 * 10^{-7} \frac{slugs}{ft} * sec} = 2.90 * 10^8$$

Refer to figures 13.1 and 13.2 to determine lifting surface correction factor and the turbulent skin friction coefficient respectively.

$$C_{fW} = 0.0017$$

$$C_{D_{0emp@M=0.6}} = 2.03 * 10^{-4}$$

$$A \frac{1}{c^{\frac{1}{3}}} = 1.26$$

$$C_{D_{empwave}} = 0.0219$$

$$C_{D_{wwavesweep}} = C_{D_{wwave}} * \cos^{2.5} \left(\Lambda_{\frac{c}{4}} \right) \quad (13.11)$$

$$C_{D_{wwave_sweep}} = C_{D_{wwave}} * \cos^{2.5} \left(\Lambda_{\frac{c}{4}} \right) = 0.0169$$

The zero-lift drag coefficient from the empennage is approximated to be.

$$C_{D_{0emp}} = C_{D_{0emp@M=0.6}} + C_{D_{empwave}} = 2.03 * 10^{-4} + 0.0169 = 0.0171$$

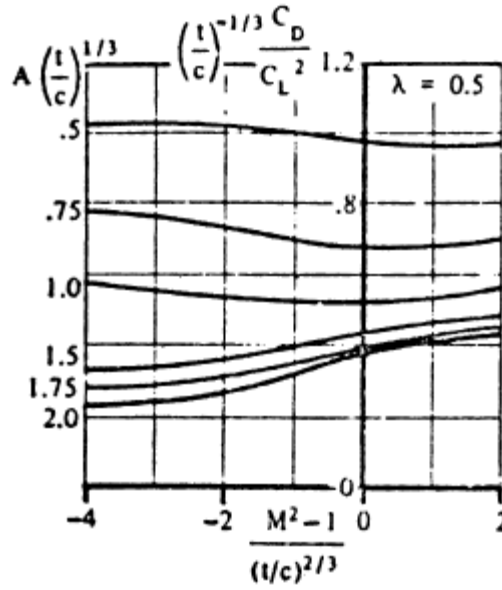


Figure 13.5. Transonic drag due to lift from the empennage [23]

$$C_{DLemp} = \frac{C_D}{C_L^2} * C_L^2 \quad (13.12)$$

$$\frac{C_D}{C_L^2} = 0.247$$

The drag coefficient from the empennage can be summarized with the following:

$$C_{Demp} = 2 * (0.0171 + 0.246C_{Lemp}^2)$$

It should be noted that:

$$C_{Lemp} = \frac{C_L}{\pi A_c e_c} * \left(\frac{S_c}{S}\right) \quad (13.13)$$

$$\text{Therefore, } C_{Demp} = 2 * (0.0171 + 0.00243C_L^2)$$

13.4 Nacelle Drag Estimation

The drag coefficient from the nacelle will be modeled as a small fuselage. Since there are two engines, the drag coefficient will be multiplied by a factor of two.

$$C_{Dnac} = 2(C_{Dofus} + C_{DLfus}) \quad (13.14)$$

The zero-lift equation can be calculated using equation 13.15.

$$C_{Dofus} = R_{wf} (C_{Dffus} + C_{Dpfus}) + C_{Dbfus} + C_{Dwavefus} * \frac{S_{fus}}{S} \quad (13.15)$$

The following values are from chapter 4 and will be used to calculate the drag coefficient of the nacelle.

- $R_{w_f} = 1$
- $C_{f_{fus}} = 0.0017$
- $S_{wet_{fus}} = 1029.47 \text{ ft}^2$
- $l_f = 24.29 \text{ ft}$
- $d_f = 11 \text{ ft}$

Like the wing and the empennage drag calculations, the Reynolds number will need to be calculated to determine the turbulent mean skin-friction coefficient.

$$R_{N_{fus}} = \frac{\rho U_1 c_{w_{fus}}}{\mu} \quad (13.16)$$

$$R_{N_{fus}} = \frac{\left(7.38 * 10^{-4} \frac{\text{slugs}}{\text{ft}^3}\right) \left(778.08 \frac{\text{ft}}{\text{s}}\right) (151.5 \text{ ft})}{3.053 * 10^{-7} \frac{\text{slugs}}{\text{ft}} * \text{sec}} = 2.85 * 10^8$$

The skin-friction coefficient from the nacelle can be used to determine fuselage skin-friction drag coefficient at Mach = 0.60.

$$C_{D_{ffus}} = \frac{C_{f_{fus}} (S_{wet_{fus}})}{S} \quad (13.17)$$

$$C_{D_{ffus}} = \frac{0.0017(1029.47)}{16,284} = 1.075 * 10^{-4}$$

The fuselage drag pressure coefficient can be calculated using equation 13.18. The skin-friction coefficient at Mach = 0.60 is like the cruise flight value based off figure 13.2.

$$C_{D_{pfus}} = C_{f_{fus@M=0.6}} \frac{(60/(l_f/d_f))^3 + 0.0025 \left(\frac{l_f}{d_f}\right) * S_{wet_{fus}}}{S} \quad (13.18)$$

$$C_{D_{pfus}} = 3.496 * 10^{-4}$$

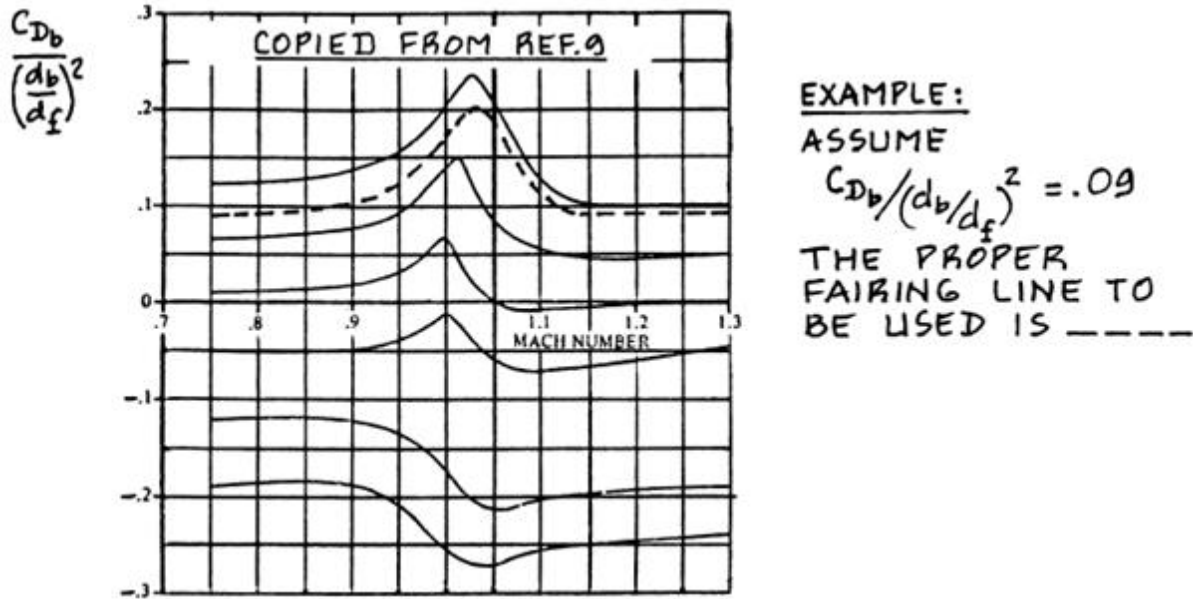


Figure 13.6. Transonic fairing for fuselage base drag coefficient [23]

$C_{D_{bfus}} = 0$, since a nacelle is a hollow cylinder, the diameter of the “base-fuselage” is effectively zero.

The fuselage wave drag coefficient can be approximated using figure 13.7.

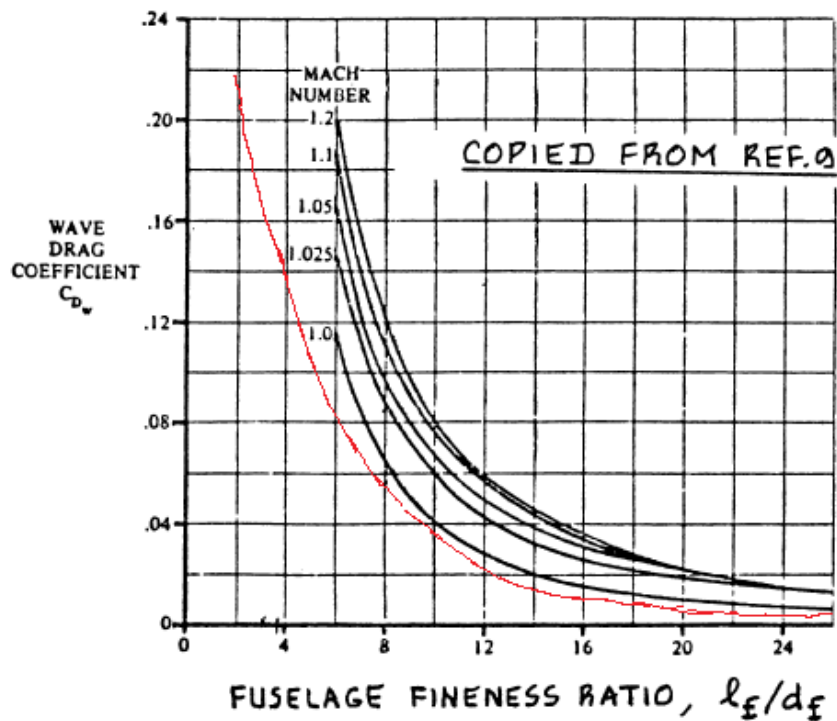


Figure 13.7. Wave drag coefficient for parabolic fuselages [23]

Through extrapolation, the wave drag coefficient of the nacelle is:

$$C_{D_{wavefus}} = 0.20$$

Summing the various zero-lift drag coefficient terms gives:

$$C_{D_{ofus}} = 1(1.075 * 10^{-4} + 3.496 * 10^{-4}) + 0 + 0.20 * \frac{1029.47}{16284} = 0.013$$

Equation 13.19 will be used to calculate the fuselage drag coefficient caused by lift.

$$C_{D_{Lfus}} = \alpha^2 \frac{S_{fus}}{S} \quad (13.19)$$

$$C_{D_{Lfus}} = \alpha^2 \frac{1029.47}{16284} = .0632\alpha^2$$

Equation 13.20 can be used to determine the angle of attack at which the airplane will be cruising at.

$$\alpha = \left(\left(\frac{W}{qS} \right) - C_{L_0} \right) C_{L\alpha} \quad (13.20)$$

$$\alpha = \frac{\left(\left(\frac{950,000}{\frac{1}{2} * 0.0237 * 778.08^2 * 16284} \right) - .12 \right)}{(3.037)} = -0.0368 \text{ radians} = -2.10^\circ$$

$$C_{D_{fus}} = 0.013 + .0632(-0.0368)^2 = 0.0131$$

$$C_{D_{nac}} = 2(C_{D_{ofus}} + C_{D_{Lfus}}) = 2(0.013 + 0.0131) = 0.0522$$

During cruise flight, the drag coefficient from the nacelles is effectively 0.0522. A more general equation for the drag coefficient caused by the nacelles is:

$$C_{D_{fus}} = 2(0.013 + .0632\alpha^2)$$

13.5 Flap Drag Estimation

Chapter 6 of this report has data pertaining to the geometry of the aircraft's flaps. Listed below are the constants and equations that will be used to calculate drag coefficient of the flaps.

- $c_f/c = 0.35$
- $\left(\frac{S_{wf}}{S} \right) = 0.30$

$$C_{D_{flap}} = \Delta C_{D_{prof_{flap}}} + \Delta C_{D_{i_{flap}}} + \Delta C_{D_{int_{flap}}} \quad (13.21)$$

To calculate the profile drag increment of plain flaps, figure 13.8 and equation 13.22 will be used.

$$\Delta C_{D_{prof_{flap}}} = \Delta C_{D_{p_{\Lambda_c=0}}} \cos \left(\frac{\Lambda_c}{4} \right) (S_{wf}/S) \quad (13.22)$$

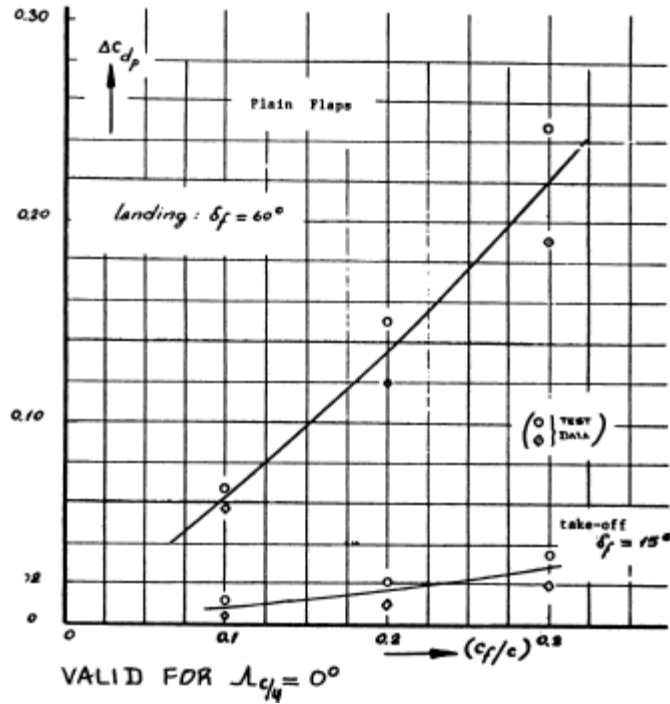


Figure 13.8. Profile drag increment: plain flaps [23]

$$\Delta C_{D_{prof\ takeoff}} = 0.25 \cos(36.81) (0.04) = 0.008$$

$$\Delta C_{D_{prof\ landing}} = 0.25 \cos(36.81) (0.30) = 0.060$$

The induced drag increment can be determined using equation 13.23 and figure 13.9. The spanwise uninterrupted flaps can be solved by dividing the area of the flaps by the chord. The aspect ratio is given from chapter 6.

$$\Delta C_{D_{iflap}} = K^2 \Delta C_{L_{flap}}^2 \cos\left(\frac{\Lambda_c}{4}\right) \quad (13.23)$$

- $\frac{b_f}{b} = \frac{\left(\frac{S_{wf}}{S}\right)}{\frac{c_f}{c}} = \frac{.30}{0.35} = 0.857$
- $A = 4.91$

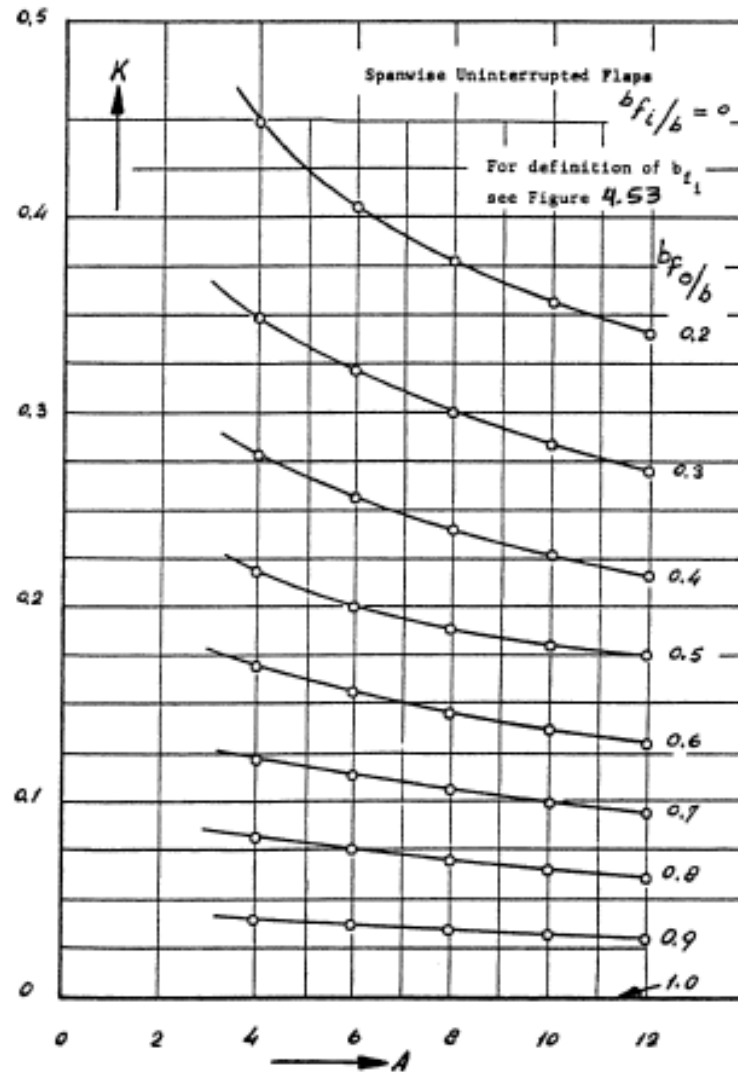


Figure 13.9. Induced drag factor for uninterrupted flaps [23]

$$\Delta C_{D_{iflap}} = (.07)^2(1.39)^2 \cos(36.81) = 0.00758$$

$$\Delta C_{D_{intflap}} = 0, \text{ since plain flaps are being used.}$$

The total drag coefficients from the flaps are calculated below:

$$C_{D_{flap_{takeoff}}} = 0.008 + 0.00758 + 0 = 0.0157$$

$$C_{D_{flap_{landing}}} = 0.060 + 0.00758 + 0 = 0.0676$$

13.6 Landing Gear Drag Estimation

The drag coefficient of a landing gear with multiple wheels per bogey is as follows:

$$C_{D_{gear}} = \Delta f_{gear} / S \quad (13.24)$$

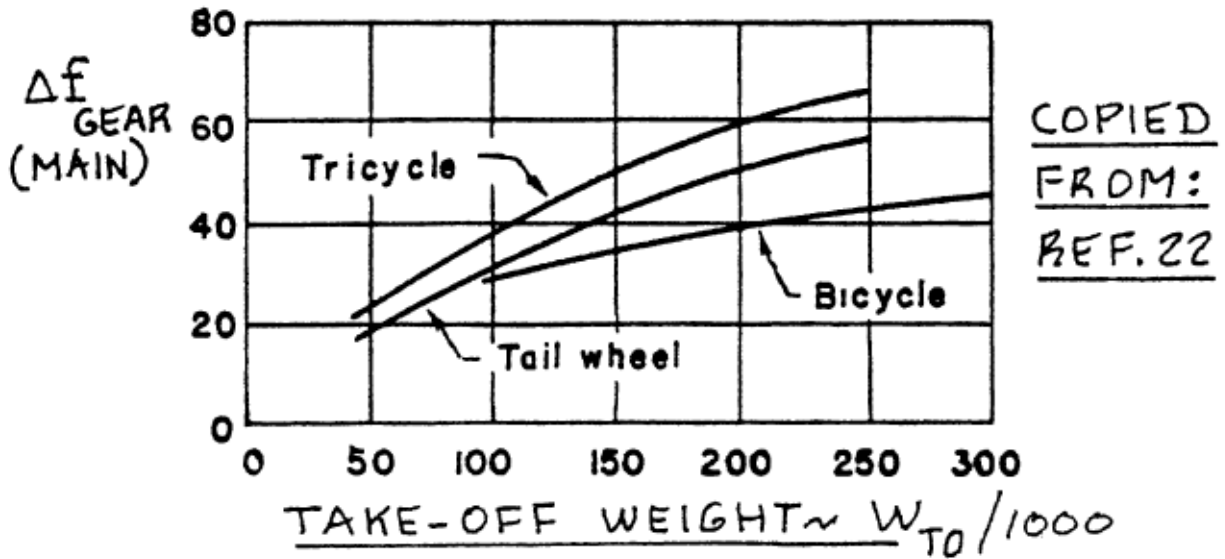


Figure 13.10. Equivalent parasitic area increment for gears with multiple wheel bogies [23]

Using Excel, a logarithmic regression equation was made to extrapolate when take-off weight was 950,000 lbs.

$$y = -78.61 + 25.61 \ln(x) \quad (13.25)$$

$$\Delta f_{gear} = 97$$

Plugging in the values from equation 13.23 gives a drag coefficient of:

$$C_{D_{gear}} = \frac{97}{16284} = 0.00595$$

13.7 Raymer's Calculations

Another method for calculating component drag coefficients is to use Raymer's equations [22]. For zero-lift drag, equations 13.25, 13.26, 13.27, and 13.28 can be used to approximate the zero-lift drag coefficients.

$$C_{D_0} = C_{f_c} FF_c Q_c S_{wet_c} / S_{ref} \quad (13.26)$$

- $C_{f_c} = 0.0030$, for a civil transport aircraft
- $Q_c = 1.0$, for the nacelle and wing and $Q_c = 1.03$, for the v-tail empennage
- FF_c represents the form factor and can be approximated as follows:

Wing, Tail:

$$FF = \left[1 + \frac{0.6}{\left(\frac{x}{c}\right)_m} \left(\frac{t}{c}\right) + 100 \left(\frac{t}{c}\right)^4 \right] \left[1.34 M^{.18} \cos^{0.28} \left(\Delta_c \frac{1}{4} \right) \right] \quad (13.27)$$

Nacelle:

$$FF = 1 + \left(\frac{0.35}{f} \right) \quad (13.28)$$

where,

$$f = \frac{l}{\sqrt{\left(\frac{4}{\pi}\right) A_{max}}} \quad (13.29)$$

The wing calculations are as follows:

$$FF = \left[1 + \frac{0.6}{0.37} (0.14) + 100(0.14)^4 \right] [1.34(0.8)^{.18} \cos^{0.28}(36.81)] = 1.530$$

$$C_{D_0} = 0.003(1.530)(1) * 2.027 = 0.00930$$

The tail calculations are as follows:

$$FF = \left[1 + \frac{0.6}{0.3} (0.12) + 100(0.12)^4 \right] [1.34(0.8)^{.18} \cos^{0.28}(25.74)] = 1.576$$

$$C_{D_0} = 2(0.003(1.576)(1.03) * 0.0759) = 0.000740$$

The nacelle calculations are as follows:

$$f = \frac{24.29}{\sqrt{\left(\frac{4}{\pi}\right) (\pi * 5.5^2)}} = 2.208$$

$$FF = 1 + \left(\frac{0.35}{2.208} \right) = 1.159$$

$$C_{D_0} = 2(0.003(1.159)(1) * \frac{1029.47(2)}{16284}) = 0.000880$$

In Raymer's textbook, drag coefficient increments are calculated with equation 13.30.

$$\Delta C_{D_{0_{flap}}} = 0.0023 \frac{b_f}{b} \delta_{flap} \quad (13.30)$$

Takeoff:

$$\Delta C_{D_{0_{flap}}} = 0.0023(0.857)(15) = 0.0296$$

Landing:

$$\Delta C_{D_{0_{flap}}} = 0.0023(0.857)(40) = 0.0788$$

The summation of the drag of the wheels and struts will determine the drag coefficient of the landing gear. In chapter 8, the planned landing gear system would have 18 wheels and tires, 5 bogeys, and 5 struts. When adding these values up and using table 13.1, the D/q value is approximately 12. According to Raymer's [22], this value is multiplied by 1.2 for mutual interference and another 1.07 for a retractable landing gear, giving a D/q value of 15.408. The D/q value can then be divided by the wing reference area to yield the zero-lift drag coefficient. This gives a value of 0.00948.

Table 13.1. Landing gear component drags [22]

	D/q Frontal area (Ft ²)
Regular wheel and tire	0.25
Second wheel and tire in tandem	0.15
Streamlined wheel and tire	0.18
Wheel and tire with fairing	0.13
Streamline strut (1/6 < t/c < 1/3)	0.05
Round strut or wire	0.30
Flat spring gear leg	1.40
Fork, bogey, irregular fitting	1.0-1.4

Lift-induced drag in Raymer's textbook [22] also uses a different method than Roskam's. Equations 13.31, 13.32, and 13.33 gives a quick calculation of induced drag of a wing.

$$K = \frac{1}{\pi A e} \quad (13.31)$$

$$e = 4.61(1 - 0.045A^{0.68})(\cos((\Lambda_{LE})^{0.15}) - 3.1) \quad (13.32)$$

$$C_{d_i} = KC_L^2 \quad (13.33)$$

Substituting the values gives the following:

$$e = 4.61(1 - 0.045(4.9)^{0.68})(\cos((36.81)^{0.15}) - 3.1) = 0.767$$

$$K = \frac{1}{\pi(4.9)(0.767)} = 0.0847$$

$$C_{d_i} = 0.0847C_L^2$$

13.8 Discussion

The total drag coefficient of the aircraft can be broken down to various drag coefficients of the different components of the aircraft. The calculations for the drag coefficient for the wing, empennage, and nacelle are during transonic flight while the calculations for the flaps and landing gear are for speeds during takeoff. Two sets of calculations were made. One using Roskam's method and another with Raymer's.

Table 13.2. Drag coefficients summary

Method	$C_{D_{wing}}$	$C_{D_{emp}}$	$C_{D_{nac}}$	$C_{D_{flight}}$	$C_{D_{flap_{toff}}}$	$C_{D_{flap_{land}}}$	$C_{D_{gear}}$
Roskam	0.0492 + 0.169 C_L^2	2 * (0.0171 + 0.00243 C_L^2)	0.026	0.118 + .171 C_L^2	0.0157	0.0676	0.00595
Raymer	0.00970 + 0.0847 C_L^2	0.000740	0.000880	0.0113 + 0.0847 C_L^2	0.0296	0.0788	0.00948

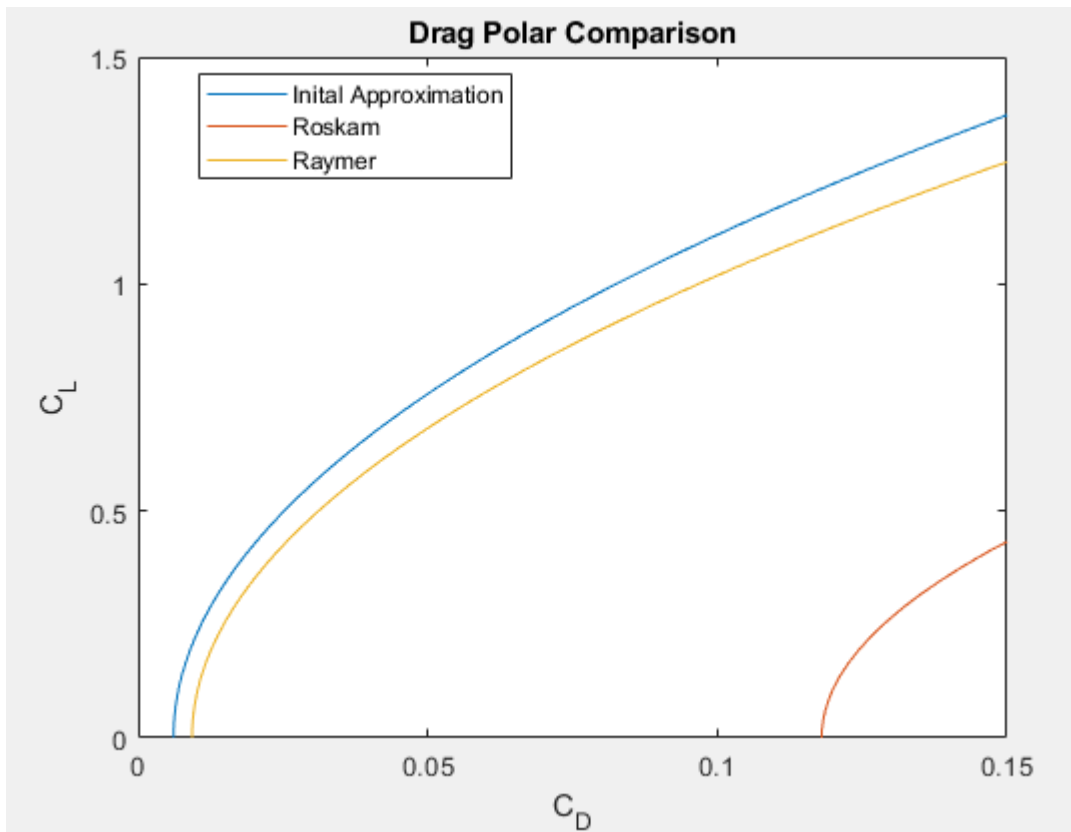


Figure 13.11. Drag polar comparison with other methods

From figure 13.11, Raymer's method is a lot closer for the initial calculations that were made earlier in the report. Roskam's method has a very high zero-lift drag coefficient when compared to the other two lines. Due to the Raymer's method being closer to the initial approximation, calculations from this method will be used in future calculations. The main reason for this is because Roskam's method calculates the drag polar based off a conventional tube and wing aircraft whereas Raymer's method is applicable to general aviation vehicles.

14. Weight and Balance Analysis – Class II

14.1 Introduction

Like chapter 9, this chapter discusses the weight breakdown of the various components in the aircraft using Roskam's method [24]. It is important to use multiple methods to calculate the weight components of the aircraft to ensure accuracy and use the set of calculations that more accurately matches the initial design. In-depth calculations using Roskam's method can be found in appendix B of the report. The following will be recorded in this section:

- Weight Breakdown in the X-Direction
- Weight Breakdown in the Z-Direction

14.2 Component Weight Breakdown

Weights of the individual components are calculated using Roskam's textbook [24]. A series of equations are provided to estimate the various individual component weights in this textbook.

Like in chapter 9, the location of the center of gravity is approximated using the SolidWorks model in chapter 4 and will be used in the same way. Roskam's equations also uses the empty weight, fuel weight, and takeoff weight calculated in chapter 2 of this report.

These values are then put into an Excel spreadsheet which approximates the center of gravity and calculates the moment arm.

Table 14.1. CG inputs in Excel for the X-location using Roskam’s method

	Weight lbs or kg	X-Location ft or m	Moment ft-lbs or kg-m
STRUCTURES GROUP	447668	83.9	37562432.5
Wing	392399	79.4	31156480.6
Horiz. Tail	0	0	0.0
Vert. Tail	34229	140.33	4803355.6
Fuselage	0	0	0.0
Total Lndg Gear	19,858	72.35	1436726.3
Nose Lndg Gear	0	0	0.0
Engine Mounts	1,182	140.33	165870.1
Firewall	0	0	0.0
Engine Section	0	0	0.0
Air Induction	0	0	0.0
			0.0
			0.0
PROPULSION GROUP	46622.0	120.8	5633268.6
Engine(s)	38632	140.33	5421228.6
Tailpipe	0	0	0.0
Engine Cooling	0	0	0.0
Oil Cooling	0	0	0.0
Engine Controls	69	15	1035.0
Starter	6604	15	99060.0
Fuel System	1317	85	111945.0
			0.0
			0.0
EQUIPMENT GROUP	46119.0	58.7	2705920.0
Flight Controls	6149	20	122980.0
Instruments,electrical,avi	6592	20	131840.0
Hydraulics	950	20	19000.0
Electrical	0	0	0.0
Avionics	0	0	0.0
Furnishings & Misc	28846	75	2163450.0
Air Conditioning	3244	75	243300.0
Handling Gear	338	75	25350.0
APU installed	0	0	0.0
Misc Empty Weight	0	0	0.0
			0.0
			0.0
			0.0
			0.0

Table 14.2. CG outputs in Excel for the X-location using Roskam's method

We-Allowance	0.0	84.9	0.0
EMPTY WEIGHT	540409.0	84.9	45901621.1
USEFUL LOAD GROUP	409591.0	76.3	31238280.0
Crew	2800	25	70000.0
Passengers			
Payload	125000	69	8625000.0
Fuel (weight available)	281791.0	80	22543280.0
Oil	0	0	0.0
			0.0
			0.0
			0.0
TAKEOFF GROSS WEIGHT	950000	81.2	77139901.1
	Fuel-Out CG	81.7	
	Payload-Out CG	83.0	

Table 14.3. CG inputs in Excel for the Z-location using Roskam’s method

	Weight lbs or kg	Z-Location ft or m	Moment ft-lbs or kg-m
STRUCTURES GROUP	447668	1.9	833341.6
Wing	392399	1.46	572902.5
Horiz. Tail	0	0	0.0
Vert. Tail	34229	16.33	558959.6
Fuselage	0	1.04	0.0
Main Lndg Gear	19,858	-16	-317728.0
Nose Lndg Gear	0	-16	0.0
Engine Mounts	1,182	16.25	19207.5
Firewall	0	0	0.0
Engine Section	0	0	0.0
Air Induction	0	0	0.0
			0.0
PROPULSION GROUP	46622.0	13.5	627770.0
Engine(s)	38632	16.25	627770.0
Tailpipe	0	0	0.0
Engine Cooling	0	0	0.0
Oil Cooling	0	0	0.0
Engine Controls	69	0	0.0
Starter	6604	0	0.0
Fuel System	1317	0	0.0
			0.0
EQUIPMENT GROUP	46119.0	0.0	0.0
Flight Controls	6149	0	0.0
Instruments	6592	0	0.0
Hydraulics	950	0	0.0
Electrical	0	0	0.0
Avionics	0	0	0.0
Furnishings & Misc	28846	0	0.0
Air Conditioning	3244	0	0.0
Handling Gear	338	0	0.0
APU installed	0	0	0.0
Misc Empty Weight	0	0	0.0
			0.0
			0.0
			0.0
			0.0

Table 14.4. CG outputs in Excel for the Z-location using Roskam’s method

We-Allowance	248588.1	2.7	672111.3
EMPTY WEIGHT	540409.0	2.7	1461111.6
USEFUL LOAD GROUP	409591.0	-1.8	-742502.0
Crew	127800	-1.4	-178920.0
Passengers			
Payload	0	0	0.0
Fuel (weight available)	281791.0	-2	-563582.0
Oil	0	0	0.0
			0.0
			0.0
			0.0
TAKEOFF GROSS WEIGHT	950000	0.8	718609.6
	Fuel-Out CG	1.9	
	Payload-Out CG	0.8	

14.4. Discussion

In chapter 2, the weight was approximated as below.

- $W_P = 127,800$ lbs
- $W_E = 440,300$ lbs
- $W_F = 374,000$ lbs

When calculating the individual components using Roskam’s equations [24] and comparing to chapter 8 Raymer values, the general weight distribution are as follows:

Table 14.5. Component weight comparison with various methods

Roskam’s Method	Raymer’s Method
$W_P = 127,800$ lbs	$W_P = 127,800$ lbs
$W_E = 540,409$ lbs	$W_E = 483,995$ lbs
$W_F = 281,791$ lbs	$W_F = 338,205$ lbs

The empty weight of the aircraft is 100,000 lbs more than estimated, which means that the fuel weight is 100,000 lbs less. This will result in roughly a 25% decrease in range. The weights of this aircraft using Roskam’s method compared to Raymer’s method are significantly different. This is because Roskam’s method is more reliable for a conventional aircraft rather than a blended winged body. In-depth calculations using Roskam’s and Raymer’s method can be found in appendices A and B.

15. V-N Diagram

15.1. Introduction

V-N diagrams are used to determine the structural load and design limits of the aircraft design. The following scenarios represent critical points that can affect the ultimate design load factor of the blended wing aircraft.

- Stall, V_s
- Cruise, V_c
- Diving, V_d
- Maneuvering, V_a
- Maximum Gust Intensity, V_b

Roskam's aircraft textbook [24] covers how to determine the velocity and design load limits for these scenarios.

15.2. V-N Diagram

The determining stall speed for this aircraft in a V-N diagram uses a similar equation from chapter 3; however, the coefficient of the maximum normal force will be used instead of the maximum lift coefficient. A good estimate for this value is 1.5 times the value for the maximum lift coefficient.

$$V_s = \sqrt{\frac{2 * \frac{W}{S}}{\rho C_{N_{MAX}}}} = \sqrt{\frac{2 * 105}{0.002378 * 1.5 * 1.1}} = 231 \frac{ft}{s} = 134 \text{ kts} \quad (15.1)$$

The design maneuvering speed is approximated using the stall speed and design load limit as seen in equation 15.2. The design limit load is approximated to be 2.5 due to Roskam's guidelines [24].

$$V_A = V_s n_{lim}^{\frac{1}{2}} = 137(2.5)^{\frac{1}{2}} = 217 \text{ kts} \quad (15.2)$$

The coefficient of lift with respect to angle of attack can be approximated from the drag polar estimation from chapter 11.

- $C_{L\alpha} = \frac{0.0524}{deg} = \frac{3}{rad}$

To determine the maximum gust intensity at various scenarios, a pair of constants, μ_g and K_g must be calculated using the following equations.

$$\mu_g = \frac{2 \left(\frac{W}{S}\right)}{\rho * c_g * C_{L\alpha}} = 2 * \frac{105}{0.002378 * 29.28 * 3} * 0.031 = 31.2 \quad (15.3)$$

$$K_g = \frac{0.88\mu_g}{5.3 + \mu_g} = \frac{31.2 * 0.88}{5.3 + 31.2} = 0.752 \quad (15.4)$$

Roskam's estimates below for gust velocities during various scenarios can be calculated [24].

$$U_{de_b} = 84.67 - 0.000933h = 84.67 - 0.000933(35,000) = 52.0 \frac{ft}{s}$$

$$U_{de_c} = 84.67 - 0.000933h = 66.67 - 0.000833(35,000) = 38.5 \frac{ft}{s}$$

$$U_{de_d} = 84.67 - 0.000417h = 33.34 - 0.000417(35,000) = 18.8 \frac{ft}{s}$$

Using equation 15.5, the design load limit in various factors can be determined using the gust velocities.

$$n_{lim} = 1 + \frac{K_g U_{de} V C_{L\alpha}}{498 * \left(\frac{W}{S}\right)} \quad (15.5)$$

$$n_{lim_b} = \frac{0.752 * 52 * 3 * V}{498(105)} = 1 + 0.00232V$$

$$n_{lim_c} = \frac{0.752 * 38.5 * 3 * V}{498(105)} = 1 + 0.00166V$$

$$n_{lim_d} = \frac{0.752 * 18.8 * 3 * V}{498(105)} = 1 + 0.000811V$$

Putting these equations in MATLAB produces a V-N gust diagram that will be used to create the V-N maneuver diagram. By finding the intersection of the limit load line of the design maneuvering speed, and the maximum gust intensity line, the velocity during maximum gust intensity can be determined to be $V_B = 160 \text{ kts}$.

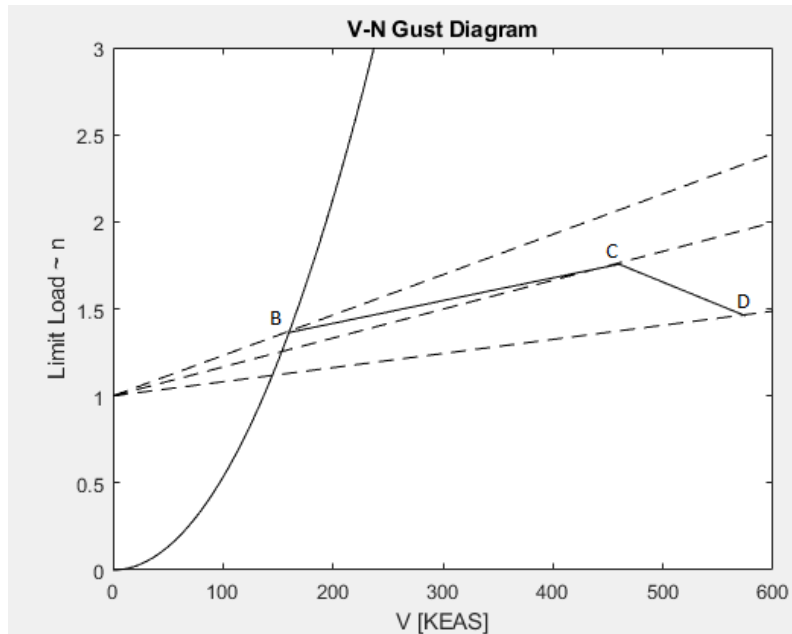


Figure 15.1. V-N gust diagram

The following velocities during cruise and diving can be approximated using a method from Roskam's textbook [24].

$$V_C \geq V_B + 43 \text{ kts} = 160 + 43 = 203 \text{ kts} \quad (15.6)$$

Since cruise velocity for the mission statement is 460 kts, it meets the minimum requirements of 203 kts.

$$V_D = 1.25V_C = 1.25(460) = 575 \text{ kts} \quad (15.7)$$

To determine the stall speed during negative load, equation 15.1 will be used; however, the maximum normal coefficient force during negative load is approximated to be 1.1

$$V_s = \sqrt{\frac{2 * 105}{0.002378 * 1.1 * 1.1}} = 270 \frac{ft}{s} = 160 \text{ kts}$$

Figure 15.2 represents the V-N maneuver diagram for the blended wing body aircraft.

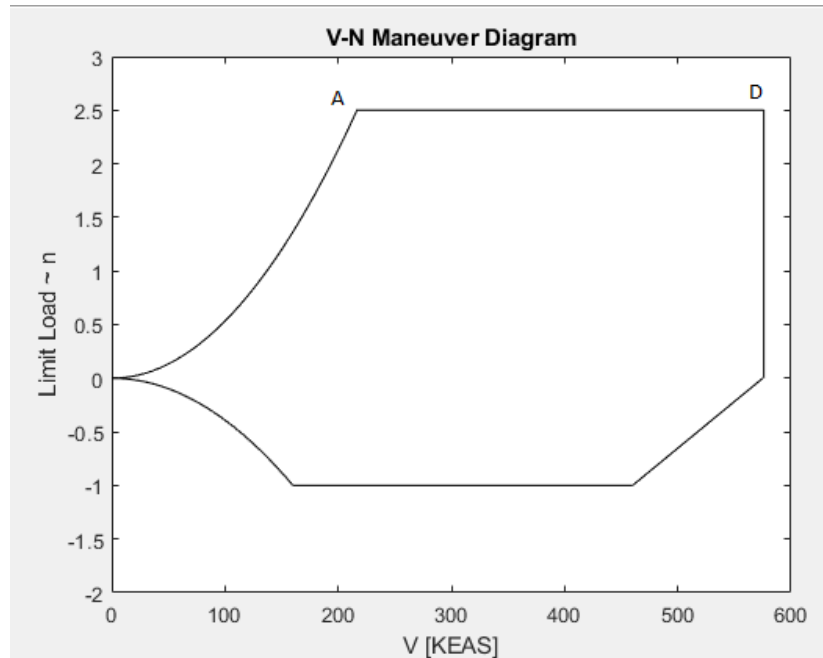


Figure 15.2. V-N maneuver diagram

16. Installed Power and Thrust Characteristics

16.1. Introduction

This chapter will discuss a method to predict the installed thrust in the blended wing body aircraft. Using chapter 4 engine manufacturer's data, the installed thrust can be predicted when considering the power extracted and thrust lost during incompressible flow. Chapter 6 of Roskam's part VI textbook, [23] provides in-depth information for these calculations.

16.2. Installed Thrust Calculations

To compute the available installed thrust, the following info must be readily available:

- Flight Mach Number
- Power Extracted
- Inlet pressure loss during incompressible flow

Once these values are determined, equation 16.1 can be used to calculate the installed thrust and be compared to the necessary thrust required for this aircraft.

$$T_{av} = T_{tst} \left(1 - 0.35 K_t M_1 \left(1 - \frac{\eta_{inl}}{inc} \right) \right) - 550 * \left(\frac{P_{extr}}{U_1} \right) \quad 16.1$$

The flight Mach number is determined by the mission requirements, which is 0.80. Due to the lack of geometric parameters from the manufacturer's data, a good estimate for inlet pressure loss during incompressible flow is, $\eta_{inl/inc} = 0.95$. The variable K_t can be determined by extrapolating from the figure below.

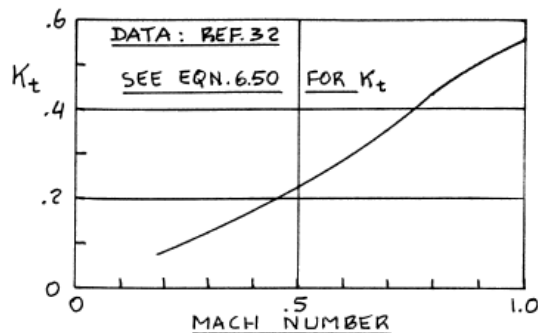


Figure 16.1. Effect of Mach number on K_t

From the figure, $K_t = 0.45$. To calculate the power extracted from the engine, a rough estimate can be determined by using the table below and equations 16.2 and 16.3.

Table 16.1. Summary of power extraction requirements

Power Extraction Type:	Electrical shp, P_{el}	Mechanical shp, P_{mech}	Pneumatic Bleed slugs/sec
Airplane Type:			
<u>Piston Propeller Driven:</u>			
Single engine, light airplanes	1-2	1-2	0
Single engine, military trainers	2-4	2-4	0
Twin engine, light airplanes	4-6	5-10	0
Multi-engine transports	20-40	30-50	0
<u>Turboprop and Jet Airplanes:</u>			
Single engine, light airplanes	2-4	3-5	0.01 $\frac{m}{a}$
Single engine, military trainers	5-7	6-10	0.015 $\frac{m}{a}$
Twin engine turboprops	6-8	7-9	0.015 $\frac{m}{a}$
Twin engine turbojets or fans	8-10	9-11	0.025 $\frac{m}{a}$
Twin jet military trainers	10-15	15-20	0.03 $\frac{m}{a}$
Jet Fighters, air-superiority	50-100	50-100	0.03 $\frac{m}{a}$
Jet Fighters, attack	100-200	100-200	0.04 $\frac{m}{a}$
Jet Transports, civil	0.00070 W_{TO}	0.00060 W_{TO}	0.03 $\frac{m}{a}$
Jet Transports, military	0.00100 W_{TO}	0.00080 W_{TO}	0.04 $\frac{m}{a}$

$$P_{neum} = \left(\frac{\dot{m}}{\dot{m}_a}\right) * \left(\frac{T_{reqd} U_1}{550}\right) = (0.025) \left(5167 * \frac{460}{550}\right) = 108 \text{ shp} \quad 16.2$$

$$P_{extr} = P_{el} + P_{mech} + P_{neum} = 9 + 10 + 108 = 127 \text{ shp} \quad 16.3$$

By plugging in the values from table 16.1 into equations 16.2 and 16.3, the total horsepower extracted from the engine can be approximated to be 127 shp. Plugging these values back in the equation 16.1, gives an installed available thrust of 229,018 lbf.

$$T_{av} = 230,600(1 - 0.35(0.45)(0.8)(1 - 0.95)) - 550 * \left(\frac{108}{460}\right) = 229,018 \text{ lbf}$$

The required thrust needed for this aircraft is 190,000 lbf during takeoff. The installed thrust of this engine more than meets the requirements of the thrust needed for this design.

17. Critical Performance Requirements

17.1. Introduction

This chapter presents methods for predicting the aircraft's critical performance and how those are compared to chapter 2 of this report. Since the blended wing body aircraft design has matured, an analysis must be performed to see if it meets those requirements. The critical performance characteristics that the design will be most interested in are the following:

- Stall
- Takeoff
- Climb
- Range
- Landing

The analysis will be performed by using equations from Roskam's part VII textbook [25].

17.2. Critical Performance Analysis

The first parameter that this design will be interested in is the stall speed. In chapter 2, the blended winged body was predicted to have a stall speed of equal to or less than 143 kts during cruise. The stall speed during takeoff and landing should also be calculated since those values will be important in the takeoff and landing analysis.

$$V_s = \sqrt{\frac{2 * W}{\rho C_{LS}}} = \sqrt{\frac{2 * 950,000}{0.002378 * 1.55 * 16,284}} = 178 \frac{ft}{s} = 103 \text{ kts} \quad (17.1)$$
$$V_{sTo} = \sqrt{\frac{2 * W}{\rho C_{LMAXTO}}} = \sqrt{\frac{2 * 950,000}{0.002378 * 1.97 * 16,284}} = 158 \frac{ft}{s} = 94 \text{ kts}$$
$$V_{sL} = \sqrt{\frac{2 * W}{\rho C_{LMAXL}}} = \sqrt{\frac{2 * 950,000}{0.002378 * 2.18 * 16,284}} = 150 \frac{ft}{s} = 89 \text{ kts}$$

Using equation 17.1, the stall speed during cruise, takeoff, and landing were calculated. The stall speed meets the requirements of under 143 kts.

The takeoff distance was expected to be less than 13,000 ft. Equations 17.2, 17.3 and 17.4 are used to determine this value. The zero-lift drag coefficient was calculated in chapter 13 and the max lift coefficient during takeoff was determined in chapter 11. The thrust to weight ratio and wing loading during takeoff was calculated during chapter 3. Other parameters that have not yet been calculated can be found in table 17.1. Since these values have already been calculated, plugging them into the equation gives a takeoff distance of 8,635 ft.

Table 17.1. Parameter values for equation 17.4 [25]

Regulation	$V_3/V_{S_{TO}}$	f_{TO}	h_{TO}
FAR 23	1.3	1.0	50 ft
FAR 25	1.25 to 1.3 (no requirement)	1.15	35 ft
AS-5263	1.2	1.0	50
MIL-C-005011B	1.15	1.0	50 ft

$$\mu' = \mu_g + 0.72 \left(\frac{C_{D0}}{C_{LMAXTO}} \right) = 0.02 + 0.72 \left(\frac{0.0504}{1.9} \right) = 0.039 \quad (17.2)$$

$$\gamma_{LOF} = 0.9 \left(\frac{T}{W} \right)_{TO} - \frac{0.3}{A^2} = 0.9(0.2) - \frac{0.3}{4.9^2} = 0.0445 \quad (17.3)$$

$$S_{TO} = f_{TO} h_{TO} \left(\frac{1}{\gamma_{LOF}} \right) + \frac{\left(\frac{V_3}{V_{STO}} \right)^2 \left(\frac{W}{S} \right)_{TO} \left(\left(\frac{T}{W} \right)_{TO} - \mu' \right)^{-1} + 1.414}{(h_{TO} \rho g C_{LMAXTO}) (1 + 1.414 \gamma_{LOF})} \quad (17.4)$$

Plugging the known values into equation 17.4 gives a takeoff field length of 8,635 ft.

$$\begin{aligned} 1.15(35) \left(\frac{1}{0.0455} \right) + \frac{(1.275)^2 (103) ((0.2 - 0.039)^{-1} + 1.414)}{(35 * 0.002378 * \frac{1}{32.17} * 32.17 * 1.9) (1 + 1.414 * (0.0455))} \\ = 885 + \frac{1,302}{0.168} = 8,487 \text{ ft} \end{aligned}$$

In addition, the liftoff speed can be approximated using equation 17.5.

$$V_{LOF} = 1.2 V_{STO} = 1.2(94) = 113 \text{ kts} \quad (17.5)$$

Since the requirement for the takeoff distance is less than 13,000 ft and the calculated takeoff distance for this aircraft is 8,635 ft. This aircraft meets the requirements and will have a liftoff speed of 114 kts.

For climb rate, it was expected to be at least 3,500 feet per minute based off data from other aircraft. Equations 17.6 and 17.7 calculate the climb rate and the gradient of this aircraft.

$$RC = 60 U_1 \left(\left(\frac{T}{W} \right) - \left(\frac{L}{D} \right)^{-1} \right) = 60(776)(0.20 - 13.87^{-1}) = 5,955 \text{ fpm} \quad (17.6)$$

$$CGR = \left(\left(\frac{T}{W} \right) - \left(\frac{L}{D} \right)^{-1} \right) = (0.20 - 13.87^{-1}) = 0.128 \quad (17.7)$$

Although there was no expected value for climb rate except for historical data, a rate of climb of 5,955 feet per minute at a 0.128 climb gradient is greater than expected and is suitable for the mission requirements.

Cruise and range values can be calculated using equations 17.8 and 17.9. As a rule of thumb from Roskam's textbook, the lift to drag ratio during cruise is 0.90 of the maximum lift to drag ratio. With known cruise speeds, specific fuel thrust consumption from GE-90 data sheet, and an expected end weight of the aircraft, the range of the aircraft can be calculated.

$$\left(\frac{L}{D} \right)_{cruise} = 0.90 \left(\frac{L}{D} \right)_{max} = 0.90(23.1) = 20.8 \quad (17.8)$$

$$R = \left(\frac{V}{c_j} \right) \left(\frac{L}{D} \right) \ln \left(\frac{W_{initial}}{W_{end}} \right) = \frac{460}{0.547} * 20.8 * \ln \left(\frac{950,000}{611,525} \right) = 7,705 \text{ nmi} \quad (17.9)$$

The lift to drag ratio was expected to be 21 from chapter 2 and the required range for the mission was 6,000 nmi. The calculated values were 20.8 for lift to drag during cruise and 7,705 nmi for the range which exceeds the mission requirement specifications.

Landing distance can be determined by the approach velocity as shown below.

$$V_A = 1.3V_{S_L} = (1.3)89 = 116 \text{ kts} \quad (17.10)$$

$$S_{FL} = 0.3V_A^2 \rightarrow 0.3(116)^2 = 4,036 \text{ ft} \quad (17.11)$$

The landing distance was expected to be less than 8,500 ft which the design met with 4,036 ft.

17.3. Discussion

The blended wing body aircraft meets all the performance requirements listed in chapter 1. Below are the summarized performance values that were calculated.

- Stall speed = 106 kts
- Takeoff Distance = 8,487 ft
- Liftoff Speed = 113 kts
- Cruise Speed = 460 kts
- Rate of Climb = 5,955 fpm
- Climb Gradient = 0.128
- Lift to drag ratio during cruise = 20.8
- Range = 7,705 nmi
- Landing Distance = 4,036 ft

The difference in actual and expected wing loading significantly affects the stall speed, takeoff distance, and landing distance. The expected wing loading was to be approximately 105 lb/ft^2 , but the actual wing loading from the designed aircraft was 58 lb/ft^2 . This drastic change in wing loading is what causes the major difference in several performance parameters. It should also be noted that the C_{LMAX} values during takeoff and landing from XFLR5 were unable to be accurately determined due to XFLR5's inability to calculate scenarios with high Reynolds numbers, such as with flaps during takeoff and landing. The inability to accurately calculate lift coefficient during takeoff and landing angle of the flaps could potentially affect the performance parameters. The engines used in this aircraft could also be optimized since the range of the aircraft far exceeds the performance requirements. Using a weaker, but lighter engine could reduce the weight of the aircraft and shift the center of gravity forward.

18. Initial Structure Arrangement

18.1. Introduction

This chapter will provide a brief overview of the structural components of the blended wing body. In particular, the wing structure and its design choices will be explained.

18.2. Discussion

In the blended wing body design, a ring frame structural arrangement will be used so the internal structural spars can wrap around the cabin. I-beam spars will be placed at the thickest part of the wing and two-thirds of wing from the leading edge of the wing. This design will help carry the bending moments through the fuselage. Multiple ribs will be attached to the two spars to transfer air loads to the spars and maintain the shape of the wing under bending.

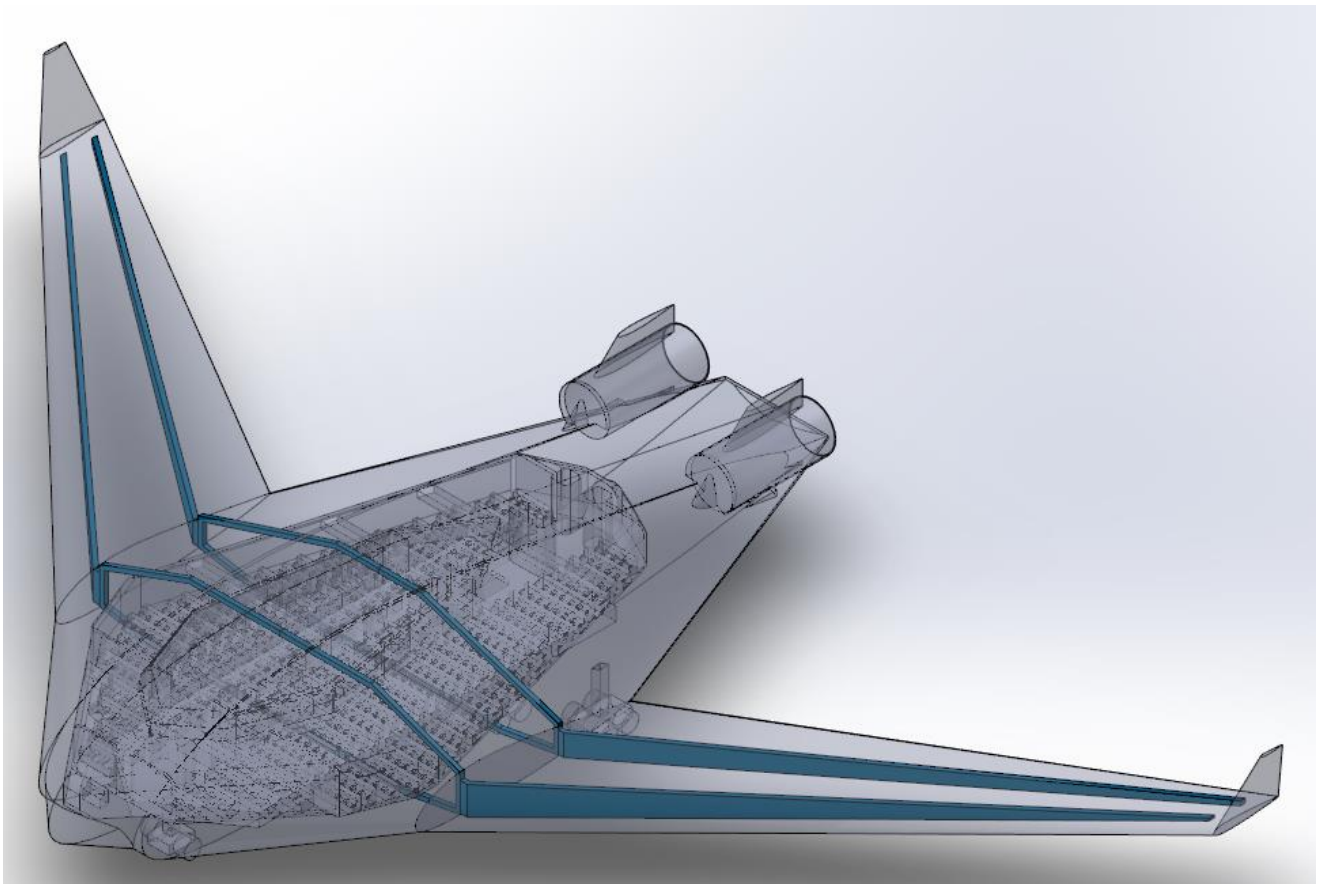


Figure 18.1. Internal wing structure arrangement iso view

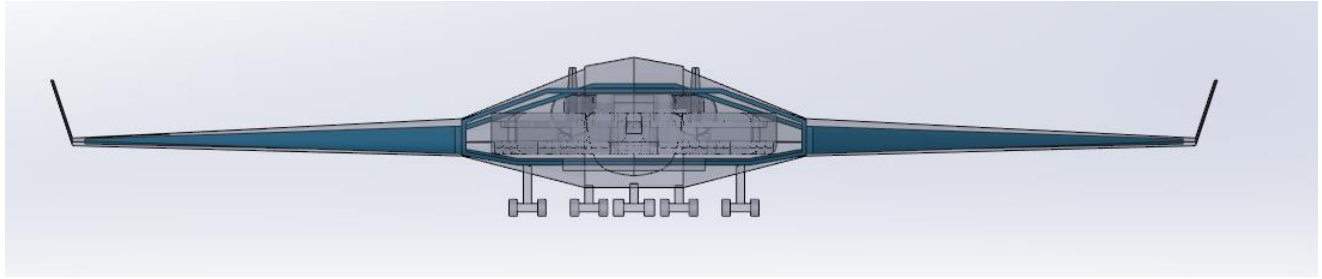


Figure 18.2. Internal wing structure arrangement front view

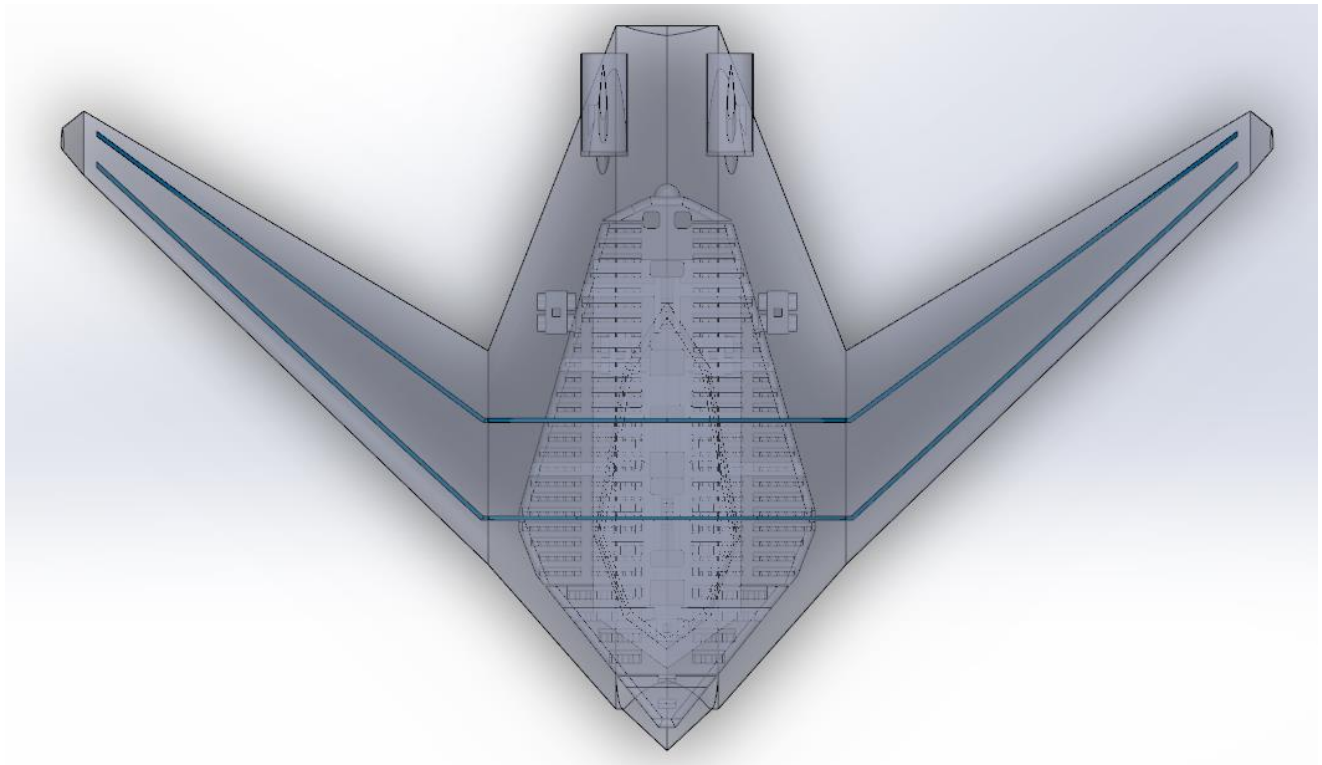


Figure 18.3. Internal wing structure arrangement top view

In addition to the ring-framed wing structure, the aircraft would have rounded walls whenever possible to help distribute the pressure within the cabin. Having a “bubble-like” cabin would greatly reduce the risk of having high stress on the walls and floors.

19. Airplane Subsystem Arrangement

19.1. Introduction

Throughout the report, the aerodynamic, design, and weight of the aircraft have been analyzed and considered; however, some of the smaller details of the aircraft have not been discussed yet. This chapter will discuss the various subsystems of the aircraft and how their layout will affect the overall performance of the aircraft. Roskam’s textbook will serve as a guide in designing subsystem layouts [26].

19.2. Flight Control Systems Layout Design

Flight control systems can be split into primary and secondary controls. Primary control systems refer to the elevator, stabilizers, rudder, ailerons, spoilers, and the canard. The secondary control systems refer to the high lifting control devices and thrust control devices.

This aircraft will use an irreversible flight control system which will rely on hydraulics and electrical components. The cockpit control systems affect the aerodynamic surface control systems, but not the other way around. In the blended wing body design, hydraulics will be used to control the primary aerodynamic surfaces. The ailerons will be driven by servos powered by hydraulics. The spoilers and elevator will be controlled using electronics, like the Boeing 767. The directional control system will also be controlled via servos.

- Service-proven system and hardware concepts
- Fly-by-wire spoilers for system simplification
- Control wheel steering through autopilot for pilot workload reduction
- Maintenance improvements—less complex line replaceable units
- Control surfaces and actuators replaceable without rerigging control cable
- Faired position of control surfaces defined by permanent indices (except ailerons)—rigging pin positions are readily accessible
- Only one hydraulic system is disturbed when a flight control actuator is replaced on the airplane
- All spoiler control valves replaceable without actuator removed
- All autopilot and yaw damper servos replaceable with control surface actuators installed

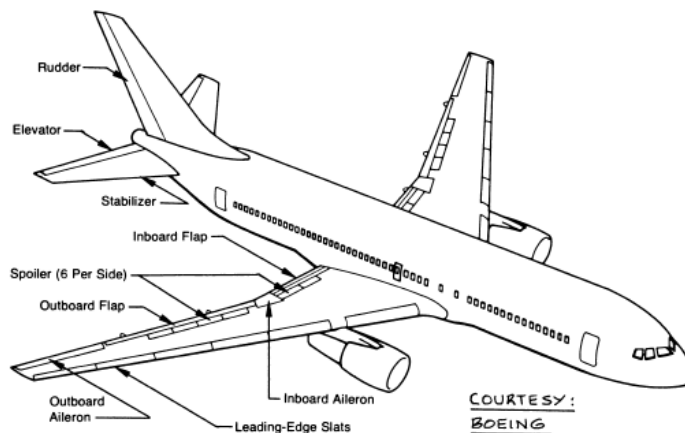


Figure 19.1. Boeing 767 flight control features [26]

19.3. Propulsion System

All airplanes require some sort of propulsion control system to help the pilot maneuver the aircraft. In a jet powered plane, the following control systems for propulsion are required:

- Ignition Control
- Starter System
- Fuel Flow
- Thrust reverser control

Ignition controls will be controlled via an electrical system like most vehicles. In addition, most airplanes will use an electric starter motor that is connected to the engine. This type of starter system will be used in the blended wing body. The engine fuel controls will be operated via a push-rod system. The thrust reverser control system is used to slow the airplane after landing and will be operated via hydraulics.

19.4. Fuel System Layout Design

The fuel will be stored inside the wings of the blended wing body. It was calculated that the aircraft will have about 338,205 lbs of fuel. This aircraft will use surge tanks as with most transportation aircraft so any excess fuel vapor can be condensed before it exits the fuel vents.

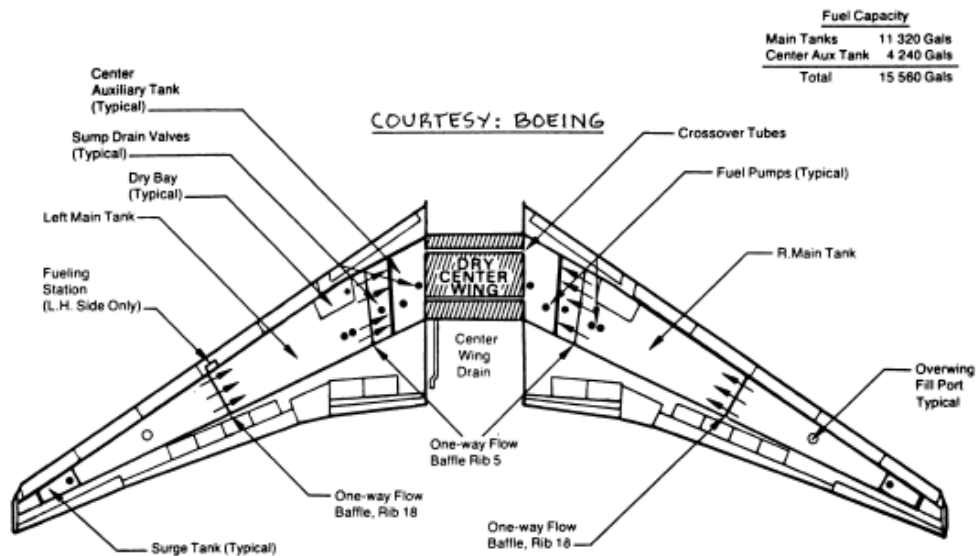


Figure 19.2. Boeing 767 fuel system layout [26]

The landing gear in the blended wing body design are positioned such that they are far away from the fuel lines. The landing gear can heat up tremendously during takeoff and landing due the friction from the tires. Similarly, the engines are positioned towards the aft of the aircraft to avoid this problem while also maintaining a favorable center of gravity for the aircraft. Like all aircraft, a fire extinguishing system will also be implemented in the chance that there is a fire caused by the fuel system.

19.5. Hydraulic System Layout Design

Hydraulics are used to mainly move primary and secondary flight controls, retract the landing gear, and control or maneuver the aircraft for the pilot. Hydraulics usually have an emergency back-up power source. Accumulators can help lower the landing gear by providing hydraulic pressure and APUs (auxiliary power units) can help power the aircraft for a short amount of time. According to Roskam's textbook [26], transport aircraft such as the Boeing 757 and Boeing 767 use a hydraulic pressure of 3,000 psi and a system flow capacity of 74 gpm. Since the blended wing body aircraft has a similar mission, these numbers will be used as a starting point for the design of the hydraulic system.

19.6. Electrical System Layout Design

Electrical power is required for all airplanes. For the blended wing body design, electricity will be used to power internal and external lighting, flight instruments and control systems, starting system, and food heating. External lighting is particularly important during takeoff and landing to allow the pilot to signal to the airports and traffic control.

Engine driven generators will be used to provide the aircraft with the necessary electrical power. The Boeing 767 uses multiple 90 KVA generators to power their electronics [26]. APUs, or auxiliary power units, can be used as a backup power source. In the blended wing body, three electrical systems will be employed with one backup system due to how essential electricity is in a transport aircraft. It is common for transport aircraft to be able to function with one failed electric system. In addition, electrical systems must be shielded from lightning strikes and must be properly spaced from each other to prevent electromagnetic interference. Lastly, the blended wing body should have some sort of way to hook up to ground power during standby.

19.7. Environmental Control System Layout Design

This section will cover the pressurization system, pneumatic system, air conditioning system, and oxygen system of the blended wing body aircraft. Pressurization is vital to a transportation aircraft due to the high altitudes and large amounts of passenger in it. An airplane's pressurization system is dependent on the pneumatic system that acts as a source of high-pressure air and a control system to provide pressure relief when necessary for the comfort and safety of the passengers. An improper pressurization system can lead to breathing problems and damage to the cabin's interior. A depressurization system is also required to prevent forced door closure should the pressurization system fail during landing. In the blended wing body's design, the rounded walls and bubble-like cabin helps stabilize pressure by distributing it equally.

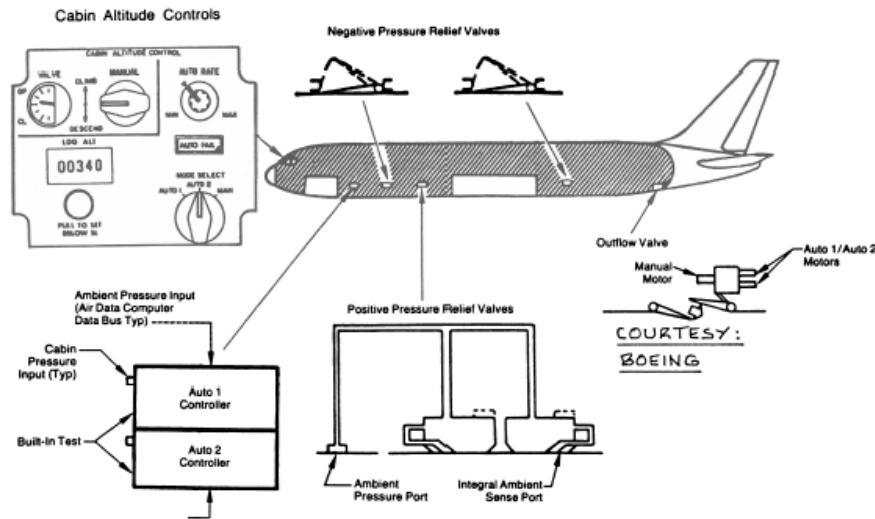


Figure 19.3. Boeing 767 pressurization system layout [26]

Pneumatic systems are used to help pressurize cabin air and provide air conditioning as well as de-icing. Air conditioning is to help regulate the temperature and humidity of the cabin for the comfort and safety of the passengers. Multiple airducts mix hot and cold air to obtain an optimal cabin environment. Oxygen systems are also required during high altitude flights in case of an emergency or failure of the cabin's pressurization system.

19.8. Cockpit Instrumentation, Flight Management and Avionics System Layout Design

The aircraft crew needs to be able to respond towards the environment. A proper environmental control system allows the crew to efficiently communicate to the ground team and respond accordingly in any situation. The cockpit instrumentation should be all laid out for the pilot to see and operate at a given notice. In addition, the aircraft will have a flight management system that will assist the pilot with the propulsion and autopilot. Many antenna systems are required to maintain stable communication with the ground team. Electrical equipment should also be in an easily accessible location as they fail rather frequently due to overheating from the high electrical power consumption from the aircraft.

19.9. De-Icing, Anti-Icing, Rain Removal and Defog Systems Layout Design

Ice formation can severely damage the aircraft's performance, especially if it occurs at the wings or the engine inlets. For these reasons, de-icing and anti-icing systems are deployed to minimize the effects of ice. The blended wing body will use an electro-impulse system to remove ice on the aircraft. This is done by using electromagnetic coils which releases mechanical impulses, shaking the ice off. In addition, an electrically heated anti-icing system will prevent the formation of ice. Since the blended wing body has a massive amount of volume, electric systems should be used to prevent additional weight while also maintaining simplicity in the design. Wind-shield wipers and rain repellent will be used to help the pilots see.

19.10. Escape System Layout Design

All passenger airliners are required to have emergency exits and escape systems. These exits will be properly marked with illuminating signs. In addition, life jackets will be provided to all passengers under the seat like most airliners. Escape hatches and escape slides will be provided throughout the aircraft. Since this is a blended wing aircraft with an auditorium-like cabin, escape hatches will also be located on the floor to allow every passenger to leave the aircraft in an emergency event. In addition, emergency rafts will be readily available during overwater flights.

19.11. Water and Waste Systems Layout Design

Water and waste systems are needed for restrooms and to put out emergency fires. In passenger transport vehicles, the amount of water in these systems approximates to 0.3 US gallon per passenger [26]. For the airliner, at least 150 US gallons of waters will be needed for the lavatories. Heat exchangers are used to supply warm running water to the lavatories. Furthermore, the drain layout must prevent ice from forming within the aircraft. Below is a water system layout for the Boeing 767. The blended wing airliner will have a similar water system to the Boeing 767 since both are passenger transport aircraft.

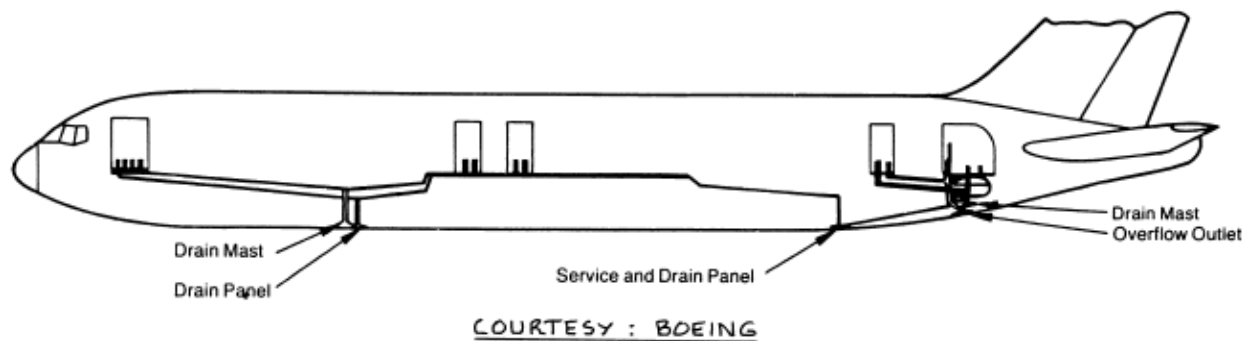


Figure 19.4. Boeing 767 water system layout [26]

19.12. Safety and Survivability Considerations

All passenger transports need to follow FAA regulations. All aircraft subsystems are separate and designed in such a way where the failure of one system does not prevent the continued safe flight and landing of the aircraft. Aircraft safety and survivability are split into preventive factors and post-crash factors. Preventive factors are areas of the aircraft where mistakes are likely to happen and every factor from software controls to the material of the aircraft needs to be inspected. Post-crash factors refer to the safety and survivability of the passengers in an aircraft during a crash scenario. Fires, emergency exits, and cabin structure and layout are the main point of focus in post-crash factors.

20. Stability and Control Analysis – Class II

20.1 Introduction

This chapter will briefly discuss about the other aspects of stability and control of this aircraft, such as trim, minimum control speed with one engine inoperative, and crosswinds. Roskam's textbook [25] provides specific calculations and in-depth detail on how these aspects affect the aircraft. Most of these areas will be discussed generally.

20.2 Discussion

A trim diagram is generally used to determine the lateral and longitudinal controllability of the aircraft. This is done by changing the angle of the ailerons, rudder, and elevator and determining when the aircraft is unstable; however, due to the elevators normally being on the horizontal stabilizer, the typical trim equation from Roskam's textbook does not apply. During one engine inoperative scenario, the aircraft should be able to land and takeoff normally due to the engines being close to the center line of the aircraft. Wan, T. & Song, B. [27] brings more insight into crosswind challenges that the blended wing body aircraft might face during cruise. Simulations were run with various angles of attacks and crosswind speeds, and it was found that even a slight change of angle of attack can cause lateral instability in the blended wing body. Although the blended wing body can land and takeoff with one engine inoperative, its ability to perform during heavy weather conditions and crosswinds is lacking and design changes will be needed for safety considerations.

21. Cost Analysis

21.1 Design and Development Cost

The research and design costs are always the most expensive, especially if it is a new unconventional aircraft design. A cost analysis model called DAPCA IV is used to approximate the development cost of an aircraft. The DAPCA IV cost model calculates the total design and development cost based off the following:

- Engineering cost
- Tooling cost
- Manufacturing cost
- Quality control cost
- Devel support cost
- Flight test cost
- Manufacturing material cost
- Engineer Production Cost

The appendix will show the DAPCA IV cost model based on Raymer's textbook. The total cost for design and development approximates to \$1.46 billion. Although the cost is extremely high for the development of one aircraft, more than half of the costs goes into R&D, testing, and tooling. Once the aircraft's design has been finalized, the total manufacturing costs are significantly less than during design and development.

21.2 Manufacturing Cost

Manufacturing costs are like the design and development costs; however, engineering costs will not be considered since the design would have already been finalized and tested. Each aircraft would cost \$297 million. The cost seems reasonable for an airliner of this size as the Boeing 747-400 costs up to \$260 million and the Boeing 747-8 costs up to \$414 million. The auditorium-like cabin allows the aircraft to pack more passenger efficiently and reduces the overall empty weight of the aircraft. This would make the aircraft cost less than conventional passenger airliners.

21.3 Operating Cost

Operating expenses can be divided into three general categories:

- Fuel costs
- Crew costs
- Material maintenance costs

Generally, fuel costs are the most expensive part of operation because of the quantity of jet fuel needed for the aircraft. For this aircraft, it is expected that \$60 million of jet fuel will be used per year. In addition to fuel costs, crew costs must be taken into consideration. For a three-man crew cost or larger, it would cost \$5,170 per hour in today's dollars for every hour of flight. This hourly cost does not include fuel and maintenance since those are generally measured in dollars per year. Maintenance and replacement parts are also needed for proper aircraft upkeep. It is approximated that the cost for yearly maintenance and material costs would be \$150,000 per aircraft.

22. Conclusion

22.1 Conclusion

Blended wing body aircraft are the future of civil transportation and need to be adopted to reduce gas emissions in the future. Their efficiency will allow airliners to burn 27% less fuel and the auditorium-like cabin will allow aircraft to hold more passengers . This report discusses a theoretical blended wing body airliner capable of carrying 500 passengers within 6,000 nmi under FAR 25 regulations. From the report, the aerodynamic characteristics of this aircraft design exceeds the conventional tube and wing design. Although the geometric design of this aircraft is unconventional when compared to other passenger airliners, many of the subsystems within the cabin can be reused due to its similar mission. One main point of interest that needs to be researched more is a cabin design capable of more evenly distributing pressure throughout the aircraft.

References

- [1] Chen, Z., Zhang, M., Chen, Y., Sang, W., Tan, Z., Li, D., and Zhang, B. "Assessment on critical technologies for conceptual design of blended-wing-body civil aircraft," *Chinese Journal of Aeronautics*, Vol. 32, 2019, pp. 1797–1827.
<https://doi.org/10.1016/j.cja.2019.06.006>
- [2] Larrimer, B. I. "The X-48 Blended Wing Body and NASA's Quest to Reshape Future Transport Aircraft," NASA, Washington, DC, 2020.
https://www.nasa.gov/sites/default/files/atoms/files/beyond_tube-and-wing_tagged.pdf
- [3] "Blended Wing Body – A potential new aircraft design," NASA, retrieved 2021.
<https://www.nasa.gov/centers/langley/news/factsheets/FS-2003-11-81-LaRC.html>
- [4] Ordoukhanian, E. & Madni, M. "Blended Wing Body Architecting and Design: Current Status and Future Prospects," *Procedia Computer Science*, Vol. 28, 2014, pp. 619-625.
<https://doi.org/10.1016/j.procs.2014.03.075>
- [5] "X-48 hybrid / blended wing body," NASA, Washington, DC, 2014.
<http://www.nasa.gov/centers/dryden/news/FactSheets/FS-090-DFRC.html>
- [6] "Imagine traveling in this blended wing body aircraft," Airbus, 11 Feb. 2020.
<https://www.airbus.com/newsroom/stories/Imagine-travelling-in-this-blended-wing-body-aircraft.html>
- [7] Bishara, M., Horst, P., Madhusoodanan, H., Brod, M., Daum, B., & Rolfes, R. "A Structural Design Concept for a Multi-Shell Blended Wing Body with Laminar Flow Control," *Energies*, Vol. 11(2), 2018, pp. 383.
doi:10.3390/en11020383
- [8] Boeing. "The right choice for the large airplane market," Arlington, VA, 2010.
https://www.boeing.com/resources/boeingdotcom/company/about_bca/startup/pdf/historical/747-400-passenger.pdf
- [9] Airbus. "A340-600," 2010.
<https://www.airbus.com/en/who-we-are/company-history/commercial-aircraft-history/previous-generation-aircraft/a340-family/a340-600>
- [10] Boeing. "Boeing 777," retrieved 9 Jan. 2022.
<https://www.boeing.com/commercial/777/>.
- [11] Northrop Grumman. "B-2 Technical Details," retrieved 9 Jan. 2022.
<https://www.northropgrumman.com/what-we-do/air/b-2-stealth-bomber/b-2-technical-details/>
- [12] Janes' Information Group. "Jane's All the World's Aircraft," 2021.
<http://janes.migavia.com/>

- [13] Cross, D., Faber, J., & Telles, R. "The B2 - Bomber: A Closer Look at the B2 Configuration," 1 Apr. 2009.
http://www.dept.aoe.vt.edu/~mason/Mason_f/B2Spr09.pdf
- [14] Roskam, J. *Airplane Design Part I: Preliminary Sizing of Airplanes*, Ottawa, S: Roskam Aviation & Engineering Corporation, 1985.
- [15] Patel, N. "Design of Medium Size Blended Wing Body Subsonic Transport Aircraft," Thesis, Aerospace Dept., San Jose State University, San Jose, CA, May 2018.
<https://www.sjsu.edu/ae/docs/project-thesis/Nishant.Patel.Sp18.pdf>
- [16] Kumar, P. & Khalid, A. "Blended Wing Body Propulsion System Design," *International Journal of Aviation, Aeronautics, and Aerospace*, Vol. 4(4), 10 Aug. 2017.
<https://doi.org/10.15394/ijaaa.2017.1187>
- [17] GE Aviation. "GE90 Commercial Aircraft Engine," 2021.
<https://www.geaviation.com/commercial/engines/ge90-engine>
- [18] Jenkinson, L., Simpkin, P. & Rhodes, D, *Civil Jet Aircraft Design*, 2001.
<https://booksite.elsevier.com/9780340741528/appendices/data-a/default.htm>
- [19] Roskam, J. *Airplane Design Part II: Preliminary Configuration Design and Integration of the Propulsion System*, Ottawa, S: Roskam Aviation & Engineering Corporation, 1985.
- [20] Gudmundsson, S., *General Aviation Aircraft Design: Applied Methods and Procedures*, Amsterdam: Butterworth-Heinemann, 2013.
- [21] Darshan, N. "Effect of Stall on Blended Wing Body Aircraft," *International Journal of Aviation, Aeronautics, and Aerospace*, Vol. 9(2), 2020.
<https://www.longdom.org/open-access/effect-of-stall-on-blended-wing-body-aircraft.pdf>
- [22] Raymer, D. P. *Aircraft design: A conceptual approach*, Washington, D.C., 1992.
- [23] Roskam, J. *Airplane Design Part VI: Preliminary Calculation of Aerodynamic Thrust and Power Characteristics*, Ottawa, S: Roskam Aviation & Engineering Corporation, 1985.
- [24] Roskam, J. *Airplane Design Part V: Component Weight Estimation*, Ottawa, S: Roskam Aviation & Engineering Corporation, 1985.
- [25] Roskam, J. *Airplane Design Part VII: Determination of Stability, Control and Performance Characteristics: FAR and Military Requirements*, Ottawa, S: Roskam Aviation & Engineering Corporation, 1985.
- [26] Roskam, J. *Airplane Design Part IV: Layout Design of Landing Gear and Systems*, Ottawa, S: Roskam Aviation & Engineering Corporation, 1985.

[27] Wan, T. & Song, B. “Aerodynamic Performance Study of a Modern Blended-Wing Aircraft Under Severe Weather Situations.” Tamkang University, 2012.
<https://core.ac.uk/download/pdf/225221083.pdf>

Appendix A: Raymer's Weight Calculations

$$W_{wing} = 0.0051 * (950,000 * 1.5 * 3 * 9.8)^{0.557} 6,291^{0.649} * 4.9^{0.5} * 0.18^{-0.4}$$

$$* (1 + 0.088)^{0.1} (\cos(36.81))^{-1.0} * 627^{0.1} = 131,216 \text{ lbf}$$

$$W_{fuselage} = 0.328 * 1.06 * 1.12 * (950,000 * 1.5 * 3 * 9.8)^{0.5} 170^{0.25} * 10,164^{0.302}$$

$$* (1 + 22.4)^{0.04} * 22^{0.10} = 228,158 \text{ lbf}$$

$$W_{vertical tail} = 2 * 0.0026 * (1 + 0)^{0.225} 950,000^{0.556} (1.5 * 3 * 9.8)^{0.536} * 14.26^{-0.5} * 702^{0.5}$$

$$* 14.26^{0.875} = 5,984 \text{ lbf}$$

$$W_{main landing gear} = 0.0106 * 1 * (950,000)^{0.888} (1.5 * 3 * 9.8)^{0.25} * 10^{0.4} 16^{0.321} * 4^{-0.5} * 242^{0.1}$$

$$= 29,410 \text{ lbf}$$

$$W_{nose landing gear} = 0.032 * 1 * (950,000)^{0.646} (1.5 * 3 * 9.8)^{0.25} * 10^{0.5} 2^{0.45} = 2,590 \text{ lbf}$$

$$W_{engine} = 19,316(2) = 38,632 \text{ lbs}$$

$$W_{nacelle} = 0.6724 * 1 * (23)^{0.1} (11)^{0.294} * (1.5 * 3 * 9.8)^{0.119} * 18,632^{0.611} * 2^{0.984} * 770^{0.224}$$

$$= 10,413 \text{ lbf}$$

$$W_{engine controls} = 5 * 2 + 0.80 * 140 = 148 \text{ lbf}$$

$$W_{starter} = 49.19 \left(2 * \frac{18,632}{1,000} \right)^{0.541} = 348 \text{ lbf}$$

$$W_{fuel system} = 2.405 * 55,820^{0.606} (1 + 0.38)^{-1.0} (1 + 0) 8^{0.5} = 3,709 \text{ lbf}$$

$$W_{flight controls} = 145.9 * 7^{0.554} \left(1 + \frac{2}{7} \right)^{-1.0} (2,000)^{0.20} (27,647,852 * 10^{-6})^{0.07} = 1,924 \text{ lbf}$$

$$W_{instruments} = 4.509(1)(1)(12)^{0.541} (2)(170 + 284)^{0.5} = 736 \text{ lbf}$$

$$W_{hydraulics} = 0.2673(7)(170 + 284)^{0.937} = 578 \text{ lbf}$$

$$W_{electrical} = 7.291 * 60^{0.782} * 20^{0.346} * 2^{0.10} = 541 \text{ lbf}$$

$$W_{avionics} = 1.73 * 1,400 = 2,422 \text{ lbf}$$

$$W_{air conditioning} = 62.36 * 512^{0.25} * \left(\frac{35,000}{1,000} \right)^{0.604} * 1,400^{0.10} = 5,241 \text{ lbf}$$

$$W_{furnishings} = 0.0577 * 12^{0.1} * 127,800^{0.393} * 10164^{0.75} = 7,608 \text{ lbf}$$

$$W_{handling gear} = 3.0 * 10^{-4} * 950,000 = 285 \text{ lbf}$$

Radii of Gyration for a Jet transport – fuselage-mounted engines:

$$\bar{R}_x = 0.24$$

$$\bar{R}_y = 0.36$$

$$\bar{R}_z = 0.44$$

Mass Moments of Inertia:

$$I_{xx} = \frac{(b^2 W \bar{R}_x^2)}{4g} = \frac{(142^2 * 950,000 * 0.24^2)}{4(32.174)} = 8,573,491 \text{ lbf} * \frac{ft}{s^2}$$

$$I_{yy} = \frac{(L^2 W \bar{R}_y^2)}{4g} = \frac{(170^2 * 950,000 * 0.36^2)}{4(32.174)} = 27,647,852 \text{ lbf} * \frac{ft}{s^2}$$

$$I_{zz} = \left(\frac{b+L}{2}\right)^2 \frac{(W \bar{R}_y^2)}{4g} = \frac{\left(\frac{142+170}{2}\right)^2 (950,000 * 0.44^2)}{4(32.174)} = 34,778,680 \text{ lbf} * \frac{ft}{s^2}$$

Appendix B: Roskam's Weight Calculations

$$W_{wing} = \frac{0.00428(16,284^{0.48})(4.9)(0.85)^{0.43}950,000(1.5 * 3 * 9.8)^{0.84}(0.088)^{0.14}}{(100 * 0.30)^{0.76} \cos^{1.54}(36.81)} = \frac{3,696,401}{9.42}$$

$$= 392,399 \text{ lbf}$$

$W_{fuselage} = N/A$, not applicable due to the lack of conventional tube design

$$W_{vertical tail} = 2$$

$$\begin{aligned} & * 0.19 \left((1 + 0)^{0.5} (950,000 * 1.5 * 3 * 9.8)^{0.363} 1,236^{1.089} (0.85)^{0.601} \right. \\ & * (154.62 - 29.28)^{-0.726} \left(1 + \frac{2(1,236)}{1,236} \right)^{0.217} 2.55^{0.337} (1 + 0.42)^{0.363} \\ & \left. * \cos(25.74)^{-0.484} \right)^{1.014} = 34,229 \text{ lbf} \end{aligned}$$

$$W_{landing gear} = 62.61 \left(\frac{950,000}{1,000} \right)^{0.84} = 19,858 \text{ lbf}$$

$$W_{engine} = 19,316(2) = 38,632 \text{ lbf}$$

$$W_{nacelle} = 3.0 * (1)((\pi * 5.5^2)^{0.5}(24.29)(15))^{0.731} = 1,182 \text{ lbf}$$

$$W_{engine controls} = 0.686(170 * 2)^{0.792} = 69 \text{ lbs}$$

$$W_{starter} = 9.33 \left(\frac{440,300}{1,000} \right)^{1.078} = 6,604 \text{ lbf}$$

$$W_{fuel system} = 80(2 + 3 - 1) + 15(3)^{0.5} \left(\frac{374,000}{6.55} \right)^{0.333} = 1,317 \text{ lbs}$$

$$W_{flight controls} = 0.64 * 950,000^{\frac{2}{3}} = 6,149 \text{ lbs}$$

$$W_{instruments,electrical,avionics} = 0.575(440,300)^{0.556} (6,000)^{0.25} = 6,952 \text{ lbs}$$

$$W_{hydraulics} = 0.001(950,000) = 950 \text{ lbf}$$

$$W_{air conditioning} = 6.75 * (124.49)^{1.28} = 3,244 \text{ lbf}$$

$$W_{furnishings} = 0.211 * (440,300)^{0.91} = 28,846 \text{ lbf}$$

$$W_{handling gear} = 3 * \frac{225}{2} = 338 \text{ lbf}$$

Appendix C: Matlab Code

C.1. Breguet's Range Equation

```
%% Jeffrey Trac-Pho
%% AE 295A Breguet's Range Equation

clc ;
clear;
close all;
%
v = 504; % kts
cj = 0.65; % lbs/lbs/hr
LDratio = 22;
Wp = 0:500000; %lbs
We = 462500; % lbs
WF = 370700; % lbs
Wi = Wp+We+WF; % lbs
Wf = Wp+We; % lbs

R = v/cj*LDratio*log(Wi./Wf);

figure,
plot(Wp,R)
title('Range vs. Payload Weight')
xlabel('Payload Weight[lbs]')
ylabel('Range [nmi]')
```

C.2. Sweep Angle Equation

```
% Jeffrey Trac-Pho  
% AE 295A Sweep Angle Equation
```

```
clc ;  
clear;  
close all;  
%
```

```
M_cruise = 0.80;  
M_cc = M_cruise/1.02;  
t_c = 0.18;
```

```
V_mph = 663 * M_cruise;  
V_fts = 5280/3600 * V_mph;
```

```
W = 950000; % lbf, slugs*ft/s^2  
rho = 7.38*10^-4; % slugs/ft^3  
A = 16306; % ft^2  
C_L = 2*W/rho/A/V_fts^2;
```

```
gamma = 1.4;
```

```
syms lambda
```

```
eqn = ((M_cc^2*(cosd(lambda))^2)/(1-M_cc^2*(cosd(lambda))^2)^(1/2)) ...
```

```
*(((gamma+1)/2)*2.64*(t_c)/cosd(lambda)+(((gamma+1)/2)*(2.64*t_c*0.34*C_L/(cosd(lambda))^3))) ...
```

```
+ ((M_cc^2*(cosd(lambda))^2)/(1-M_cc^2*(cosd(lambda))^2))*(((gamma+1)/2)*(1.32*t_c/cosd(lambda))^2) ...
```

```
+ (M_cc^2*(cosd(lambda))^2)*(1+((gamma+1)/2)*(0.68*C_L/(cosd(lambda))^2)+((gamma+1)/2)*((0.34*C_L)/(cosd(lambda))^2)-1) ...  
== 0;
```

```
S = solve(eqn,lambda,'Real',true)  
fplot([lhs(eqn) rhs(eqn)], [0 90])  
ylim([-1 1])  
xlabel('Sweep Angle [degrees]')  
ylabel('Value of LHS and RHS of the Equation')
```

C.3. CG Excursion Equation

```
%% Jeffrey Trac-Pho
%% AE 295A CG Excursion

clc ;
clear;
close all;
%
x_MTOW = 78.0; % [ft]
x_no_fuel = 76.9; % [ft]
x_no_payload = 79.4; % [ft]
x_bar = 29.28; % [ft]
MAC = 96.84; % ft
MTOW = [(x_MTOW-x_bar)/MAC,950000]; % [dimensionless, lbf]
no_fuel = [(x_no_fuel-x_bar)/MAC,611795]; % [dimensionless, lbf]
no_payload = [(x_no_payload-x_bar)/MAC,483995]; % [dimensionless, lbf]

location = [MTOW(1), no_fuel(1), no_payload(1),MTOW(1)];
weights = [MTOW(2), no_fuel(2), no_payload(2),MTOW(2)];

x_np = 87.725; %ft
SM_forward = (87.725-76.9)/MAC;
SM_aft = (87.725-79.4)/MAC;
forward_CG = (x_np-MAC*(SM_forward)-x_bar)/MAC;
aft_CG = (x_np-MAC*(SM_aft)-x_bar)/MAC;

figure,
plot (location, weights)
xline(forward_CG)
xline(aft_CG)

xlabel('% of MAC')
ylabel('Weight [lbs]')
title('CG Excursion Diagram')
```

C.4. Drag Polar Graph Equation

```
%% Jeffrey Trac-Pho
%% AE 295A Drag Polar Graph Estimate

clc ;
clear;
close all;
%
Cd0 = 0.0061;
e = 0.85 ;
CL = linspace(-3,3,200);
AR = 4.9;
CD = Cd0 + CL.^2/(pi*e*AR);

Cd0_takeoff_up = 0.016;
e_takeoff = 0.80 ;
CL = linspace(-3,3,200);
CD_takeoff_up = Cd0_takeoff_up + CL.^2/(pi*e_takeoff*AR);

Cd0_takeoff_down = 0.031;
CL = linspace(-3,3,200);
CD_takeoff_down = Cd0_takeoff_down + CL.^2/(pi*e_takeoff*AR);

Cd0_landing_up = 0.016;
e_landing = 0.75 ;
CL = linspace(-3,3,200);
CD_landing_up = Cd0_landing_up + CL.^2/(pi*e_landing*AR);

Cd0_landing_down = 0.031;
CL = linspace(-3,3,200);
CD_landing_down = Cd0_landing_down + CL.^2/(pi*e_landing*AR);

figure,
plot(CD,CL)
hold on
plot(CD_takeoff_up,CL)
hold on
plot(CD_takeoff_down,CL)
hold on
plot(CD_landing_up,CL)
hold on
plot(CD_landing_down,CL)

title('Drag Polar [Estimated]')
xlabel('C_D')
ylabel('C_L')
xlim([0 0.15])
ylim([0 1.5])
legend('Clean','Take-off Flaps, Gear Up','Take-off Flaps, Gear Down', ...
       'Landing Flaps, Gear Up','Landing Flaps, Gear Down','Location','Best')
```

C.5. Drag Polar Graph Equation of Raymer's and Roskam's Methods

```
% Jeffrey Trac-Pho
% AE 295B Drag Polar Estimation Comparison

clc ;
clear;
close all;
%
Cd0 = 0.0061;
e = 0.85 ;
CL = linspace(-3,3,200);
AR = 4.9;
CD = Cd0 + CL.^2/(pi*e*AR);

% Roskam
CD_roskam = 0.118 + .171*CL.^2;

% Raymer
CD_raymer = 0.0124 + .0874*CL.^2;

figure,
plot(CD,CL)
hold on
plot(CD_roskam,CL)
hold on
plot(CD_raymer,CL)

title('Drag Polar Comparison')
xlabel('C_D')
ylabel('C_L')
xlim([0 0.15])
ylim([0 1.5])
legend('Initial Approximation','Roskam','Raymer','Location','Best')
```

C.6. V-N Diagram

```
%% Jeffrey Trac-Pho
%% V-N Diagram

clc ;
clear;
close all;
%
V = linspace(0,600,601);
n_lim_a = (V/134).^2;
n_lim_b = 1+0.00232*V;
n_lim_c = 1+0.00166*V;
n_lim_d = 1+0.000811*V;
n_lim_neg = -(V/160).^2;

v_bc = V(1:301);
n_bc = n_lim_a(161)+(n_lim_c(461)-n_lim_b(161))/(461-161).*v_bc;
v_cd = V(1:116);
n_cd = n_bc(end)+(n_lim_d(576)-n_lim_c(461))/(576-461).*v_cd;
n_ef = -1+(1)/(576-461).*v_cd;

figure,
plot(V,n_lim_a,'k')
hold on
plot(V,n_lim_b,'k--')
hold on
plot(V,n_lim_c,'k--')
hold on
plot(V,n_lim_d,'k--')
hold on
plot(V(161:461),n_bc,'k')
hold on
plot(V(461:576),n_cd,'k')
hold on

title('V-N Gust Diagram')
xlabel('V [KEAS]')
ylabel('Limit Load ~ n')
ylim([0 3])

figure,
plot(V(1:218),n_lim_a(1:218),'k')
hold on
plot([V(218),576],[2.5,2.5],'k')
hold on
plot(V(1:161),n_lim_neg(1:161),'k')
hold on
plot([V(161),V(461)],[-1,-1],'k')
hold on
plot(V(461:576),n_ef,'k')
hold on
plot([576,576],[2.5,0],'k')
hold on
```

```
title('V-N Maneuver Diagram')
xlabel('V [KEAS]')
ylabel('Limit Load ~ n')
ylim([-2 3])
```

C.7. DAPCA IV Cost Model

```
%% Jeffrey Trac-Pho  
%% AE 295B Cost Analysis
```

```
clear;  
clc;
```

```
We = 483995; % Empty Weight [lb]  
V = 500; % Maximum velocity [kts]  
v_c = 460;  
Q = 150; % Production Quantity  
FTA = 6; % Flight Test Aircraft  
C_eng = 4140000*2; % Engine costs  
C_avi = 2000*483995; % Avionics costs  
H_e = 4.86*We^0.777*V^0.894*Q^0.163;  
H_T = 5.99*We^0.777*V^0.696*Q^0.263;  
H_m = 7.37*We^0.82*V^0.484*Q^0.641;  
H_Q = 0.133;  
C_D = 45.42*We^0.630*500^1.3;  
C_F = 1243.03*We^0.325*V^0.822*FTA^1.21;  
C_M = 11*We^0.921*V^0.621*Q^0.799;  
R_e = 160.70;  
R_T = 165.05;  
R_Q = 150.64;  
R_M = 136.23;  
RD = 1.2*(H_e*R_e+(H_T*R_T+H_m*R_M+H_Q*R_Q+C_D+C_F+C_M+C_eng+C_avi)/Q)  
% 1.2 for composite/titanium parts for secondary structures  
mfg_cost = 1.2*(H_T*R_T+H_m*R_M+H_Q*R_Q+C_D+C_F+C_M+C_eng+C_avi)/Q  
  
c_fuel = 4.81*338205/6.74*2500 % $4.81 for 2022 Jet Fuel Price  
c_crew = 2.719*(47*(460*950000/10^5)^0.3+118)*2.719  
  
material_cost = 15*3.3*(mfg_cost-C_eng)/10^6+7.04+(58*(C_eng/10^6)-13)*2
```